NuMI-NOTE-1491-v1
September 7, 2014

Measuring the Number of Protons-on-Target (POT) in the NuMI Beamline

Phil Adamson [1], **Mary Bishai**[2], **Daniel Cherdack**[3], **Sam Childress**[1], **Mark Dierckxsens**[2], **Jim Hylen**[1], **Aisha Ibrahim**[1], **Dharma Indurthy**[4], **Doug Jensen**[1], **Gordon Koizumi**[1], **Sacha Kopp**[4], **Peter Lucas**[1], **Alysia Marino**[1], **Brian Rebel**[1], **Brett Viren**[2], **Bob Zwaska**[1]

[1] *Fermi National Accelerator Lab.*
[2] *Brookhaven National Lab*
[3] *Tufts University*
[4] *University of Texas, Austin*

The absolute measurement of the number of protons delivered to the NuMI target is a key ingredient of the MINOS experimental program. The NuMI beamline instrumentation provides measurements of the absolute intensity of the proton beam as well as its profile and position at the target. In this report, we examine the measurements of the NuMI beam intensity, profile, position-on-target and stability for the 2005 dataset. We present a detailed account of the estimation of the systematic uncertainties on the measurement of number of protons-on-target for the first 1×10^{20} protons in MINOS.

Contents

List of Tables

List of Figures

1 Introduction

The absolute measurement of the number of protons delivered to the NuMI target is a key ingredient of the MINOS experimental program. For Near Detector physics analysis it is a critical component

in the normalization of the neutrino flux. The NuMI beamline is the most highly instrumented fixed target beamline to date. A schematic of the different instrumentation and the location along the beamline is shown in Figure 1. Two Toroid Intensity Monitor Integrators measure the proton

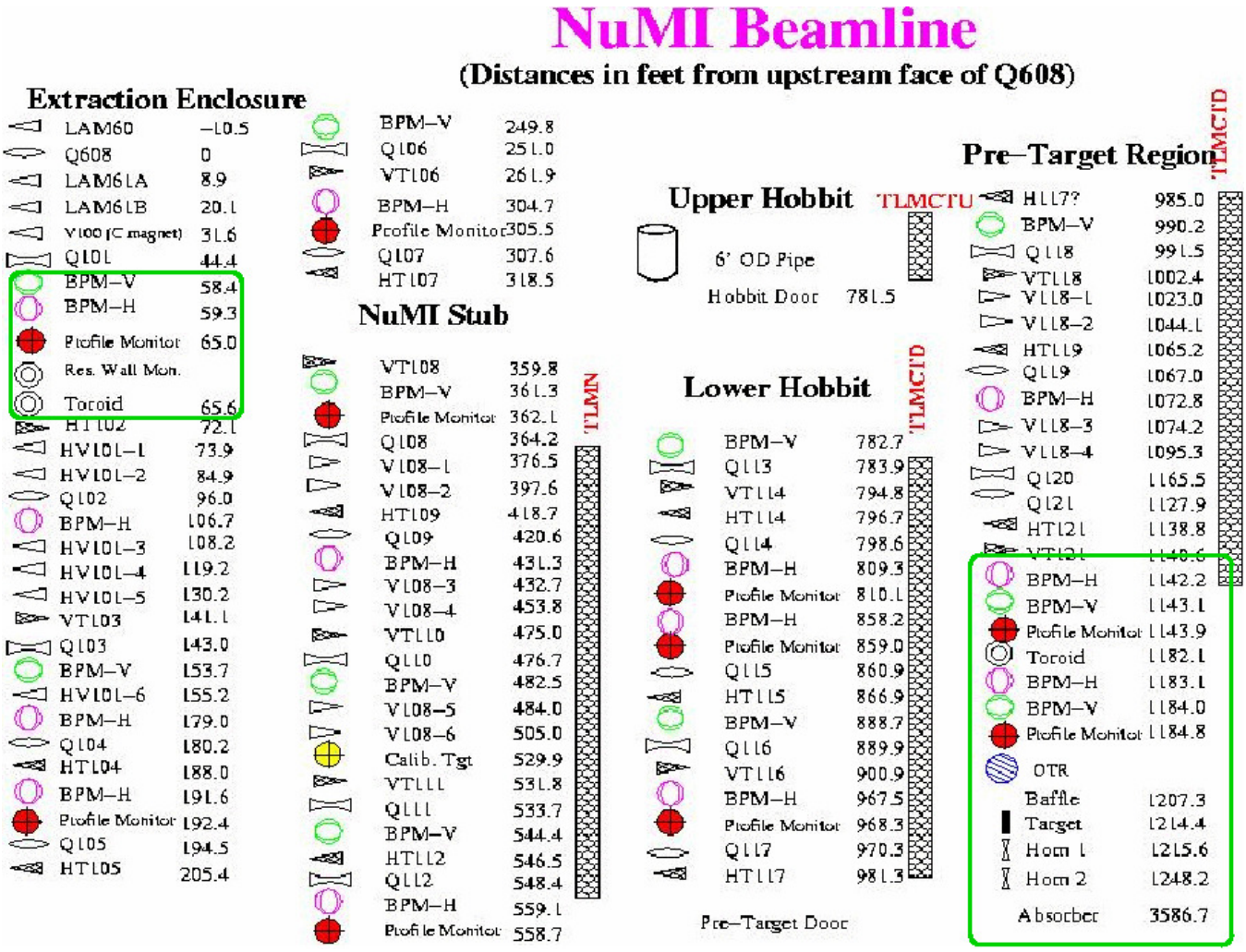

Figure 1: NuMI beamline instrumentation.

beam intensity at the beginning of the 400 meter beamline and at a distance of ≈ 9 meters from the target. The toroids are read out with different ADCs with different precision, the most precise being a 16 bit readout which provides an intrinsic resolution of up to 0.006% at the nominal beam intensity of 25 teraprotons per spill. Adjustable integration gates allow for optimization of the intensity measurements to reduce noise and pedestals.

The number of protons on target is determined not only by the number of protons in the beam, but also the fraction of these protons that are actually incident on the target. There are 24 beam position monitors (BPMs) which provide information on the location of the beam along the NuMI beamline (13 horizontal and 11 vertical BPMs). Each BPM consists of two cylindrical electrodes. The difference in charge induced on each electrode by the beam allow for a precise measurement of the beam position in the horizontal or vertical. In the pretarget region there are two pairs of horizontal and vertical BPMs beyond the last focusing and bending magnet. The pre-target region instrumentation stations are approximately 40 feet apart and the center of the target in the low energy (LE) position is 30 feet from the nearest instrumentation station. The BPMs in the pre-

target region have a nominal measurement precision of 0.05mm rms within ±6 mm for 3 to 9.5×10^{10} protons per bunch. The NuMI BPM front-end electronics determine the position and intensity of each of the 6 proton batches in a spill. The pretarget BPMs are used to project the location of the beam maximum at the target. The autotune program runs in real time and uses feedback from the BPMs to adjust the trim magent currents in the NuMI beamline on a spill-by-spill basis such that the beam stability at the target is carefully controlled.

The hadron spectrum from the NuMI target depends not only on the total number of protons hitting the target, but where each proton hit. Hadrons produced near the edge of the target are more likely to escape and reinteract less in the target. Protons hitting the graphite protection baffle 1meter upstream of the target produce hadrons that are focused differently by the horns and produce a higher energy neutrino spectrum. Therefore, to properly model the hadron production in the NuMI target, we need to know the profile of the beam as well as its location on the target. Ten Segmented Electron Multipliers (SEM) made from 5 μ m thick Ti foil [1] are deployed along the NuMI beamline. Each SEM has two sheets of segmented foils which measure the beam profile in the horizontal and the vertical. The foil segments are 0.25 mm thick and are spaced 1 mm apart in the transport region and 0.5 mm apart in the pre-target region. In addition to measuring the beam profiles, the SEMs also measure the beam position with comparable precision as the BPMs. The SEMs measure the profile and position of the beam once during a spill averaged over all batches. To minimize losses, only the SEM closest to the target is kept in the beamline at all times.

In this note we summarize the calibrations of the NuMI toroids and the measurements of the NuMI beam intensity, profile, position-on-target and stability for the 2005 dataset. From these studies, we present an estimate of the systematic uncertainties on the measurement of the total number of protons delivered to MINOS in 2005.

2 Measuring the absolute proton intensity in NuMI

2.1 NuMI toroids

The proton beam intensity in the NuMI beamline is measured using Toroid Intensity Monitor Integrators. There are two such devices in the NuMI beamline: TOR101 is located 65 feet from Q608, the first quadrupole in the NuMI beam line, and TORTGT located 1185 feet from Q608 and 30 feet from the NuMI target. Each toroid has a high-precision and low-precision readout. E:TOR101 and E:TORTGT are the ACNET device names used for the lower precision ADC readout. E:TR101D and E:TRTGTD are the corresponding ACNET device names for the higher precision ADC readout which is 16 bit for both toroids. The following are the technical specifications of the NuMI toroids:

- Pearson Current Transformers (Model 3100) @ 0.5V/Amp
- Resistance on Single-turn calibration winding ≈ 51.01
- Cable Length ≈ about 175ft for TOR101 and 394ft for TORTGT
  - 3/8" Heliax for calibration cable to send test pulse to toroid
  - Trumpeter TWC2-78 for signal cable from toroid to electronics
- Sampled Integrator :
  - DC Gain ≈ 2200 (66.9dB)

  - Integrator low frequency corner ≈ 48.2Hz
  - Integration time constant ≈ 1.7usec
  - Integration gated window ≈ 0.1usec to 99.9usec (increments of 0.1usec)
  - 16Bit 250KHz ADC after integrator (Effective gain of 4 through to DAC output)

- Outputs integrated intensity reading:
  - Full-scale for all readouts: 5.21E13 / 10V
  - Ignoring ACNET control pathways, Vnoise (i.e. pulse to pulse error) ≈ 276 μ Vrms
  - Integrator electronics uses 16bit ADC and DAC (76uV LSB, 2's complement)
  - E:TOR101 ≈ signed 12-bit MADC readout LSB: 0.0254E12 (4.88mV)
  - E:TORTGT ≈ signed 14-bit MADC readout LSB: 0.0064E12 (1.22mV)
  - E:TR101D and E:TRTGTD ≈ signed 16-bit C284 readout LSB: 0.0016E12 (305.2uV) Fastest readback is limited by C284 card to 15Hz

A brief description of the FNAL accelerator complex timing and synchronization signals is presented in Appendix A. As of 3/29/05 the timing triggers for the readback of the NuMI toroids are as follows:

- E:TS101D ≈ main sample trigger for TOR101 and TR101D
  MIBS $74 with 17.068027 MREV delay / 189usec (prior to July 18, 2005)
  MIBS $74 with 19.967687 MREV delay (after July 19, 2005)
  1 bucket resolution from 479 timing card

- E:TC101D ≈ clear/reset trigger for TOR101 and TR101D
  TCLK $25 with 1 usec delay
  70 bucket resolution from 377 timing card

- E:TSTGTD ≈ main sample trigger for TORTGT
  MIBS $74 with 17.068027 MREV delay / 189usec (prior to July 25, 2005)
  MIBS $74 with 19.967687 MREV delay (after July 25, 2005)
  1 bucket resolution from 479 timing card

- E:TCTGTD ≈ clear/reset trigger for TORTGT and TRTGTD
  TCLK $25 with 1 usec delay
  70 bucket resolution from 377 timing card

The external trigger's rising edge causes the integration gate to open. The toroid readout is determined by the ACNET calibrations applied and the integration gate widths. The initial integration gate widths were 99.9 μ seconds for both toroids. The TOR101 gate width was changed from 99.9 μ to 13.1 μ seconds on July 19, 2005. On July 25th E:TSTGTD delay was changed from 17.068027 MRev to 19.967687 MRev to match TOR101. For TORTGT the gate width was changed from 99.9 μ seconds to 13.1 μ seconds on July 25th, 2005. After the integration window closes the data is held for 3-4 μ sec to latch intensity into the toroid modules 16 bit digital buffer. This provides the C285 digital readout. The C285 is converted into an analog signal for MADC readout using a 16 bit DAC. The MADC signal is readout via ACNET.

3 Toroid Calibrations

3.1 Absolute calibrations of NuMI toroids

The schema for calibrating the toroids is shown in Figure 2. The calibration method is described

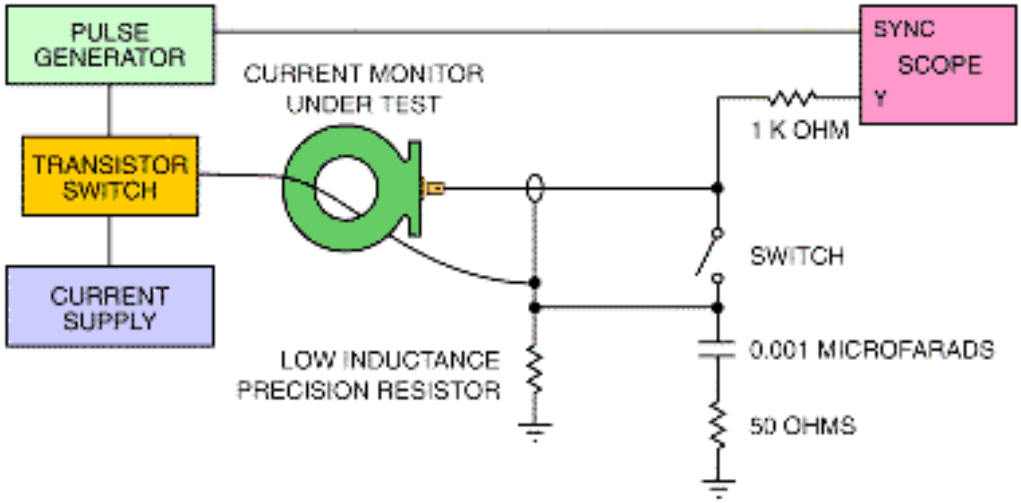

Figure 2: Calibration schema for Pearson Current Transformers

in [2] as follows: "A current pulse is generated by a current power supply switched by a transistor switch under control of a pulse generator. The pulse current passes through the current monitor and through the calibrated low inductance resistor to ground. The voltage drop across the resistor is subtracted from the voltage produced by the Current Monitor and the difference signal is observed on an oscilloscope." The first set of absolute calibrations of the NuMI toroids was carried out on 2/3/2005. The calibration pulse and gate used is shown in Figure 3. A comparison of the

Figure 3: Scope trace of the calibration pulse and TORTGT gate.

ACNET readback of the toroids before and after corrections are applied is shown in Figure 4 and 5. The result of a straight line fit to measured vs expected values is shown in Figures 4 and 5. Measured and expected values are found to agree within 0.3% for both TORTGT and TOR101. The insets in Figures 4 and 5 show the fractional difference in measured vs expected before and after the calibration constants are applied to the ACNET readout. The % errors on the readout of the toroids is found to be large for beam intensity values below 0.5 E12 even after the proper

calibrations are applied. Pedestal values are found to be -0.04E12 and -0.08E12 for TOR101 and TORTGT respectively. Based on these calibrations, the expected uncertainty on the toroid readout

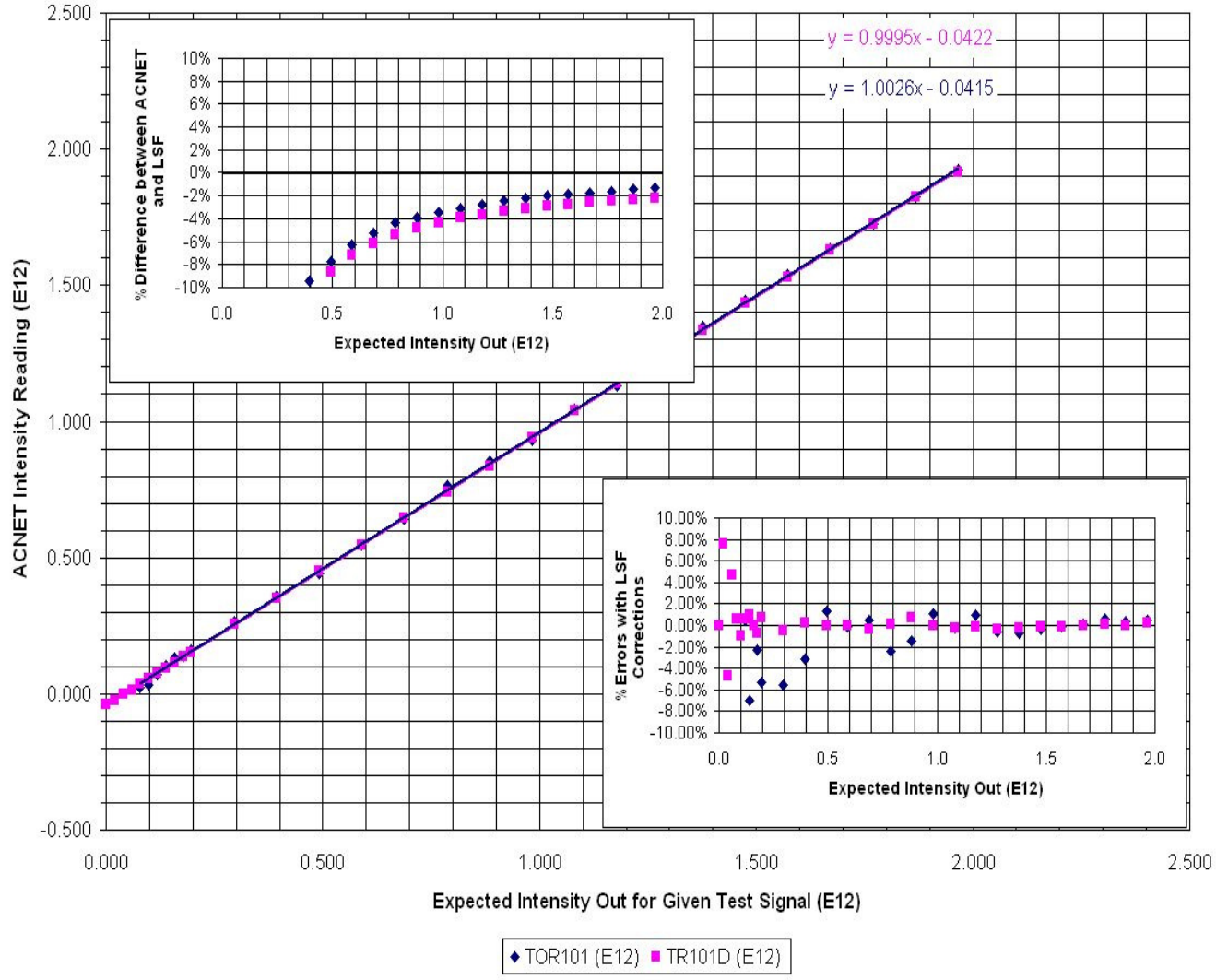

Figure 4: Calibration of TOR101 with a current source on 2/3/05

using the calibrated ACNET readout for intensities > 1.0 E12 is good to 0.5% (?????).

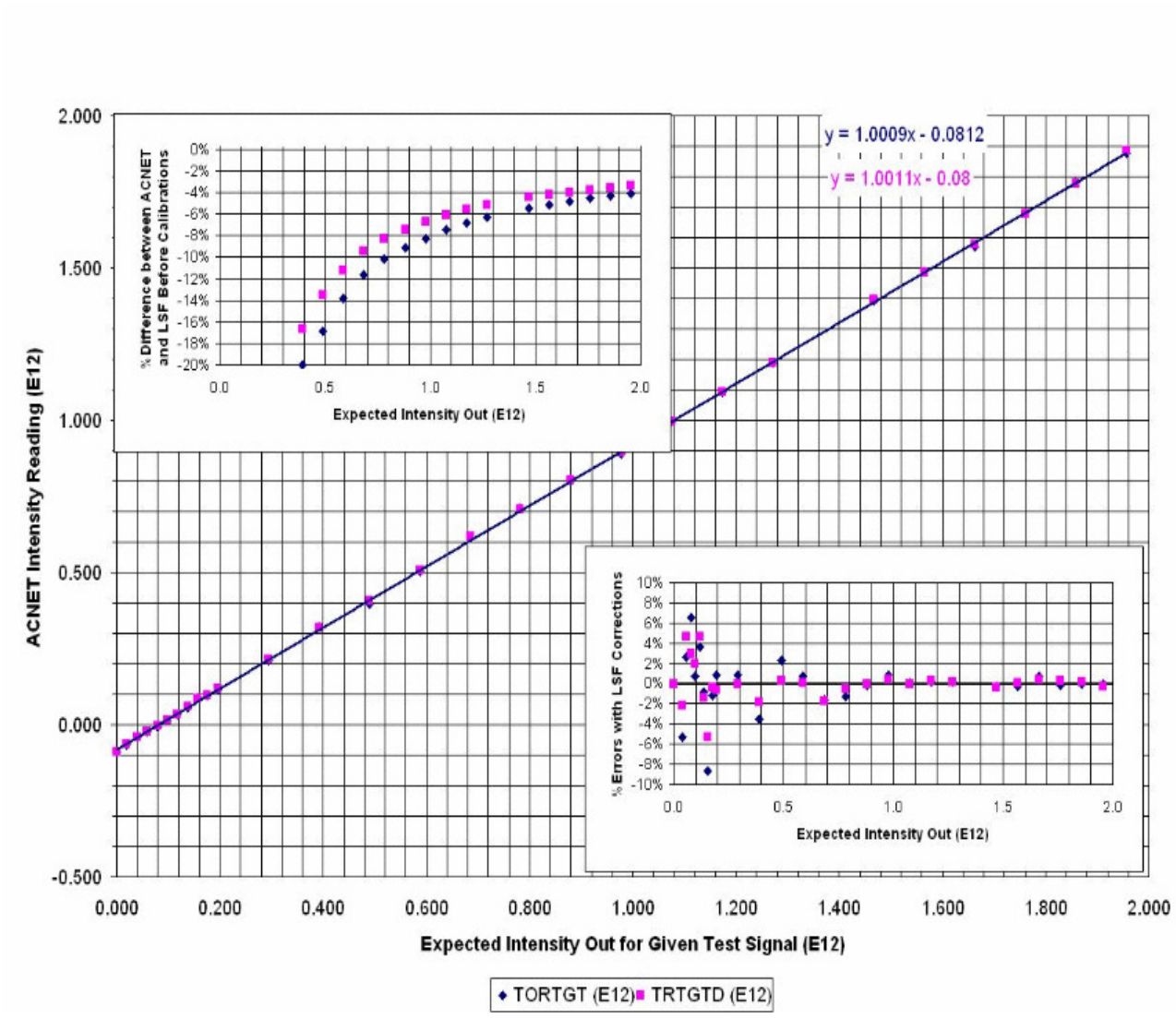

Figure 5: Calibration of TORTGT with a current source on 2/3/05

The gate widths for were changed from 99.9 μ second to 13.1 μ seconds for TOR101 and TORTGT on July 18 and July 25, 2005 respectively. In addition, on July 26th the gate timing for TORTGT was changed to properly capture the 1st batch signal in NuMI only 6 batch mode. The absolute pulse calibrations for the toroids were repeated when the gate width changed are shown in Figures 6 and 7. This calibration was performed for intensities up to 1E13. The insets

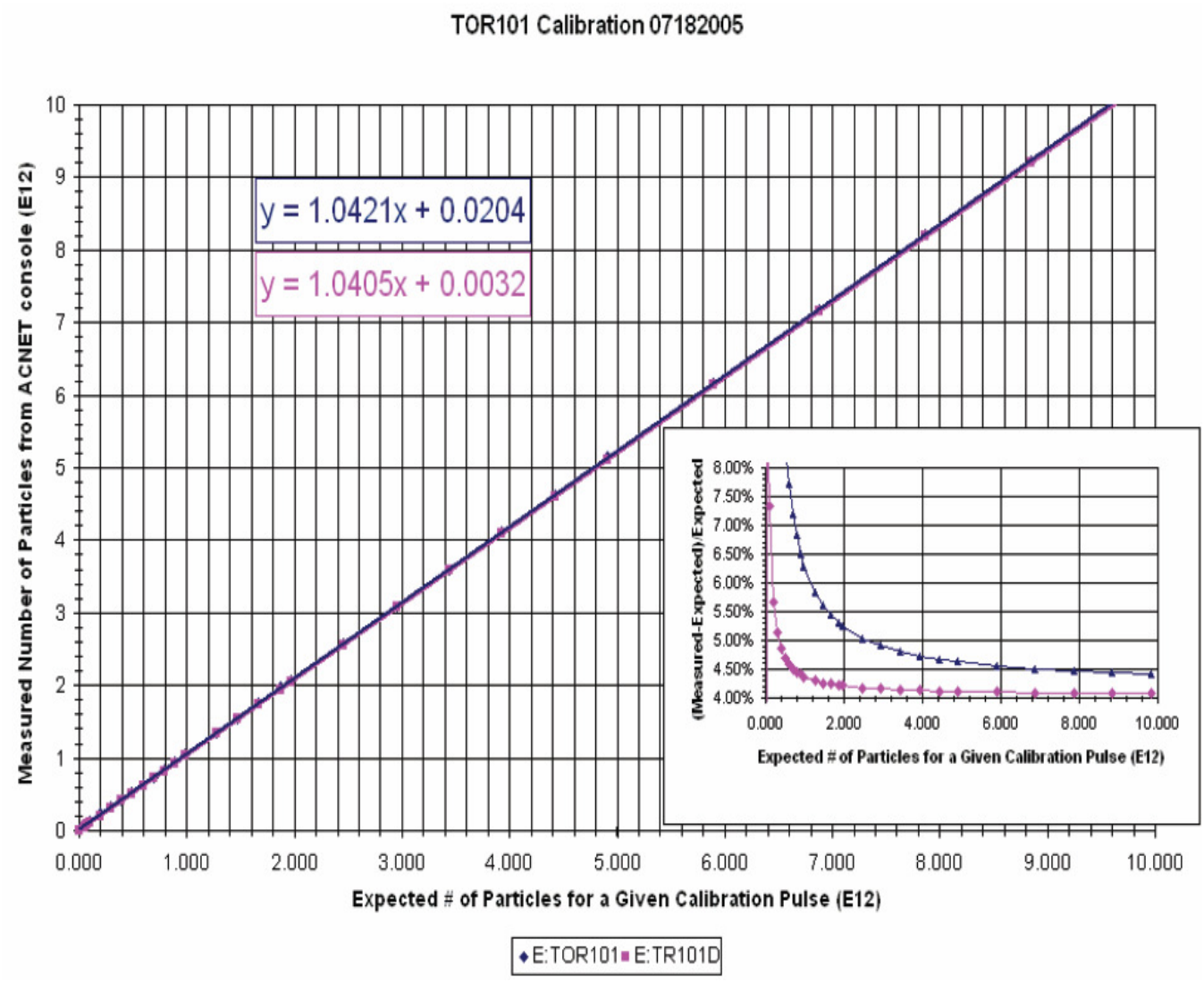

Figure 6: Calibration of TOR101 with a current source and 13.1 μ sec gate on 7/18/05

in the figures display the calibration corrections needed as a function of intensity for all 4 readouts. The ACNET readout from the toroids has calibration corrections applied based on the measurements shown in Figures 6 and 7. For TOR101 (TR101D) the average calibration correction is -4% (-3.7%) after July 18 and for TORTGT the average correction is -13% (-14%). These calibrations are applied as a function of proton intensity (???). The accuracy of these corrections for the data acquired with the smaller gate width is xxx % for intensities $>$ 1.0 E12.

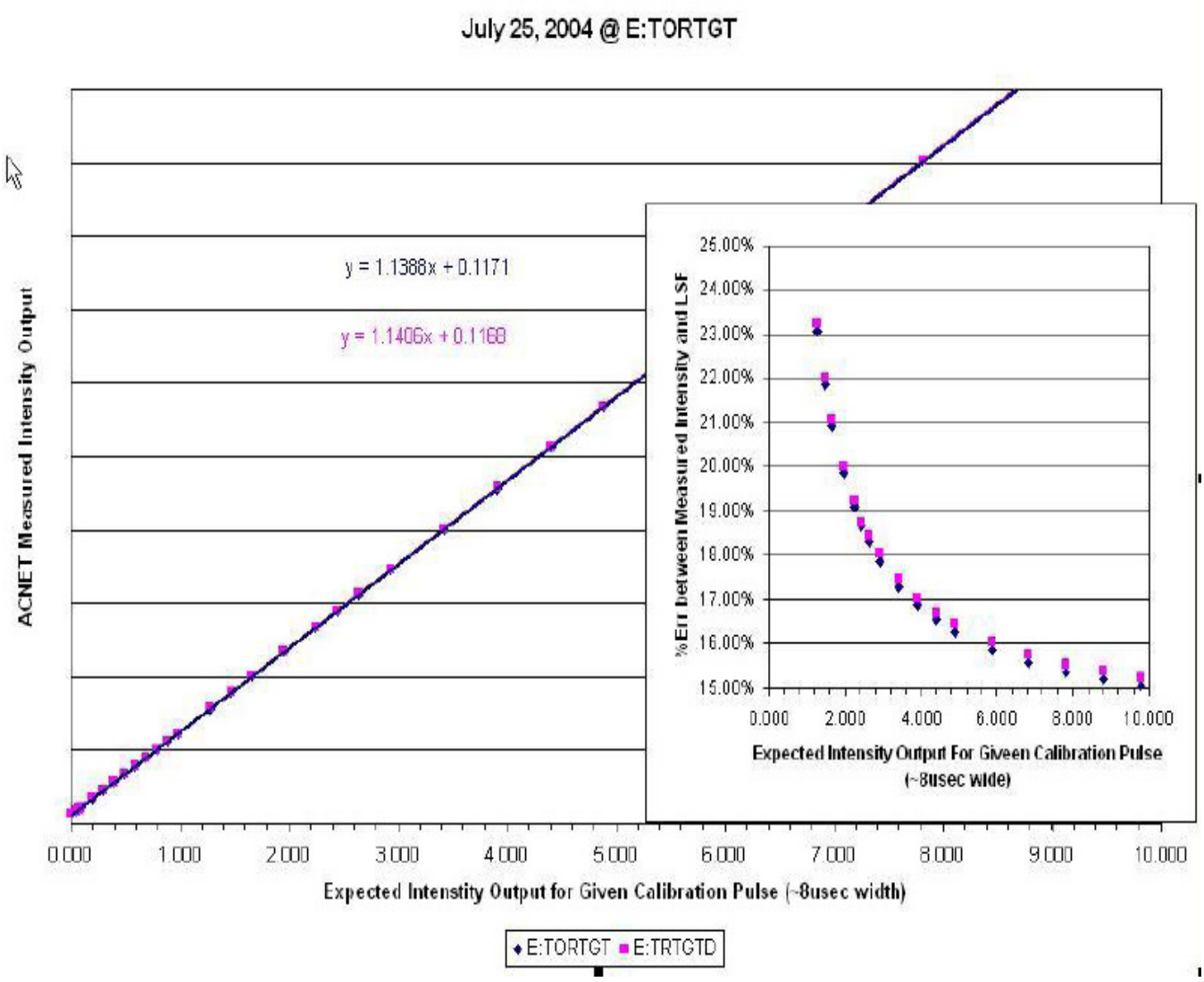

Figure 7: Calibration of TORTGT with a current source and 13.1 μ sec gate on 7/25/05

3.2 Integration Gate Widths

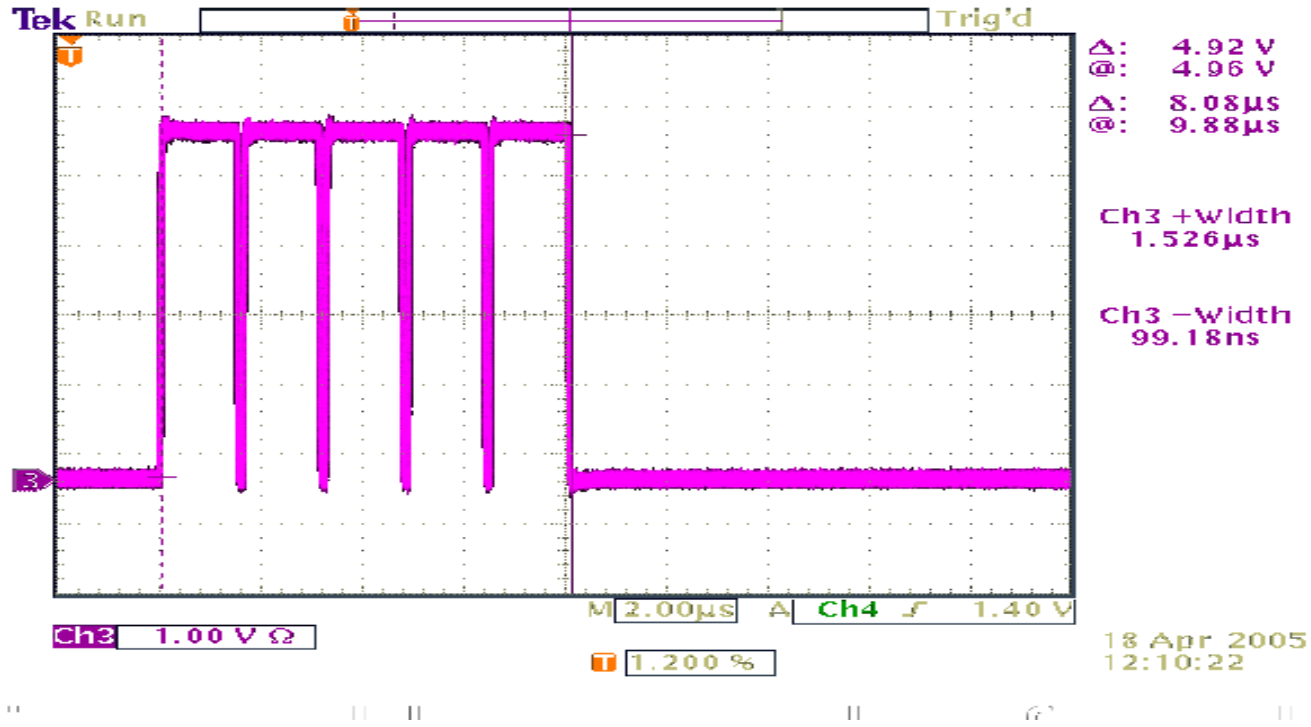

Figure 8: Scope trace of the calibration pulse used for gate width studies.

Prior to July 18, both TOR101 and TORTGT both had 99.9 μ sec integration gates. A study of the measured readout of TR101D versus expected as a function of the relative timing between the tail edge of a calibration pulse and the 99.9 μ sec integration gate edge [3] is shown in Figure 9. The measured readout from ACNET has calibration constants applied assuming the pulse is furthest from the end of the integration gate. The calibration pulse used was chosen to match the 5 batch structure of the beam as shown in Figure 8. The results shown in Figure 9 demonstrate that the closer the calibration pulse is relative to the end of the integration gate, the higher the measured value is w.r.t to the expected value and the response is very linear as a function of time between the end of the calibration pulse and the end of the integration gate. The decrease in the integrated charge as the pulse moves away from the end of the integration window (and hence the beginning of digitization) has been attributed to charge leakage from the integrating capacitor on the toroid. The study demonstrates that we lose 0.15 % of the charge per 1 μ second delay between the end of the pulse and the end of the integration gate.

The current MINOS pME and pHE dataset was acquired when the toroid integration gate width was 99.9 μ seconds and the beam pulse is close to the start of the gate. From the scatter in the last set of points in Figure 9, which show the fractional deviation from expected after corrections have been applied, we estimate the uncertainty in the ACNET calibration for the 99.9μ second gate width is $\sim$ 1%. We have included in this uncertainty our current lack of knowledge of how well the calibration pulse matches the real beam pulse in the time placement within the gate. The 1% uncertainty in the ACNET read out corresponds to a 5 μ second uncertainty in the location of the beam pulse as compared to the calibration pulse.

The integration gate widths changed to 13.1 μ seconds on July 19 for TOR101 and July 25 for TORTGT. The number of batches in a NuMI spill varies between 5 and 6 batches. In NuMI-mixed

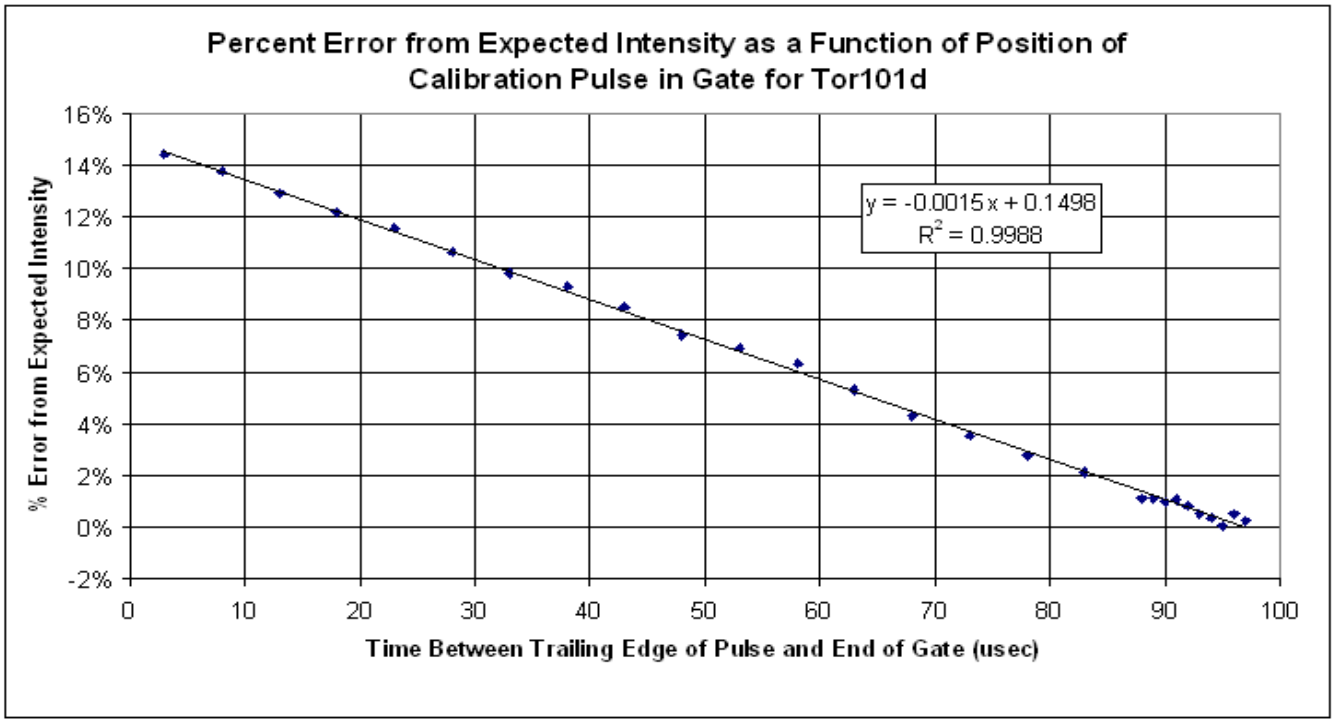

Figure 9: Percent difference between expected and measured beam intensity (from ACNET) as a function of the time between the falling edge of the calibration pulse and the end of the integration gate. Note that the ACNET readout already has calibration corrections applied to it assuming the time between the falling edge and the gate end is xx μ seconds. This causes an overcorrection being applied to the measured value when the pulse moves closer to the end of the integration gate. [3]

mode running the first batch is sent to pbar production and only 5 MI batches are sent to NuMI [1]. For 6 batches the beam pulse is 10 μ second wide and for 5 batches the beam pulse is 8 μ seconds wide. For the 5-batch NuMI spills [2] more charge is likely to leak off the integrating capacitor of the toroid before digitization. For the 13.1 μ second gate we estimate the maximum charge loss from the integrating capacitor for a 10 μ second 6-batch pulse is $\sim 0.5\%$ and for an 8 μ second 5-batch beam pulse the fraction of charge lost is $\sim 0.8\%$. The ACNET calibrations applied include corrections for the fraction of the charge lost due to leakage. A single correction is applied in ACNET regardless of the number of batches or their timing within the integration gate. The accuracy of the calibration will depend on how well the calibration pulse matches the timing of the real beam pulse. To be conservative, we recommend a 0.5% uncertainty be applied on the toroid readout for the 13.1 μ second gate width due to variations in charge leakage from the integrating capacitor.

In Figure 10, the scope traces from the real minos beam pulse at TOR101 for a 6 and 5 batch spill in NuMI-only and NuMI-mixed mode respectively are shown. The snapshots were taken on Feb 20, 2006. The traces in 10 reveal that the real beam pulse has a small tail at the trailing edge of the last batch which is not duplicated by the calibration pulse. The beam in the trailing edge is still contained within the 13.1 μ second integration gate with the present timing and we condsider the uncertainty on the beam intensity measurement due to beam outside the integration gate to be negligible.

[1] The location of the last batch w.r.t to the MIBS \$74 signal that generates the toroid integration gate is the same in 6-batch NuMI-only and 5-batch NuMI-mixed mode running

[2] Earlier in 2005 NuMI only spills had only 5 not 6 batches.

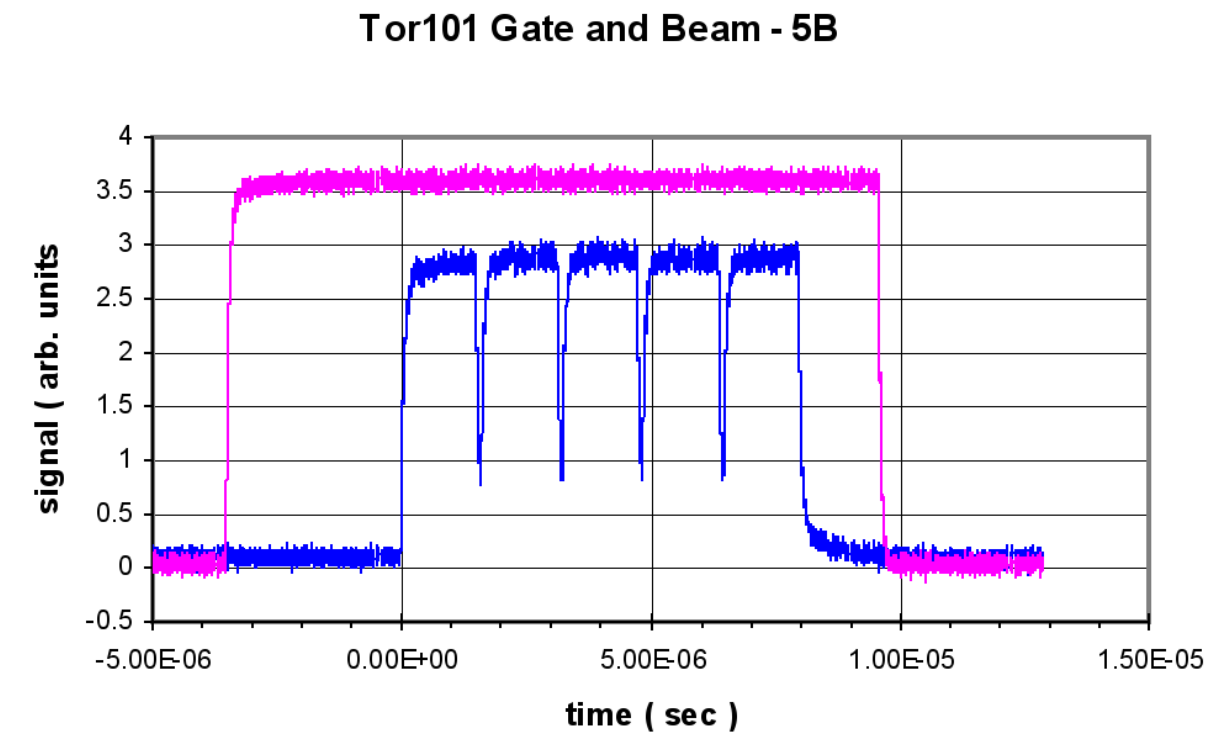

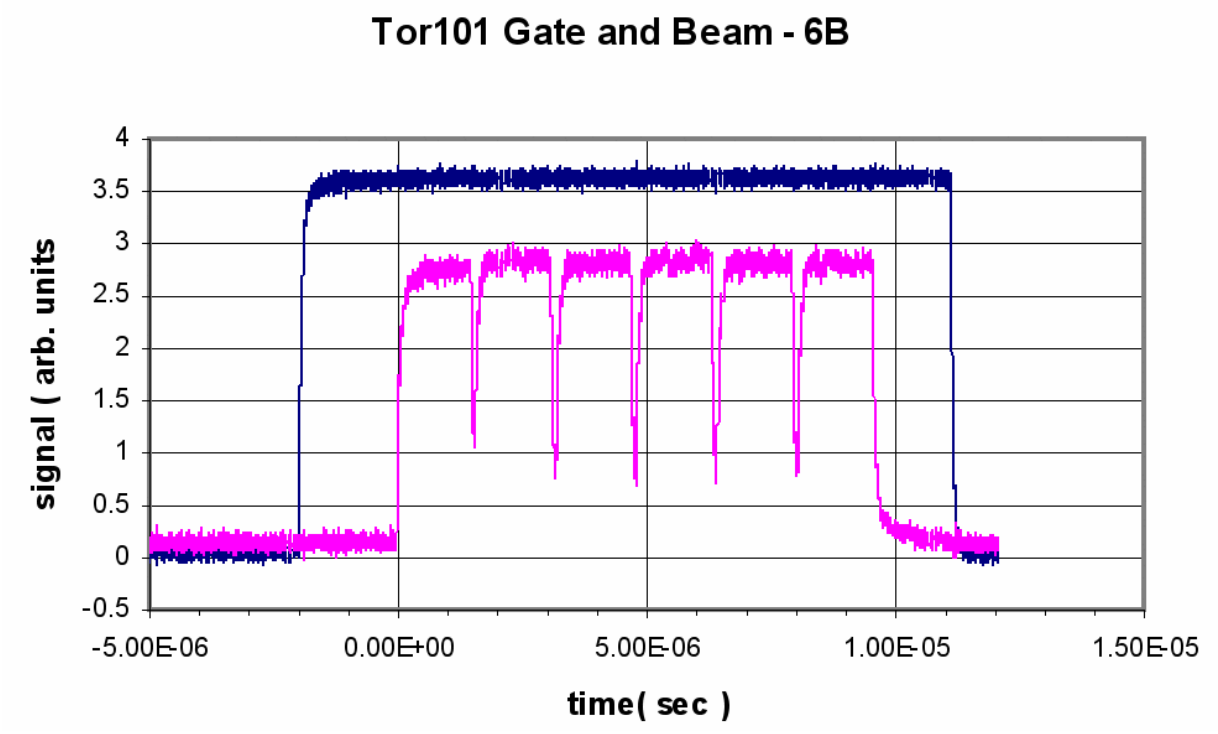

Figure 10: Timing of the beam pulse in TOR101 after gate width change to 13.1 μ seconds. 10,000 scope acquisitions taken on Feb 20, 2006

3.3 Pedestals

The ACNET readout of the beam intensity using the toroids does not correct for the pedestal values. The pedestal values for TOR101,TR101D, TORTGT and TRTGTD versus time is shown in Figure 12. Changes in the gate widths of TORTGT on Feb 27 and July 26, 2005 resulted in different pedestal mean pedestal values and noise before and after those dates. TOR101 gate widths were changed in early June, 2005 and July 19, 2005. We use the TORTGT and TRTGTD readout as the absoulte reference for the POT measurements in MINOS. The pedestal distribution before and after the July 26th, 2005 gate change is shown in Figure 12 [3]. The mean of the pedestal and the RMS for different running periods is listed in Table 1.

Table 1: Pedestal offsets for TORTGT. The data is presented in the form MEAN $\pm$ RMS E12.

Date	TORTGT	TRTGTD
Feb 1st - Feb 27	0.080 ± 0.011 E12	0.084 ± 0.010 E12
Feb 27 - March 31, 2005	-0.016 ± 0.017	-0.019 ± 0.016
May - July 26	0.014 ± 0.015	0.017 ± 0.013
July 26 - Dec, 2005	-0.0019 ± 0.0080	-0.0013 ± 0.0056

The uncertainty on the measurement of the beam intensity due to toroid noise can be estimated from the RMS of the pedestal distribution. We find that for TORTGT the value is 0.015E12 and 0.008E12 before and after July 26,2005 respectively. For TRTGTD the values are 0.013E12 and 0.006E12. At the nominal spill value of 25E12 POT, the uncertainty due to toroid noise is negligible being $< 0.03\%$.

[3] The data presented here is from the MINOS beam data stream which had the wrong ACNET calibration constants applied to TORTGT from July 26 to August 1st - which is why the pedestals seem to jump by 13% for TORTGT. An offline corretion is applied to correct for this.

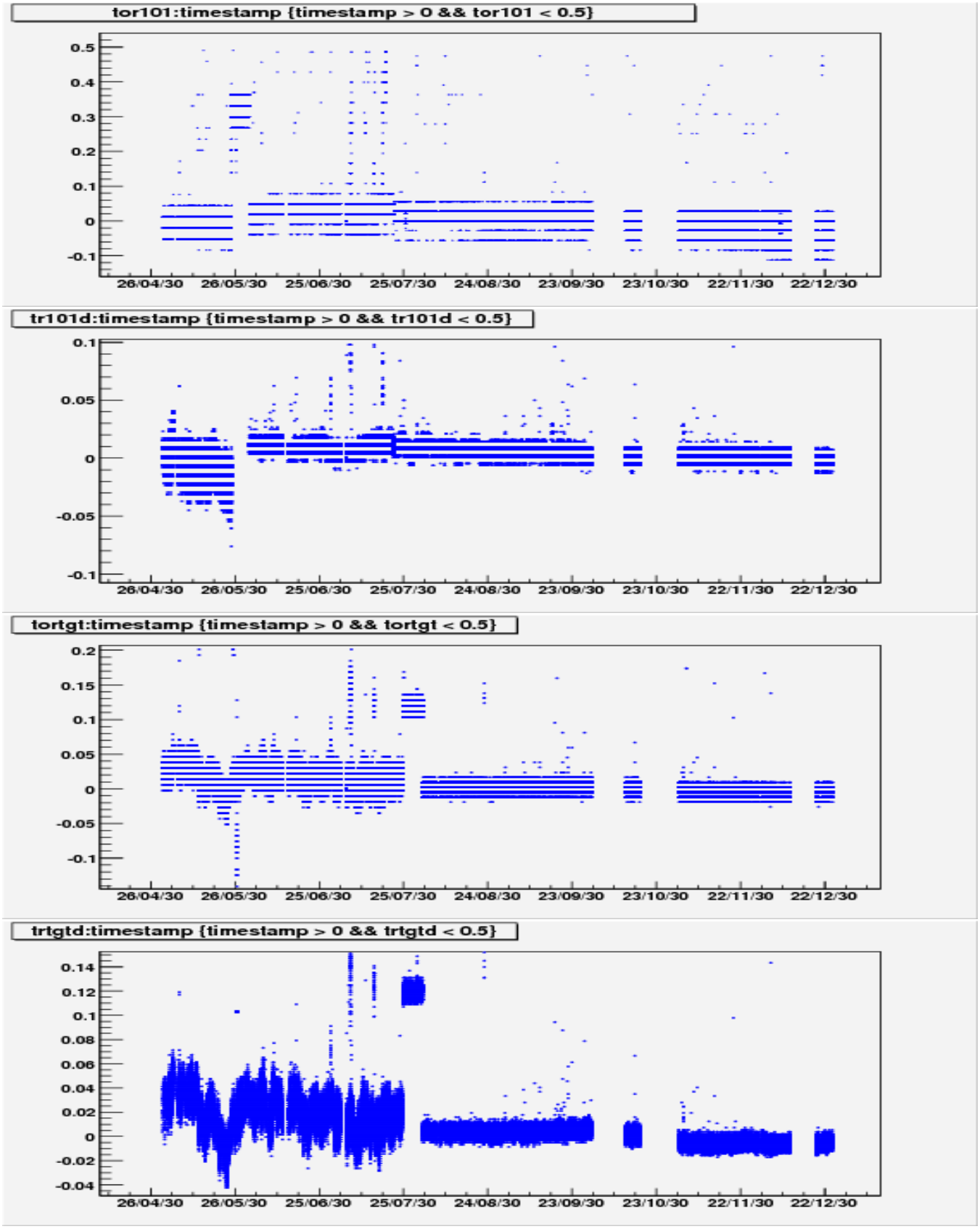

Figure 11: TOR101,TR101D, TORTGT and TRTGTD pedestals vs time.

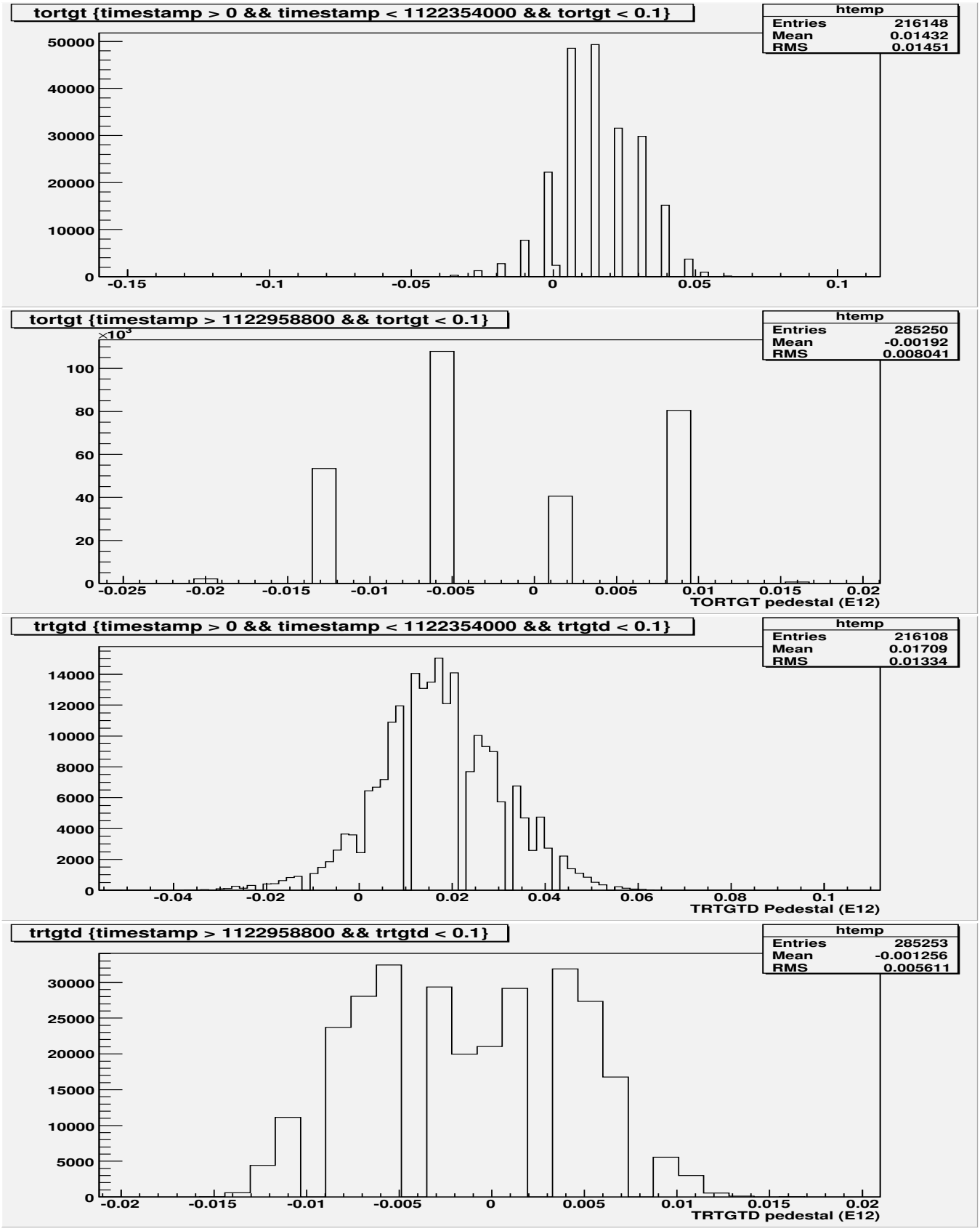

Figure 12: TORTGT and TRTGTD pedestals before and after the gate change on July 26th, 2005.

3.4 Comparison of NuMI toroids and MI DCCT

The beam intensity in the Main Injector before extraction to the NuMI beamline is measured by a DC current transformer (DCCT). To estimate the extraction efficiency from Main Injector to the NuMI beamline the readout from the NuMI toroids is compared to the DCCT readout. For the data from Feb - Mar 22 the comparison with TOR101 and TORTGT is shown in Figures 13 and 14. We find that the relative response is linear from 5 to 20E12, but the NuMI toroids were consistently reading out 4-5% higher than DCCT during this time period. In addition, below 5E12 the relative response of TORTGT as compared to DCCT shows a non-linear response that varies by about 2%.

In table 2 the average value of the ratio of the NuMI toroids to DCCT for various time periods from March to Dec, 2005 is listed. Prior to July 18, the comparison with DCCT shows varying differences. We find that after the gate width change and calibrations or TOR101 and TORTGT on July 18 and 25th, 2005, agreement with DCCT and relative agreement of TOR101 and TORTGT is good to < 1 % and stable to 0.4%. The performance of TOR101 and TORTGT as compared with DCCT for the 13.1 μ second gate widths is shown in Figures 15 and 16 for data collected Nov 1st, 2005 through Jan 31st, 2006. Given that the relative measurement of the toroid values as compared to DCCT stabilized after the recalibration and the reduction of the gate widths, we estimate that an additional corrction of -4% is to be applied to the toroid readout prior to July 18 for TOR101 and July 25 for TORTGT. The uncertainty on this correction is estimated to be 3% to account for the variations observed in March and May of 2005.

Table 2: NuMI Toroid readout as compared with Main Injector DCCT sampled on different dates throught 2005.TOR101 calibrations where changed on July 19 and TORTGT calibrations where changed on July 25.*The distribution is not Gaussian but has two peaks.

Date	TR101D/DCCT	TRTGTD/DCCT	TRTGTD/TR101D
Feb 27	1.06	1.023	0.965
Mar 7	1.081*		0.989
Feb 18 to Mar 22	1.0525	1.0424	0.990
Mar 22			0.990
May 5th	1.017	1.012	0.994
May 22	1.012	1.005	0.993
May 30	1.037	1.040	1.004
July 19	1.035	1.036	1.002
July 20	0.994	1.037	1.043
July 25	0.994	0.991	0.997
Sept 26	0.995	0.993	0.997
Nov 1	0.997	0.995	0.997
Nov 12	0.997	0.995	0.998
Nov 28	0.997	0.993	0.997
Dec (?)	0.995	0.993	0.997

We have also considered the difference in the readout from TOR101 as compared to TORTGT - which is the transport efficiency down the the NuMI beamline. In principal, the losses in the NuMI beamline are negligible and any difference observed in the readout of the two NuMI toroids is attributed to uncertainties on the relative calibration. From the study shown in Figure 17 we see that the relative calibration of TR101D to TRTGTD changed during the period March 1st through July 6, 2005. The overall variation is within 1% and is taken as an additional systematic

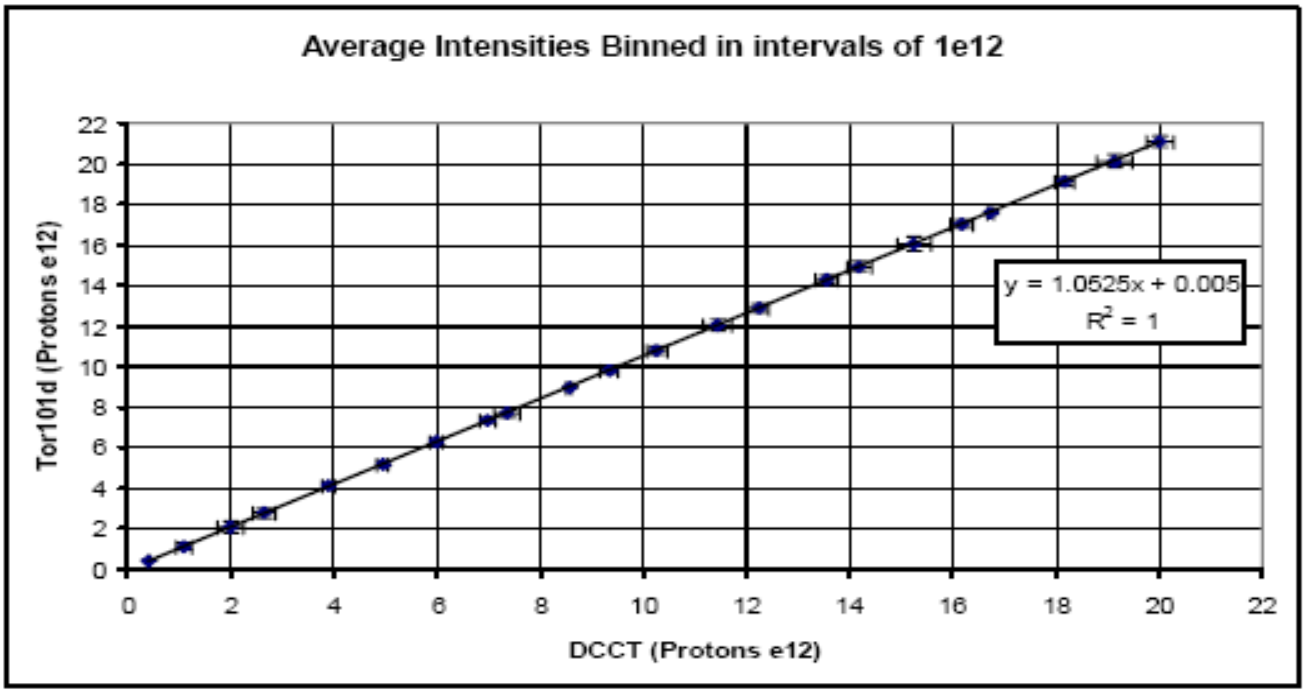

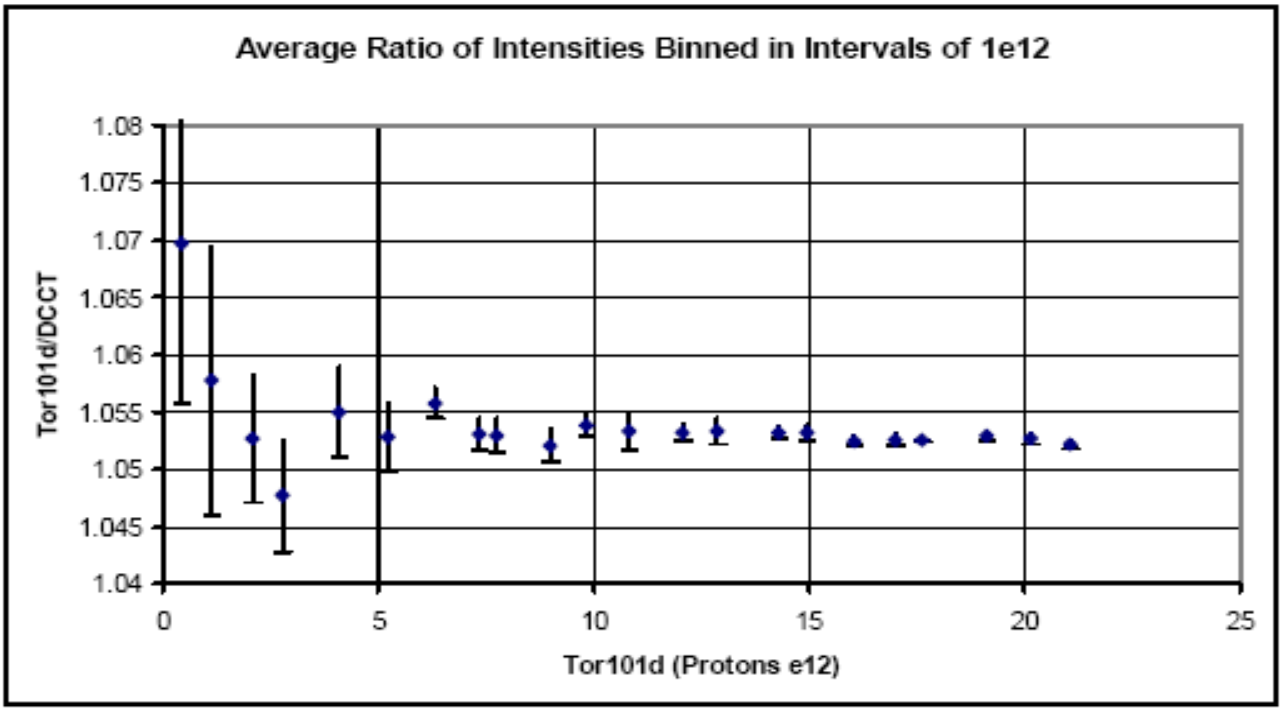

Figure 13: TR101D vs DCCT [3]. Feb 18 to Mar 22, 2005

uncertainty. A comparison of the relative readout from TRTGTD and TR101D after the gate change and calibrations in July 18 (TOR101) and July 25 (TORTGT) is shown in Figure 18. We find that the fractional difference between the toroids after recalibration is 0.2% and the relative calibration of the two toroids is very stable. The relative response as a function of intensity has several features in it but the RMS of the distribution, if taken as a measure of the overall sensitivity of the D devices, indicates that the average measured sensitivity of the devices is $\approx 0.06\%$.

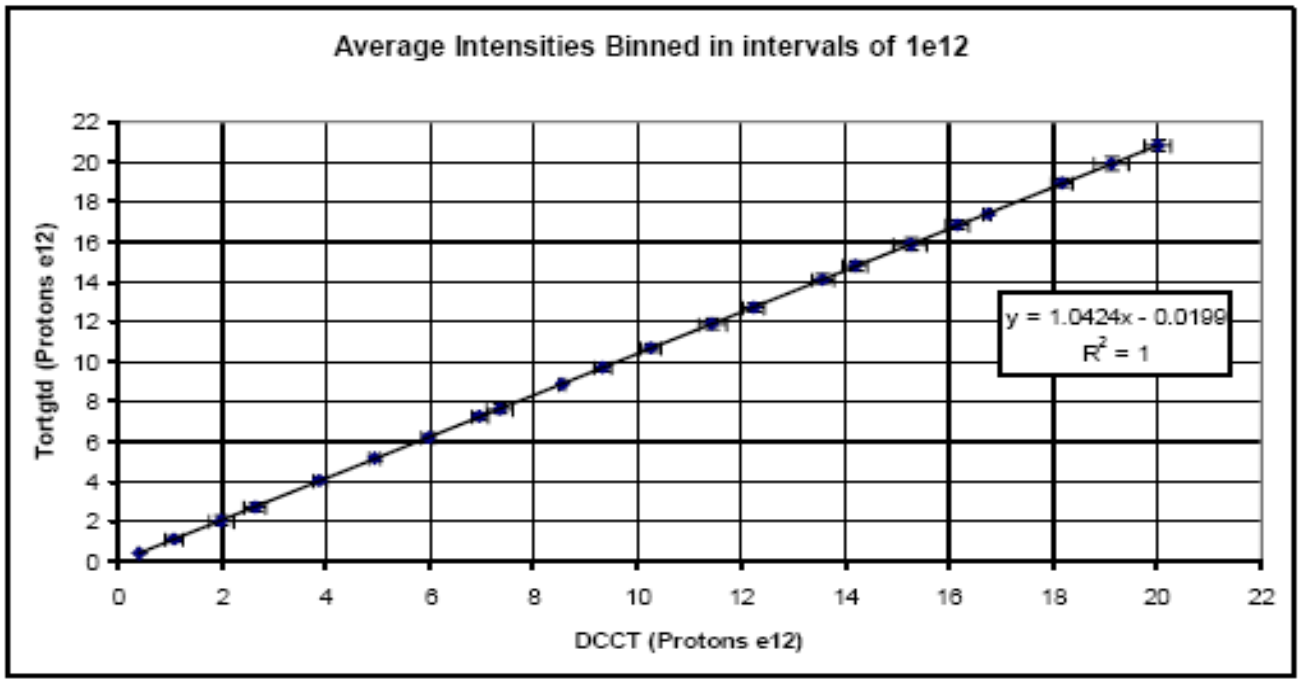

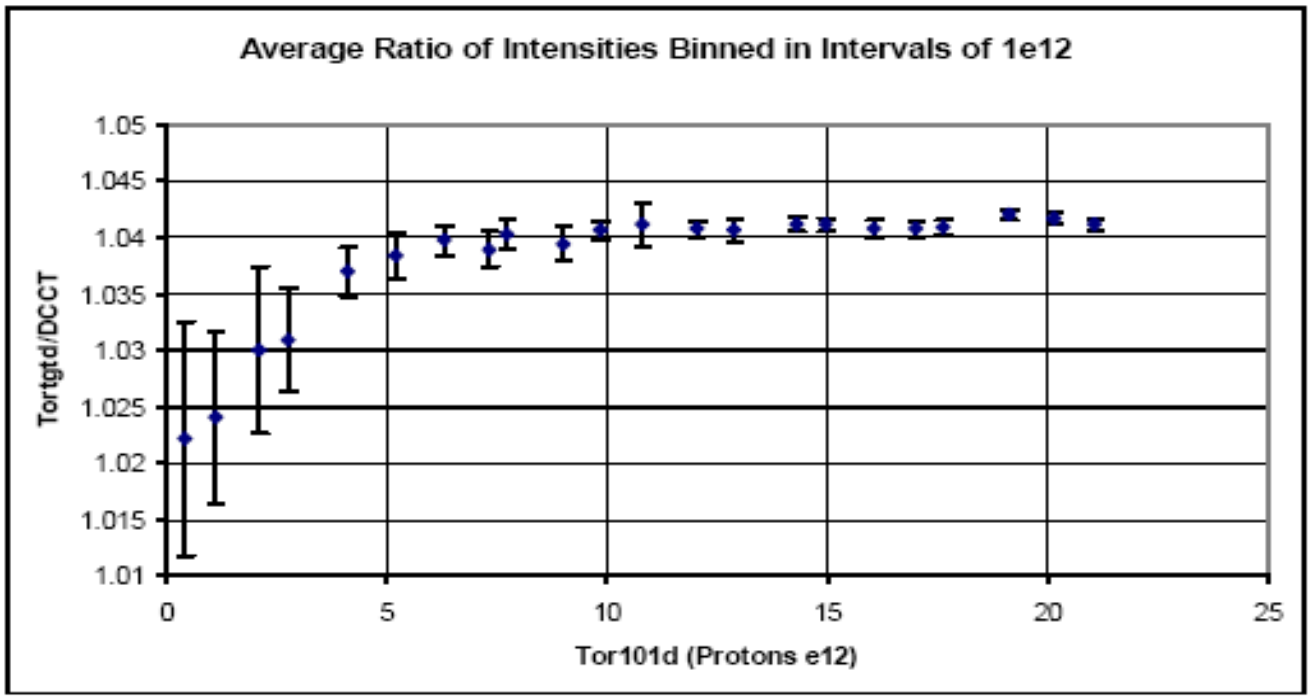

Figure 14: TRTGTD vs DCCT [3]. Feb 18 to Mar 22, 2005

3.5 Toroid measurement stability

From the previous comparison of the toroid values as compared to DCCT, we conclude that after the gate width change to 13.1μ seconds, the overall relative stability of the toroid measurement from July to Dec,2005 is of the order $\pm 0.2\%$. We have observed a dependance of the toroid readout on the Main Injector cycle used for NuMI. The data shown in Figure 19 plots the difference in the

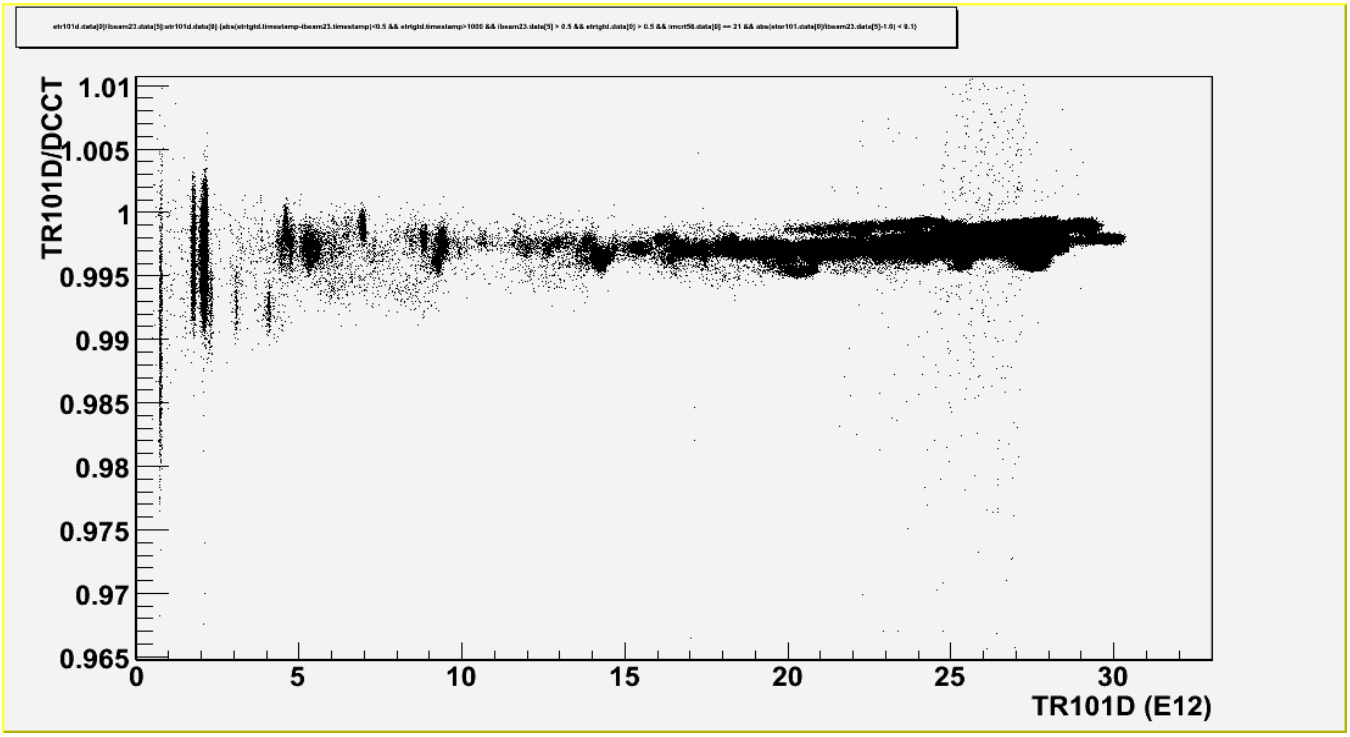

Figure 15: TR101D vs DCCT. November, 2005 to January, 2006

ratio of TR101D/TRTGTD during a period of time where NuMI mixed-mode (1st MI batch is used for pbar production) and NuMI only mode where interleaved. The difference in the relative readout of the two toroids is of the order 0.1%. We do not currently know the reason for this discrepancy.

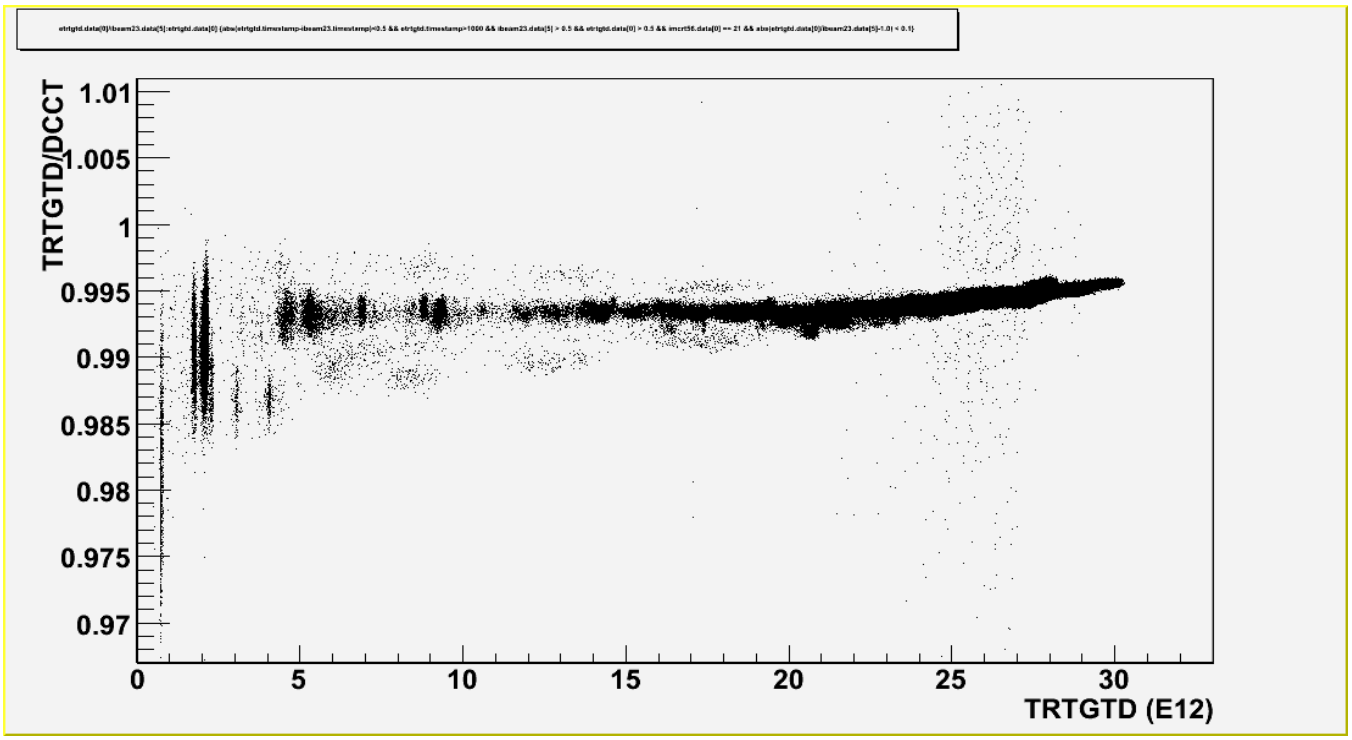

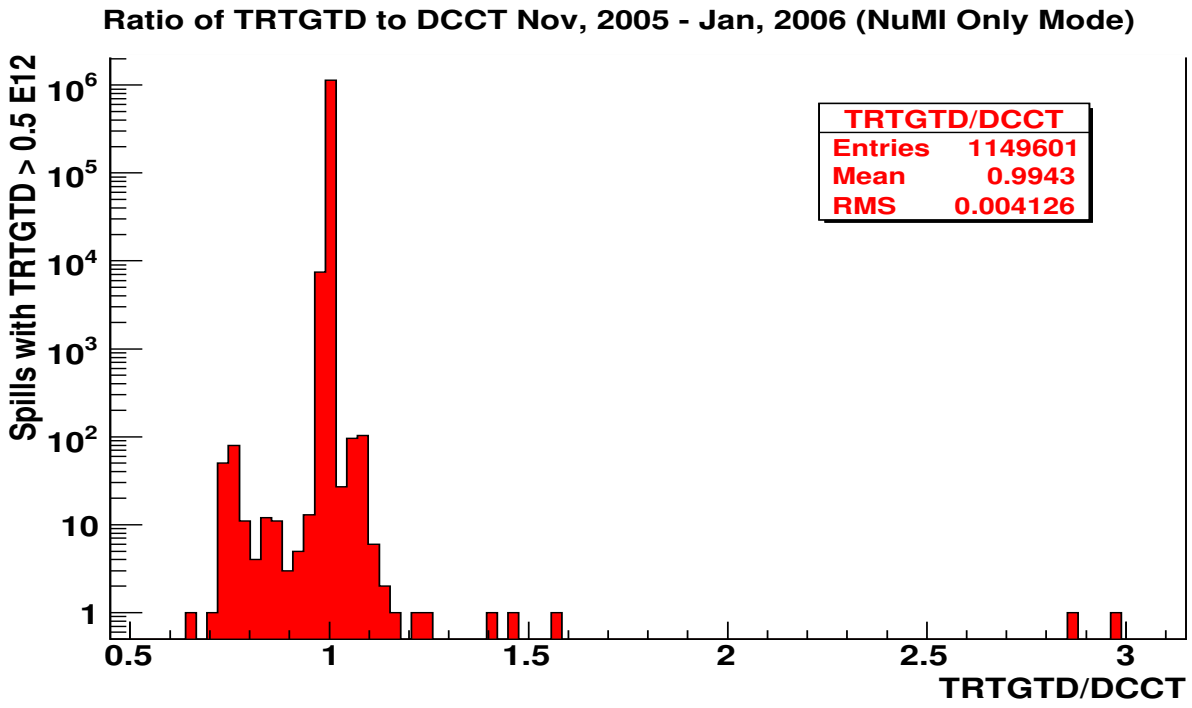

Figure 16: TRTGTD vs DCCT. November, 2005 to January, 2006

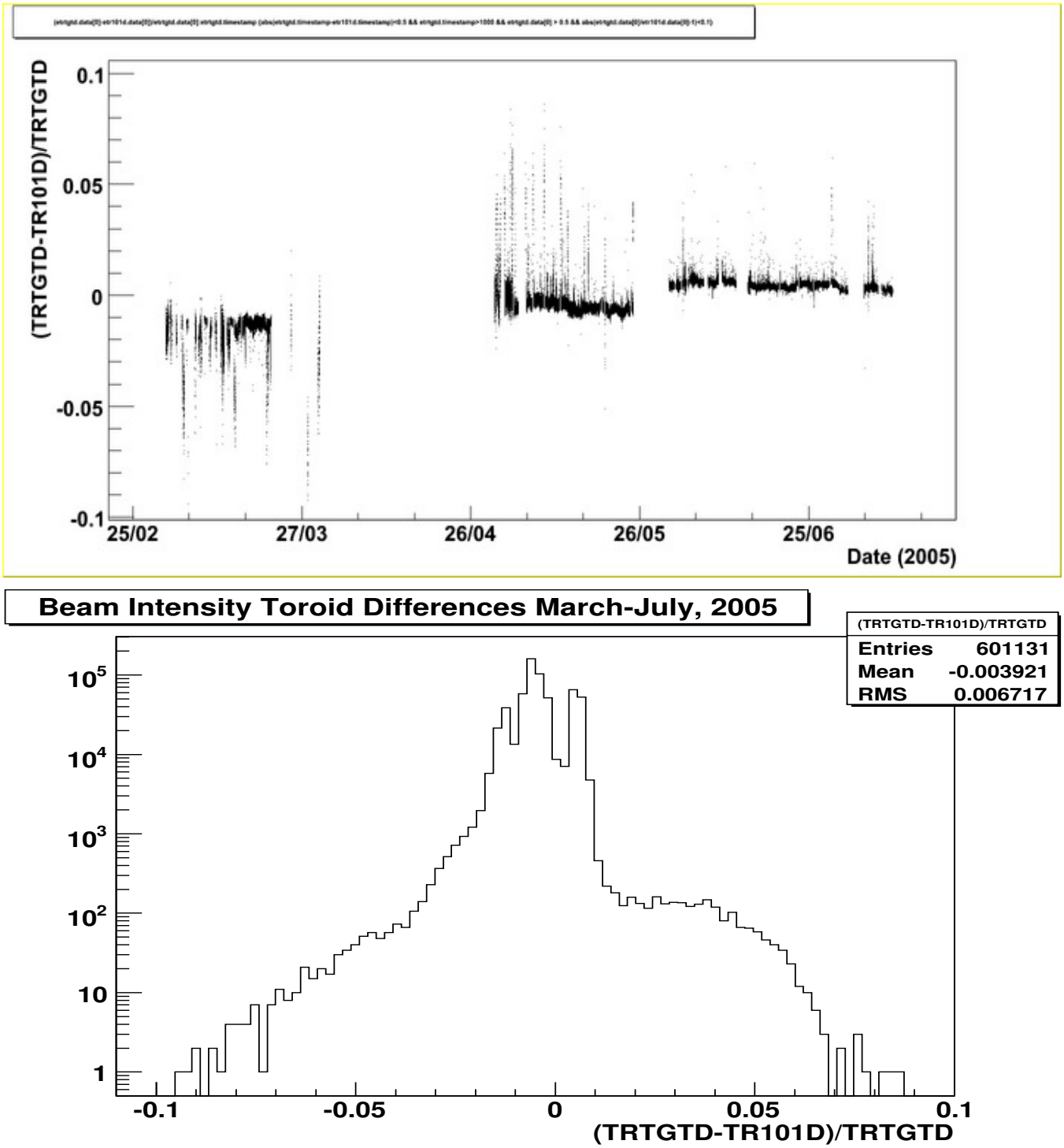

Figure 17: Comparison between the intensity measurements of TRTGTD and TR101D for data taken from Mar 1st, 2005 - Jul 6,2005 using only the calibrations applied by ACNET system.

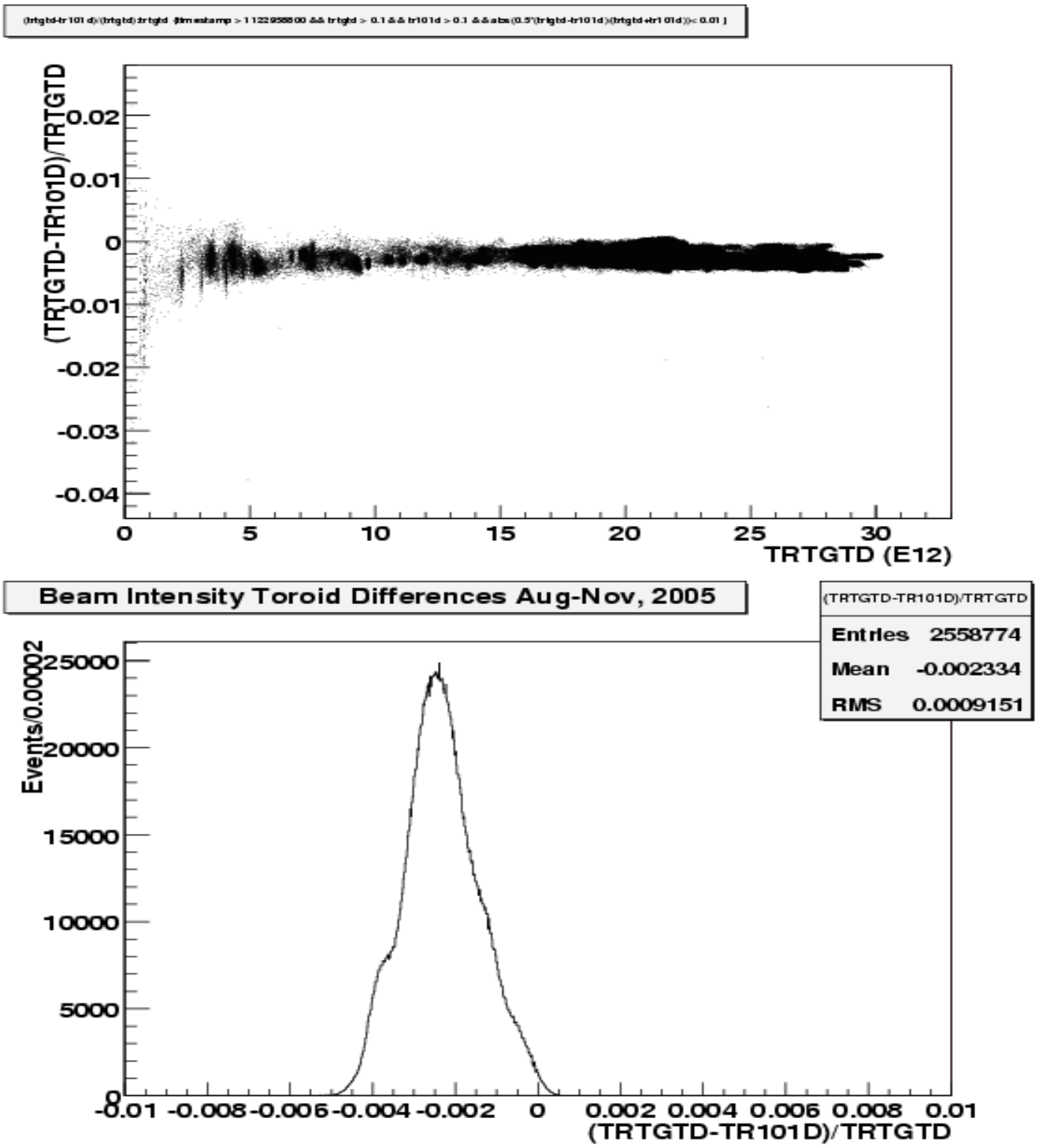

Figure 18: Comparison between the intensity measurements of TRTGTD and TR101D for data taken from Aug 2nd, 2005 - Nov 31,2005 using only the calibrations applied by ACNET system. The top figure shows the linearity of the response as a function of total beam intensity. The figure at the bottom shows the fractional difference in the measurements between TRTGTD and TR101D. Assuming both toroids have the same sensitivity the RMS of the plot $\approx \sqrt{2}\delta_{toroid}/intensity \Rightarrow$ sensitivity of the D devices is 0.06%

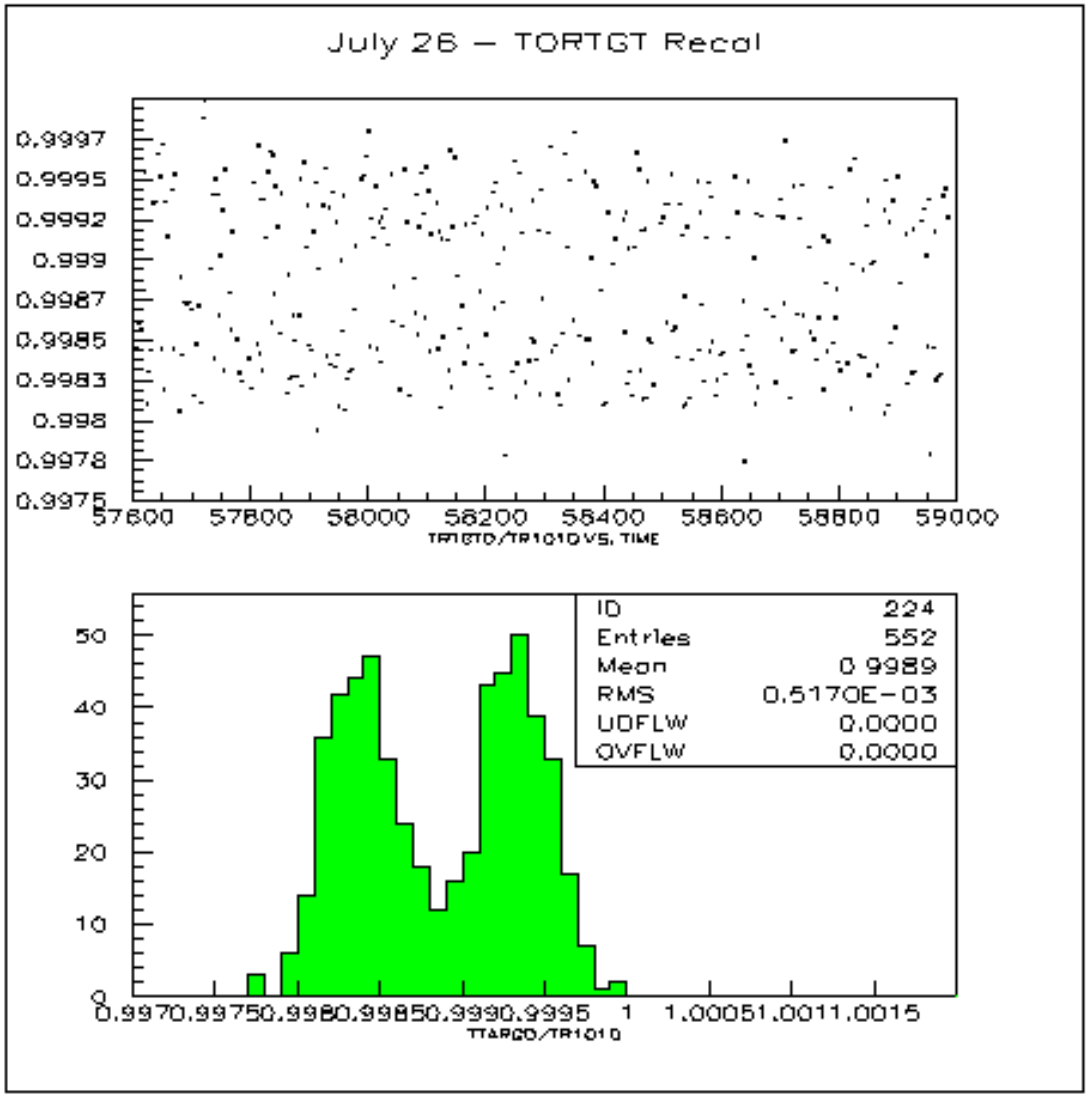

Figure 19: Variations in the beam intensity measurements as a function of MI cycle. The ratio of TRTGTD to TR101D is shown here for a period of time when the MI was running interleaved NuMI only and NuMI mixed-mode cycles.

3.6 SUMMARY

The list of systematic uncertainties on the absolute beam intensity measurements from the NuMI toroids is summarized in Table 3

Table 3: Uncertainties on the absolute beam intensity measurements. *This correction is applied offline and so is not included in the overall estimate of the uncertainties.

Description	99.9 μ sec. gate	13.1 μ sec. gate
Absolute calibration with a current source	$< 0.5\%$ for > 1 E12	$< 0.5\%$ for > 1 E12
Calibration w.r.t. DCCT	$\sim -4\%$*	-0.6%
TOR101 vs TORTGT difference	1%	0.2%
Stability (compared to DCCT)	3%	0.4%
Sensitivity (D devices)		0.06 %
Charge leakage	1%	0.5%
Pedestals	< 0.09 E12	~ -0.0016 E12 (TORTGT)
Noise	< 0.02 E12	~ 0.008 E12 (TORTGT)
Total	$\approx 3.4\%$	$\approx 1\%$

4 Logging the proton intensity data

There are several dataloggers that record the ACNET data from the NuMI toroids as well as most of the NuMI beamline ACNET instruments. It should be noted that all known dataloggers are logging the same data from the ACNET front end readouts. They main differences between different loggers are 1) The path the data takes to disk and 2) when the data is polled from the front end. In addition, the Near Detector GPS timing system also records the GPS times of all MIBS \$74 signals issued by the accelerator. This system is completely independent of the ACNET DAQ systems and records only the GPS times of the physical MIBS \$74 signal sent to the ND DAQ.

In this section we will discuss the relative performance of two ACNET datalogging processes:

1. The Accelerator Division Dataloggers: there are two of these as discussed below.
2. The MINOS datastream Beam Data Process (BDP): this process obtains ACNET information via an XML-RPC server operated by the controls division using a dedicated Data Acquisition Engine to interfact to the ACNET front ends.

For the POT counting it is important to understand how data from the toroids is acquired by the ACNET system: TOR101/TORTGT is set on \$74+19.967 MRev + 16 microseconds for electronics (after July 12). A \$74, which is an MIBS event, occurs at \$A5+1.240052 seconds, where \$A5 is the MI extracted beam reset. So the toroid is sampled at \$A5+1.24029 seconds. The sample is cleared on a \$25, start ramp flattop, which occurs at \$A5+1 second.

4.1 Accelerator Division Dataloggers

There are two AD dataloggers: the "Clock Logger" and the "NuMI logger". The Clock logger records E:TOR101 at \$A5+1.4 seconds. The NuMI logger records E:TOR101 at \$A5+1.5 seconds. The sample and hold is cleared 0.25 seconds before it is sampled again and the loggers wait 0.15 sec and 0.25 sec later to record the data. A comparison between the POTs from TRTGTD logged

by both loggers during November, 2005 is shown in Figure 20. The NuMI logger is heavily loaded while the clock data logger has a lighter load. Differences on the order of 0.2% are observed with the NuMI data logger consistently logging fewer POTs than the clock logger.

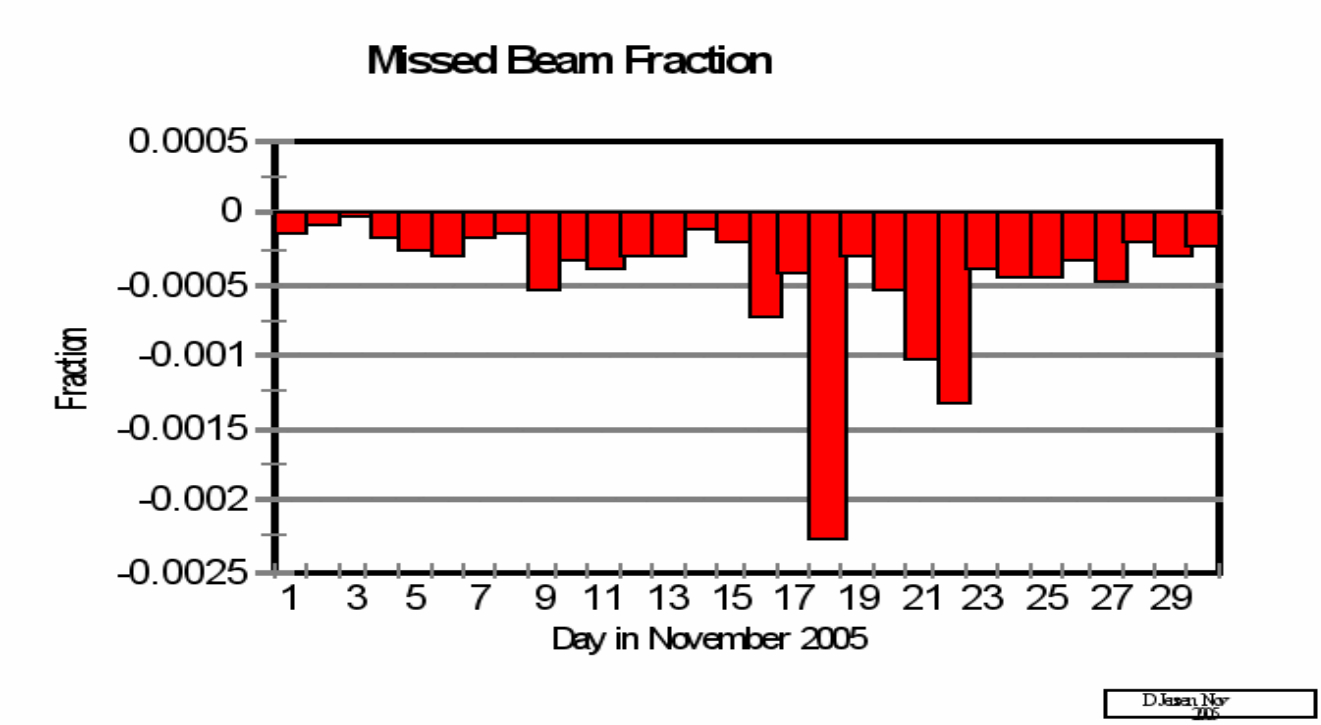

Figure 20: Fractional difference between POT from TRTGTD logged by the NuMI and Clock data loggers. Fraction = (NuMI-Clock)/Clock.

4.2 MINOS Beam Data Process Logger

A detailed description of the MINOS Beam Data Process (BDP) that logs the beam data in the MINOS datastream can be found in [4]. A brief description follows:

Figure 21 illustrates the path data from the ACNET front ends takes to reach the BDP MINOS data stream. A dedicated Data Acquisition Engine (DAE) [5] from the Accelerator Division's controls department polls the data from the NuMI ACNET front ends, after a programmed delay time, upon recieving notification that an "A9" clock event has occured. A "CLOCK" process listens to a 15hz TCP/IP telecast of the various clock process from a Universal Clock Decoder front end which decodes TCLK signals. Its the "CLOCK" process that informs the MINOS DAE when a particular clock signal has occured. The DAE then broadcasts the data using an XML-RPC server process. Any XML-RPC client from anywhere inside or outside Fermilab can recieve that data. The Beam Data Process is an XML-RPC client that requests and recieves data from the DAE and sends it to a ROTOROOTER process to be encoded in the ROOT based MINOS data format. Data is then written to disk on a dedicated computer in the MINOS control room. The raw MINOS beam files are closed every 8 hours at which time a process is initiated which reads in the beam data from the most recent closed file and fills the BEAMMONSPILL database table with a summary of the spill information. Offline MINOS reconstruction queries BEAMMONSPILL and fills the same information into an NtpBDLite ROOT TTree which is written out in the same file as the near and far detector data ntuples.

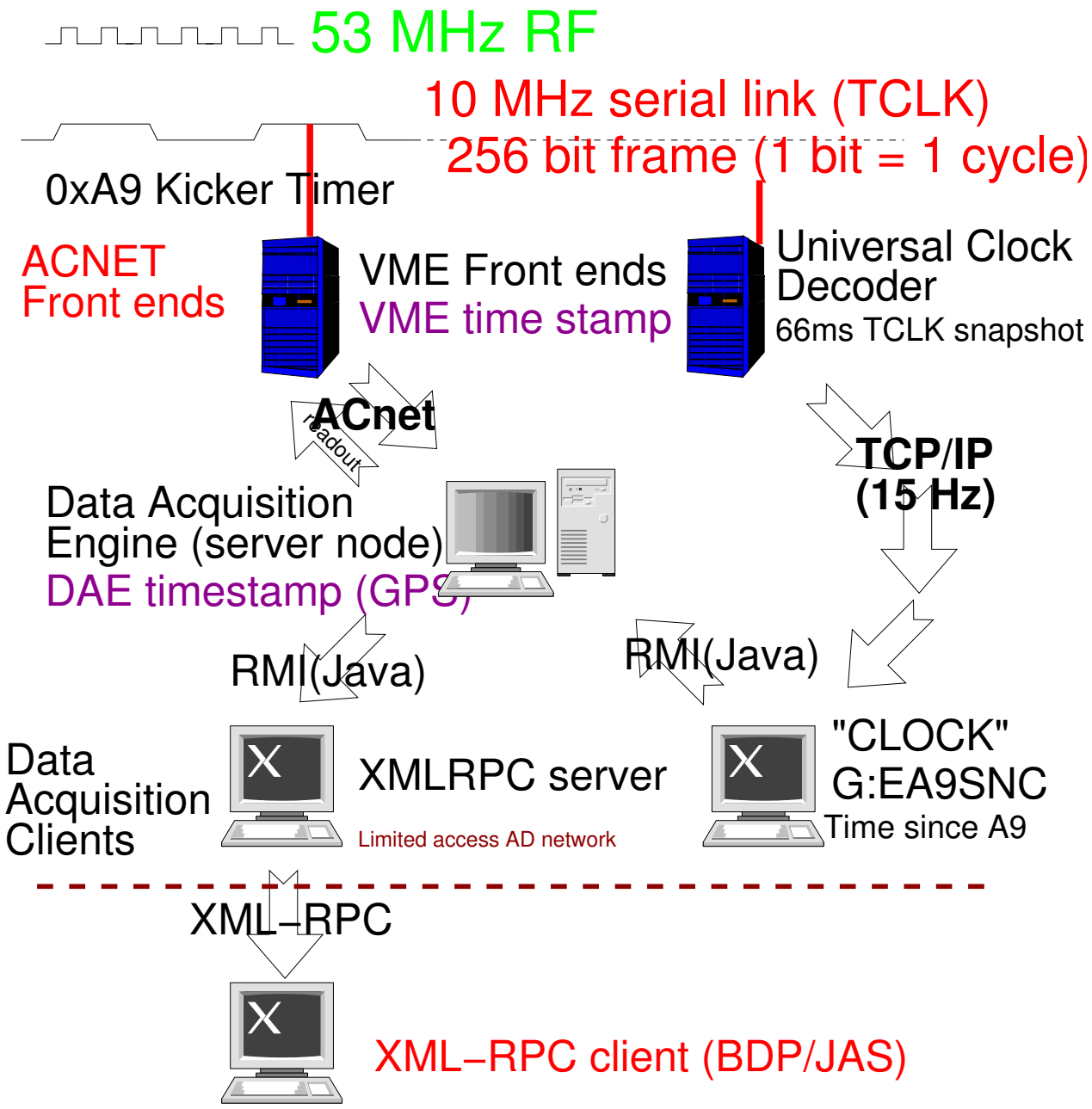

Figure 21: Illustration of the data path from the ACNET front ends to the MINOS beam data process and JAS.

For the period from May 4 - Dec, 2005, the MINOS BDP requests data from all NuMI devices to be logged at 0.5 seconds after the $A9 signal which occurs xxx seconds after the $A5. Since there is some delay time between when the $A9 occurs and when the DAE recieves the trigger from the CLOCK process over a 15 Hz TCPIP connection, the toroid readout recieved by the MINOS datastream is usually sampled sometime >$A5+1.5 seconds.

We have compared identical spills from the MINOS datastream and the NuMI datalogger. A sample of the TORTGT readings in the BDP and NuMI datalogger for identical spills is listed in Table 4. We find that the TORTGT values from identical spills recorded by the two different loggers

Table 4: A sample of identical spill intensities as recorded in the NuMI Datalogger (DL) and the MINOS datastream (BDP). The difference is BDP-DL.

BDP Timestamp	DL TORTGT	BDP TORTGT	Difference
1123036711	19.60540	19.6054	0.0
1123036713	20.20616	20.19185	-0.01431
1123036715	20.68534	20.67818	-0.00716
1123036717	21.00002	20.99286	-0.00716
1123036727	18.96889	18.96889	0.0
1123036729	20.75685	20.75685	0.0
1123036731	20.72109	20.7139	0.0
1123036733	9.263910E-3	9.263910E-3	0.0
1123036743	9.263910E-3	9.263910E-3	0.0
1123036745	9.263910E-3	9.263910E-3	0.0
1123036747	-5.03984E-3	-5.03984E-3	0.0
1123036749	20.56375	20.56375	0.0
1123036758	19.66262	19.66262	0.0
1123036760	20.64242	20.63527	-0.00715
1123036762	21.13590	21.14305	-0.00715

can differ by 0.00715 - 0.0143 E12 with the numbers in the MINOS datastream being consistantly lower. The quantization of the differences is a multiple of 0.00715E12 which is consistent with the ADC resolution for this device of $\approx$ 0.0064 E12. Based on this analysis, for a typical spill intensity of 25E12 the differences between the data logged in the MINOS data stream and the dataloggers is not expected to exceed 0.06%.

4.2.1 BDP efficiency and uncertainties

To estimate the BDP MINOS data logging efficiency we have two options with which we can compare performance:

1. The ND GPS system which records the GPS time of each MIBS $74 signal recieved. This is the closest system we have to a hardware spill counter. The ND GPS processes that log the MIBS $74 time are not tied to the ND DAQ run state. On the other hand, the processes can be shut down, crash, or the TPC can be powered down, all of which will kill the ND GPS logger. These are all unusual, but it does happen occassionally. Also, data transfer to the database-maker can get shut down, which will delay the database table creation. Although not a 100% efficient, we expect this system to have the highest efficiency of counting spills.

2. The Accelerator Division Dataloggers. The efficiency of these loggers is as yet unknown.

The following is a list of all the currently known BDP failures/inefficiencies affecting the period May-Dec, 2005:

- After long periods of downtime, the rotorooter process shuts down for as yet unknown reasons. This affects both the BDP process and the backup process. We lost data on the following dates due to this failure mode: May 15, May 31st, June 1st, June 13-14, July 5th ,2005.

- Network failures and/or rebooting of the computer on which the BDP process was running. At least one such failure occured on August 1st but the data was recovered from the backup BDP process which did not crash.

- Two or more callbacks were initiated at the same time from the BDP xmlrpc client to the server. This caused duplicate spills and data from different spills to be mangled together. This affected data in the period Oct 18-31st and Nov 3rd and 4th, 2005. The feature of the BDP process control GUI that allows mutiple identical callbacks has been disabled. Most of the data has been recovered offline.

- The process that fills the DB with spill information after the BDP raw root file is closed every 8 hours encountered a failure mode where it was being restarted every 5 minutes. This caused a large CPU and I/O load on minos-beamdata and interfered with the performance of the BDP logger. This affected data logging efficiency on Nov 9-10, 2005.

First, we compared the BDP process performance by counting the number of spills recorded by the BDP process which were in the BEAMMONSPILL database table with the number of spills recorded in the SPILLTIMEND table. We believe this is the best measure of the BDP process logging efficiency. The results for each month are list in Table 5. We find that the total number of spills recorded by the beam data process from Feb - Dec 11th, 2005 is 98.2% of the number of MIBS \$74 signals detected by the ND GPS system. We note that in July, 2005 the BDP process actually logged more spills than the ND GPS system. This has been attributed to problems with the GPS computer sometime in July. We counted the number of the BDP spills where TORTGT failed to readback properly (flagged by a DAE timestamp of 0) and found that for this time period only 0.1% of spills recorded by the BDP had no valid TORTGT readout. To be able to ascertain the quality of a given spill the minimum information needed is:

1. The number of POT in this spill.

2. The horizontal and vertical batch position projected at the target center

3. The beam profile measured at the profile monitor in the pretarget region.

4. The horn current readout.

The minimum set of ACNET devices needed to determine the above spill conditions is : TORTGT, HP121, VP121, HPTGT, VPTGT, MTGT and NSLINA-D. This set is hereby referred to as "critical devices". The number of spills where all critical devices read back successifully is noted in Table 5. In general $> 99\%$ of spills recorded by the BDP have valid data in the critical device set. The notable exceptions are data prior to May 4th, 2005 when the BDP was requesting readback on the beam position monitors after the reset signal and August 16-18,29 2005 when the VME sequencer for the profile monitor MTGT failed.

Table 5: Beam data process spill logging efficiency measured w.r.t to SPILLTIMEND in 2005. Good readout refers to total number of spills where the following critical ACNET devices all readout properly: TORTGT, HP121,VP121, HPTGT, VPTGT, MTGT,NSLIN*. These are the minimum set of devices needed to determine the spill quality.

Month	SPILLTIMEND	BEAMMONSPILL	Good readout	BDP eff.	ACNET +BDP eff.
February,2005	5440	5201		95.6 %	
March	113285	100878	67821	89 %	60%
May	610381	604838	592897	99.1 %	97.1 %
June	699687	666471	662447	95.3 %	94.7 %
July	764926	765096	761825	100.0%	99.6 %
August	900635	899091	857593	99.8 %	95.2 %
Sept	931116	923427	921773	99.2 %	99.0 %
Oct	515528	502413		97.5 %	
Nov	889945	861680		96.8 %	
Dec	673535	671907	665821	99.8 %	98.9%
Jan, 2006	982163	977416	974927	99.5 %	99.3%
Feb	706536	702743	678011	99.5 %	96.0%
Total	7793180	7681160		98.6 %	

From the analysis of the BDP spill logging efficiency as compared to the ND GPS timing system we find that >98% of spills have been logged by the BDP with valid TORTGT readout. In principal, this should approximatly correspond to the total number of POT recorded by the BDP as compared to the total delivered. As a useful cross-check we also compared the number of POT recorded by the BDP process to that recorded in the NuMI dataloggers. As mentioned previously, we do not actually know what the logging efficiency of the AD dataloggers is. The daily POT recorded by TORTGT from 00:00:00 CDT to 00:00:00 CDT by both the BDP process and the NuMI datalogger for the period May 1st - Dec 10th, 2005 are shown in Figures 22 to 26. A correction of 0.874 is applied to the BDP TORTGT values for spills taken from July 26 2:17:41 UTC to August 1st 22:43:23 UTC. This is to correct for the fact that the TORTGT ACNET calibration changed on July 26th and the new calibration values where not picked up by the BDP process until August 1st. The monthly totals are listed in Table 6 As noted earlier, known problems with the operation of the BDP process occured on the following dates: May 15, May 31st, June 1st, June 13-14, July 5th. Oct 18-31, Nov 3-4 and Nov 9-10,2005.

Table 6: Summary of raw number of POTs logged by the NuMI ACNET dataloggers and MINOS beam data stream from Dec 3rd, 2004 through Dec 10th, 2005. The POT numbers are from TORTGT with no calibration corrections applied.

Month	DL POT	BDP POT	Difference
Dec-April	8.714 E17	0.342 (feb) 7.04 (March) +0.097(april)	-14%
May	68.1 E17	67.4 E17	-1%
June	107.9E17	103.7 E17	-4%
July	129.4E17	130.9 E17	+1%
August	170.6 E17	170.5 E17	-0.06%
Sept	193.6 E17	192.1 E17	-0.8%
Oct	103.4 E17	101.4 E17	-1.9%
Nov	190.5 E17	185.6 E17	-2.6%
Dec	147.7 E17	147.3 E17	-0.3%
Jan, 2006	198.4 E17	197.5 E17	-0.5%
Feb	96.7 E17	96.7 E17	-0%
Total	1.415 E20	1.401 E20	-1.0%

A Gaussian fit to the difference of BDP and NuMI Dataloggers daily POT from a 156 running days (May, June, July, August, Sep, Nov, Dec 1-10) is shown in Figure 27. We find that the mean difference is 0.03% with a standard deviation of 0.09%.

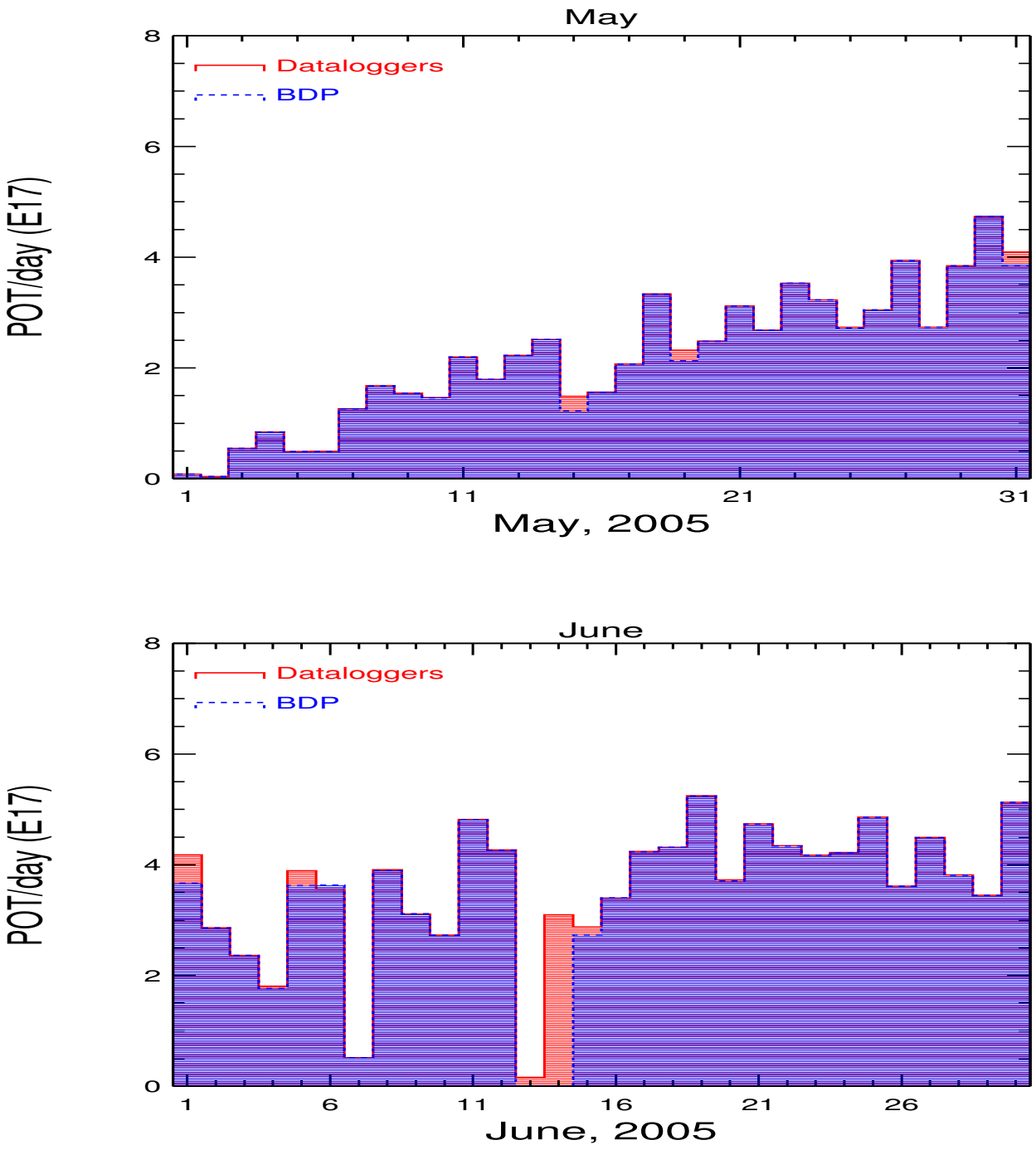

Figure 22: Comparison of POT logged by BDP and NuMI Dataloggers for May, June 2005

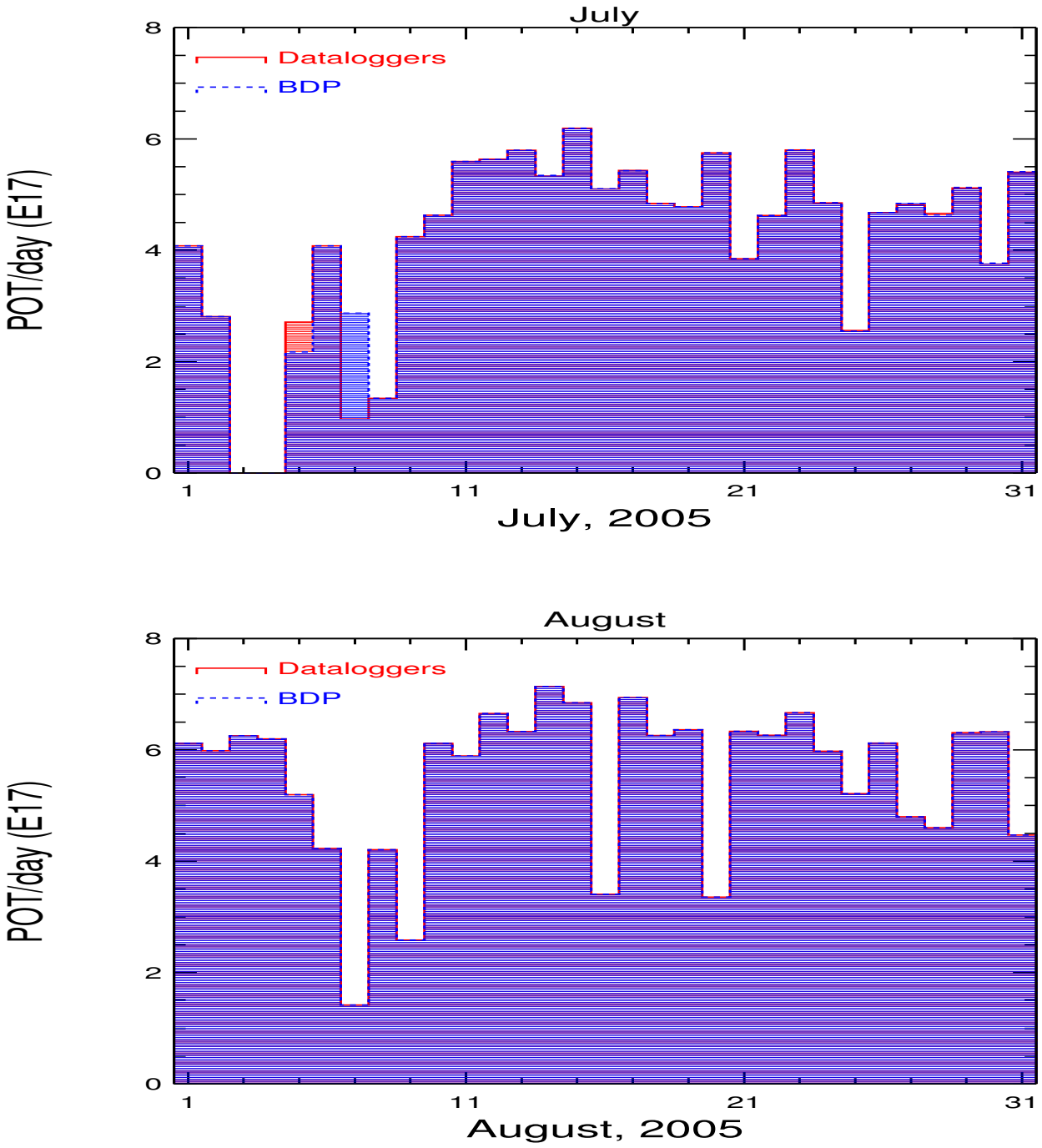

Figure 23: Comparison of POT logged by BDP and NuMI Dataloggers for July,Aug 2005

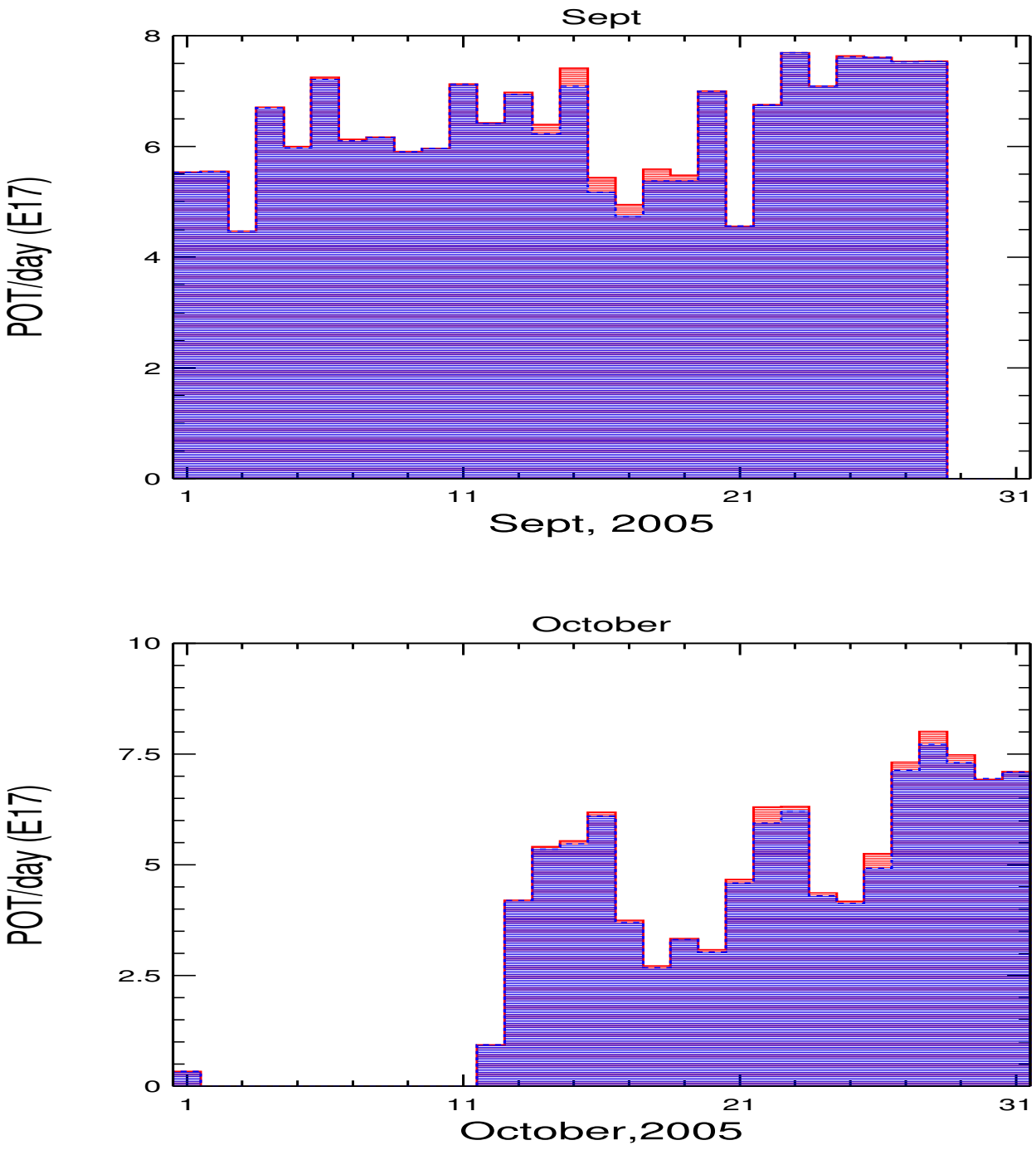

Figure 24: Comparison of POT logged by BDP and NuMI Dataloggers for Sept,Oct 2005

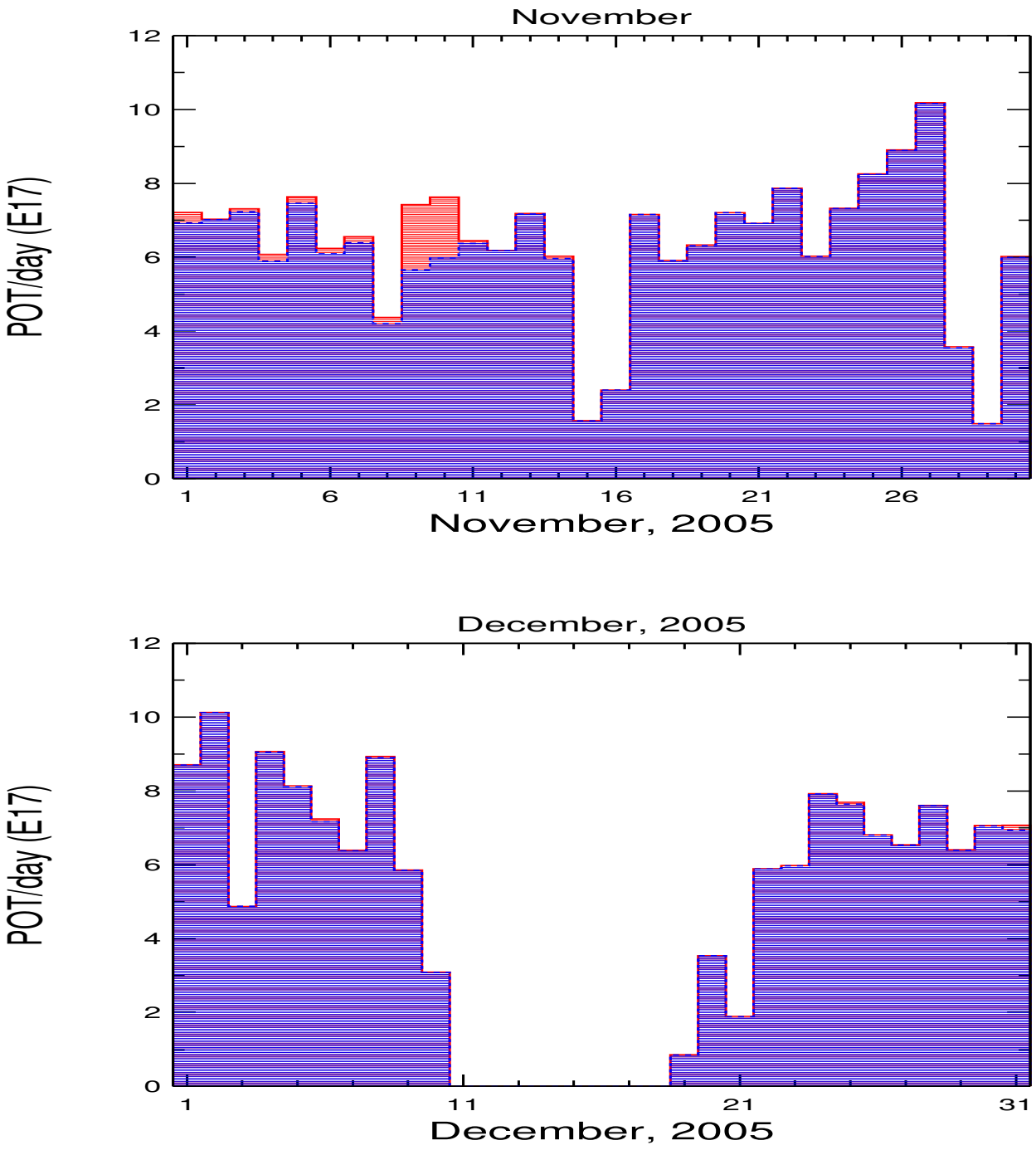

Figure 25: Comparison of POT logged by BDP and NuMI Dataloggers for Nov,Dec 2005

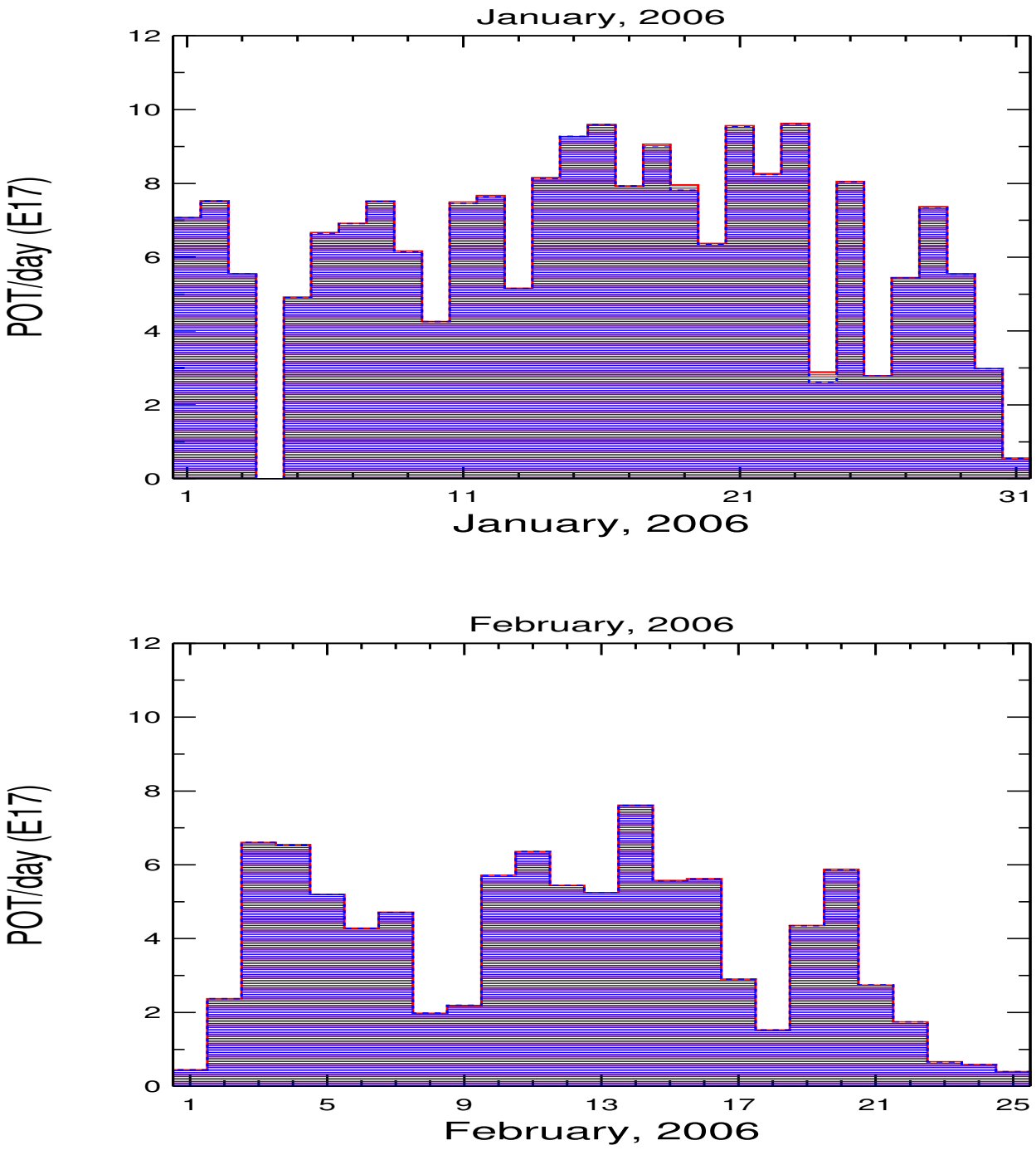

Figure 26: Comparison of POT logged by BDP and NuMI Dataloggers for Jan,Feb 2006

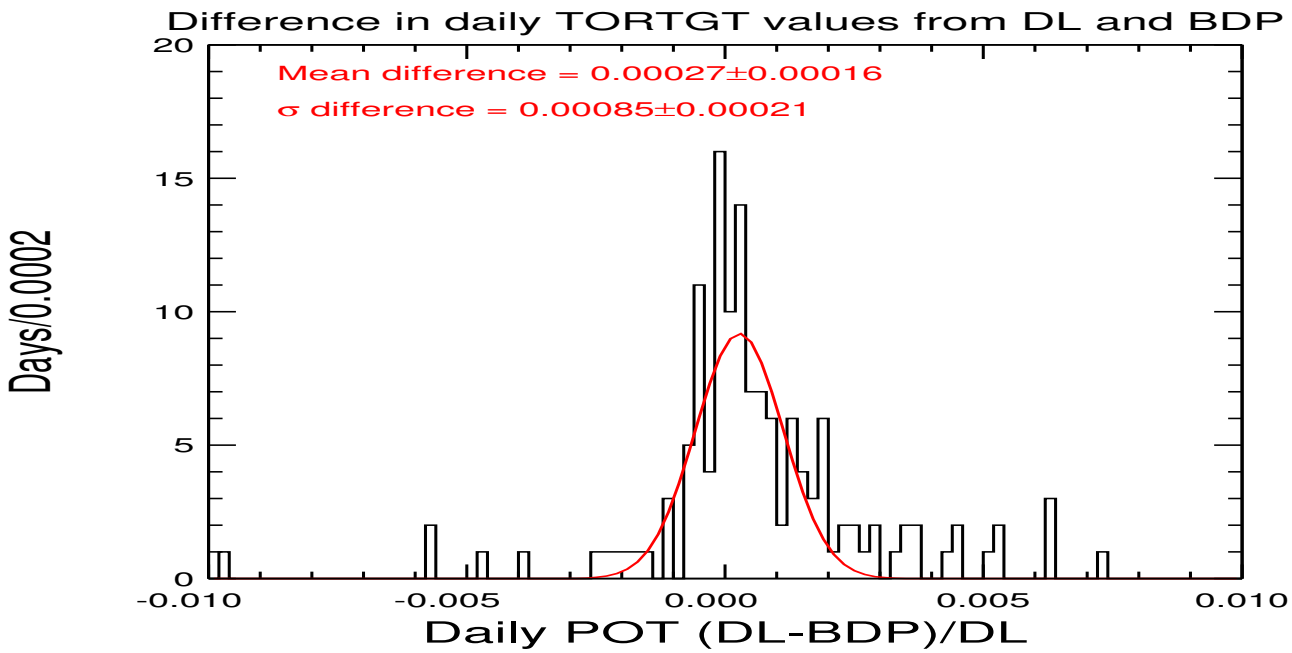

Figure 27: The distribution of the fractional difference in POT logged by the NuMI dataloggers (DL) and the BDP for 156 running days from May, June, July, August, Sept, Nov, Dec 1-10th, 2005. The red curve is from a Gaussian fit to the distribution.

4.2.2 Matching BDP spills with Near and Far Detectors

For ND and FD analysis on MINOS, we need to be able to query beam conditions and measure POT on a spill-by-spill basis. This neccesitates the ability to match ND and FD snarls with beam spills. There are two sources of GPS timestamps available from the NuMI ACNET devices with which we can match ND and FD snarl times:

1. The DAE timestamp: The DAE computer that collects the ACNET data from the ACNET front ends adds a timestamp to the data it recieves from each device. The local DAE clock is synched to the Accelerator Divisions Stratum 1 GPS time servers. For each device in each spill, the DAE timestamp is obtained by subtracting the known DAE delay between receipt of the "A9" and the extraction of the data from the front ends. This delay is typically 0.5-1 second. The DAE timestamp has a time resolution limited by the 15Hz clock signal telecast and system and data transmission overheads. Typically the resolution is only good to $\mathcal{O}(100)$ millisecsonds.

2. The VME timestamp: Several NuMI devices have VME frontends. This is true of the NuMI profile monitors and the Hadron and Muon monitors [4]. Data from these devices is acquired via custom made SWIC electronics. After the data is digitized in the SWICs it is sent via a dedicated ARCNET link to the front end VME processor. The VME processer recieves an \$8F hardware clock signal every second which synchs the on board clock with the AD GPS time servers. When the digitized data is recieved from the SWICs the VME front end then applies a timestamp. The VME frontends also carry out some onboard computations such as pedestal subtractions, profile monitor fits. This processed data is added as extra blocks to the raw SWIC data block and transmitted to the DAE. Although in principal, the VME timestamps could be accurate to $\mathcal{O}(10)\mu$ seconds, ARCNET speeds and VME overhead effectively limit the resolution to $\mathcal{O}(10)$ milliseconds.

The earliest DAE and VME timestamp from all ACNET devices read out successfully in a spill is recorded in the BEAMMONSPILL database and in the NtpBDLite Tree in the reconstructed ntuple files. Figure 28 shows the time difference between the GPS ND spill time from the SPILLTIMEND database and the DAE and VME timestamps.

We find that there is 16 milliseconds delay offset between both the DAE and VME timestamps and the ND GPS spill time. The DAE timestamps match within a 100 millisecond time window and the VME timestamps match the ND GPS within a 30 millisecond time window. We conclude that the resolution of the VME timestamp is more than adequate to match unambiguously spill data from the ACNET beamline devices with near detector GPS spill times. On rare occasions when none of the devices with VME frontends reads out successfully during a spill, the DAE timestamp can also be reliably used to match the beam spill data with the MINOS spills.

Using beam and near detector data taken from May 1st through Sep 30th 2005 we investigated the efficiency of matching beam data spills with near detector spills. The results are summarized in Table 7. We find that the efficiency of matching near detector snarls with beam data spills is 98.2% which is consistent with the average BDP spill live time as described in Table 5.

[4] The NuMI Beam Position Monitors also have VME front ends but we do not record the raw VME data from these devices in the MINOS datastream and as such we do not have access to these timestamps

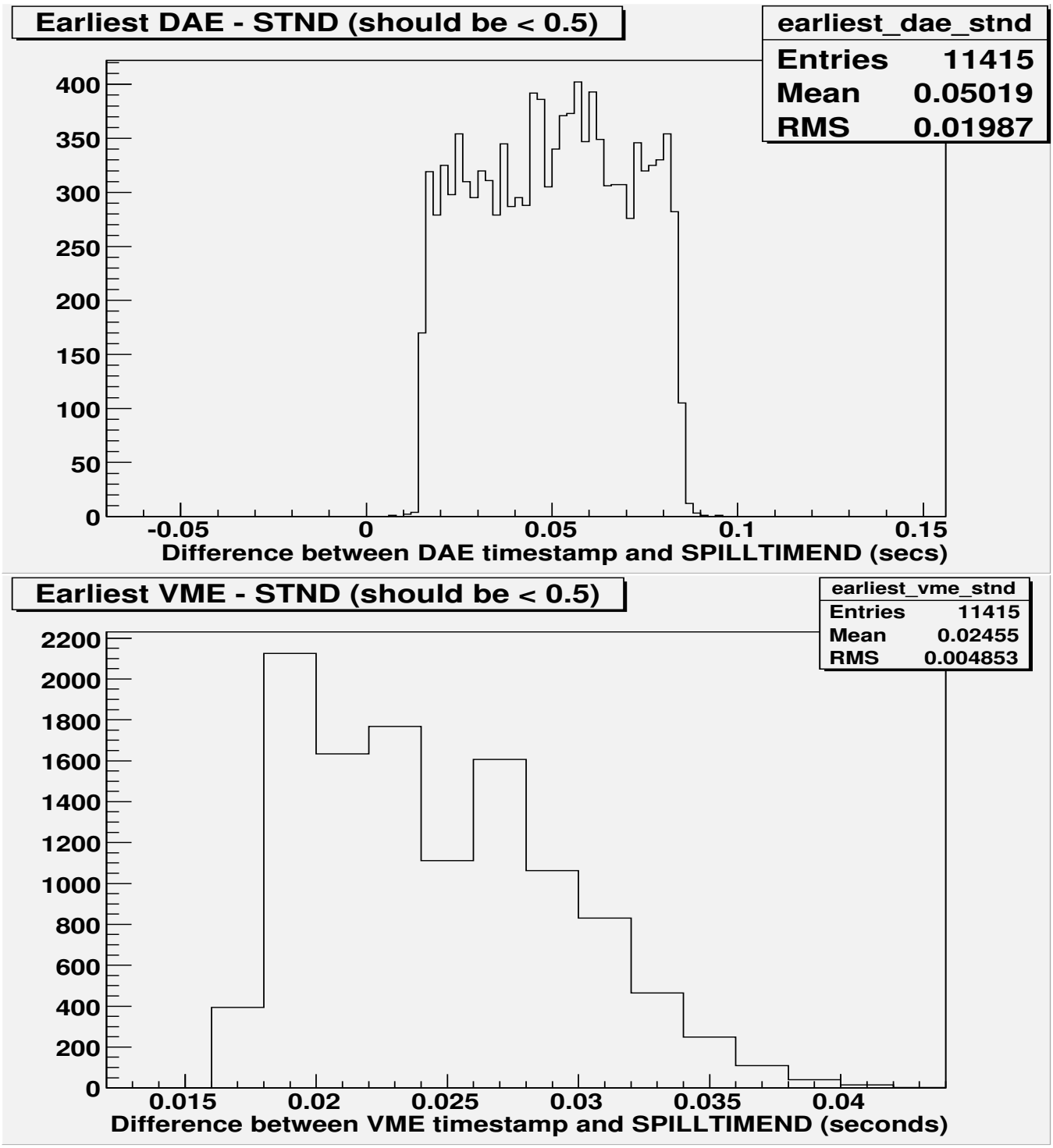

Figure 28: The distribution of time difference between ND GPS spill time and the closest ACNET beam spill time using the earliest VME and DAE timestamps.

Table 7: Matching ND snarls with beam spills for data taken from May 1st through September 30th.

Number of SPILLTIMEND spills	3906439
Number of BEAMMONSPILL spills	3858923
Number of ND snarls	3853039
Number of ND snarls matched with beam spills	3785397

4.3 SUMMARY

We have identified all sources of the MINOS Beam Data Process (BDP) failure modes with >1% loss in efficiency for the period Feb 1st,2005 - Feb 28, 2006. Almost all the failure modes identified have been addressed and preventative measures implemented. For the period Feb 1st, 2005 - Feb 28, 2006 the ND GPS system recorded 7.79M spills whereas the BDP process logged 7.68M spills. We find the overall BDP spill logging efficiency to be 98.6% when compared to the number of spills recorded by the ND GPS system. The BDP spill logging efficiency has been > 99.5% for the period Dec, 2005 through Feb, 2006. The fraction of BDP recorded spills where the NuMI toroids failed to readout is negligible; being $\sim 0.1\%$.

We have compared the total number of POT recorded by the BDP to the NuMI dataloggers. We find occasional differences in spill intensity values for TORTGT recorded in the NuMI dataloggers and by the BDP for the same spill. The difference in recorded intensity for the same spill is on the order of the ADC resolution which is 0.03% at 25E12. Overall, we find the Dataloggers record on average 0.03% higher daily POT values as compared to the BDP when both systems are operating normally which is consistent with the differences in individual spill values noted earlier. We consider this source of uncertainty on the torioid POT values to be negligible. We find that the NuMI datalogger recorded a total of 1.415 E20 POT (raw) for the period Feb 1st, 2005 through Feb 25, 2006 and the BDP recorded a total of 1.401E12 (raw) [5]. The difference in the total POT logged by the NuMI dataloggers and the BDP is $\sim 1\%$ and is consistent with the BDP spill logging efficiency of $\sim 98.6\%$.

The timeline breakdown for different beam configurations is discussed in Appendix C. Table 8 summarizes total POT integrated for different beam configurations after correcting for toroid calibrations [6] and including the uncertainties on the toroid readout discussed in Section 3.

Table 8: Integrated POT as recorded by the BDP for different beam running conditions. For data collected from Jan 21, 2005 through Feb 25, 2006.

Target location	Horn current	BDP POT
-250 cm	-200 kA	1.60 ± 0.05E18
-100 cm	-200 kA	1.20 ± 0.04E18
0 cm	-200 kA	0.676 ± 0.023E18
-10cm	0 kA	2.915 ± 0.030E18
-10cm	-170 kA	1.466 ± 0.015E18
-10cm	-200 kA	1.366 ± 0.014E18
-10cm	-185 kA	1.297 ± 0.013 E20
All	All	1.390 ± 0.014 E20

We studied the accuracy of beam data timestamps compared to the ND GPS timing system. We find that the accuracy of matching the beam data timestamps with the ND GPS spill times is better than 100 milliseconds. The efficiency of matching ND snarls with beam data spills is consistent with the BDP livetime.

[5] No toroid calibrations have been applied to these numbers

[6] The calibrations applied are a reduction of 4% on all TORTGT readings recorded prior to the gate change on July 26, 2005

5 Further corrections to POT measurements

In previous sections of this document, we discussed the mearsurement of the beam intensity in the NuMI beamline. The NuMI target is a 6.4 mm wide x 22 mm high x 1m long graphite target located more than 9 meters away from the pretarget region beam instrumentation. An upstream cylindrically shaped graphite baffle protects the target cooling lines from the proton beam. A cartoon of the cross-section of the target and baffle transverse and parallel to the NuMI beamline is shown in Figure 29. To correctly estimate the number of protons hitting the NuMI target we need

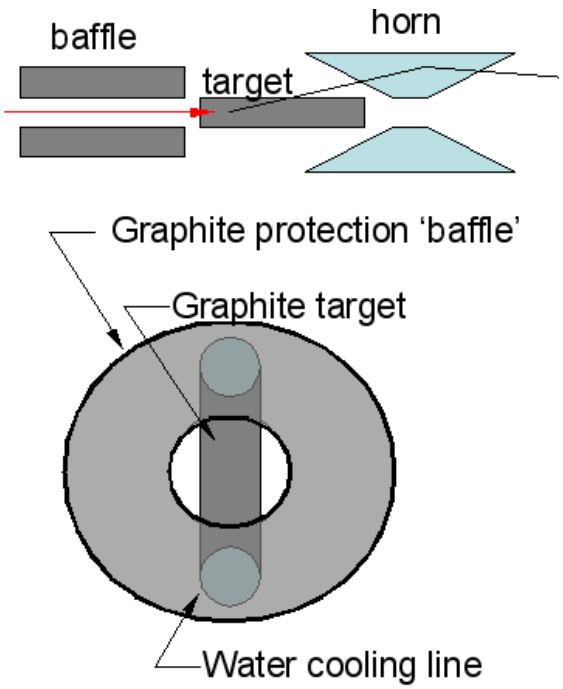

Figure 29: Conceptual drawing of the target and baffle layout along the NuMI beamline

to correct the total beam intensity measured in the toroids by the fraction of the beam actually hitting the target. The design specifications of the NuMI beam are a Gaussian beam profile 1mm in width both horizontally and vertically. In practice, beam widths of 1.5 mm in the horizontal and up to 2mm in the vertical have been observed during operating periods where the Booster beam quality has been bad. In addition to variations in the beam profiles, $>$ 1 mm variations in the beam position at the target during stable running have been observed. In this section we will attempt to address the following issues which are pertinent to the fraction of the beam actually hitting target:

1. Where is the target with respect to beamline instrumentation?
2. What is the accuracy and stability of the beam position monitors used to measure the beam positions at the target?
3. How stable is the beam position on the target?
4. What is the profile of the beam at the target?
5. How stable is the beam profile?
6. Are there any significant beam losses?

5.1 Target/baffle alignment

In this study, we use the data from proton beam scans to estimate the alignment of the target, baffle and horns relative to the beam and the stability of the alignment as a function of time. For a more detailed study of alignment using beam scans see [7]. Target scans are conducted using only a single proton batch with low intensity - typically < 1 E12 POT/spill. The beam is steered horizontally and vertically by varying the horizontal and vertical dipole magnet trim currents at HT121 and VT121 such that the beam travels in a straight line to the target. The hadron and muon monitor intensities normalized to the absolute beam intensity measurement at TORTGT are recorded at each scan location. The beam position monitors at location 121 and TGT are used to project the beam position in the horizontal and vertical to a given location along the beamline in the target region. Additional scale factors need to be applied to the BPM ACNET data. The scale factor for the pretarget area BPMs used is given in Table 9 [7]. The locations used for the pretarget

Table 9: Scale factors for target region BPMs

BPM	Multiplicitive scale factor
HP121	0.945
VP121	0.945
HPTGT	0.934
VPTGT	0.946

area BPMs and the target center are obtained from the survey of Jan 19th, 2005 and are listed in Table 10.

Table 10: Beamline axis locations of pretarget BPMs, pretarget profile monitors and the target center obtained from the Jan 19, 2005 survey. The target center in the LE-10, pME and pHE positions is taken to be 10cm, 100cm and 250 cm upstream of the LE surveyed position noted below.

Device	Distance from Q608 in feet
HP121	1142.21625
VP121	1143.13925
M121	1143.92041
HPTGT	1183.05649
VPTGT	1183.97315
MTGT	1184.76065
Target center in LE position	1215.99

Using the correction factors and alignment numbers noted in Tables 9 and 10, data from the horizontal target position scans taken with the hadron monitor on May 20th, July 19th, July 29th, Aug 19th, Sept 9th and Nov 18th, 2005 are examined [8]. In a horizontal scan the charge in the hadron monitor is minimal at the target center and increases as we move from the target center

[7] The scale factor for the upstream BPM's is between 0.965 and 0.981

[8] Due to BDP logging failures data from the Jun 3rd and Oct 20th scans are not included in this study.

towards the gap between target and baffle. When the beam moves onto the baffle, the charge in the hadron monitor decreases once more. The distribution of the hadron monitor charge as a function of the beam position at is shown in Figure 30. The horizontal beam position at the target in these distributions is obtained using the horizontal beam position measured by the two pretarget area BPMs HPTGT and HP121 to project the beam position at the target using the alignment data in Table 10. In order to determine the target center emperically from the scan data, the distribution of hadron monitor intensities near the target center is fit using a symmetrical 4th order polynomial function of the form

$$\begin{aligned}\text{Normalized had. intensity} = \quad & NORM + \\ & POLY02 * (x - OFFSET)^2 + \\ & POLY04 * (x - OFFSET)^4\end{aligned}$$

where x is the projection of the target position at the target using the pretarget area BPMs. The fit value of $OFFSET$ is the location around which the distribution is symmetric and is therefore taken to be the target center favored by the data. The fit results overlaid with the scan data are shown in Figure 30. The value of the target center horizontally obtained from the fits to LE-10 horizontal scans are summerized in Figure 31. Drifts in BPM calibrations could cause a shift in the target center w.r.t. to the BPMs. We fit the horizontal target positions obtained from the data over a 6 month period (May-Nov, 2005) to a straight line as shown in Figure 31. The data is consistent with a flat line. The average target position in the horizontal is found to be $target^x_{center} = -1.14 \pm 0.011$ mm w.r.t to the pretarget BPMs.

A closer inspection of the data distributions in Figure 30 reveals an asymmetry in the amount of charge deposited in the hadron monitor when the beam is passing through the right and left gaps between target and baffle. A study of the value of the integrated charge in the hadron monitor as a function of a target-center to baffle-center misalignment in the horizontal is shown in Figure 32. We conclude that the asymmetry in hadron monitor charge observed in the target scans is most probably due to a misalignment between target and baffle in the horizontal on the order of 0.5 mm.

The data from two vertical scans of the target position taken on May 12th, 2005 using BPMs to project to the target center is shown in Figure 33. In a vertical scan the hadron intensity decreases as we move away from target center and more towards the baffle. An emperical fit to a 4th order polynomial symmetric around the target offset from BPM center is shown. The values of the target offset preferred by the fits are 1.46 ± 0.02 and 0.62 ± 0.03 for the scan on May 12th and Nov 18th, respectively. For the period May-Dec,2005 we combine these two numbers and estimate $target^y_{center} = 1.0 \pm 0.4$ mm.

Target scans were also used to determine the horn/target/beam relative alignment. The results are discussed in Appendix B.

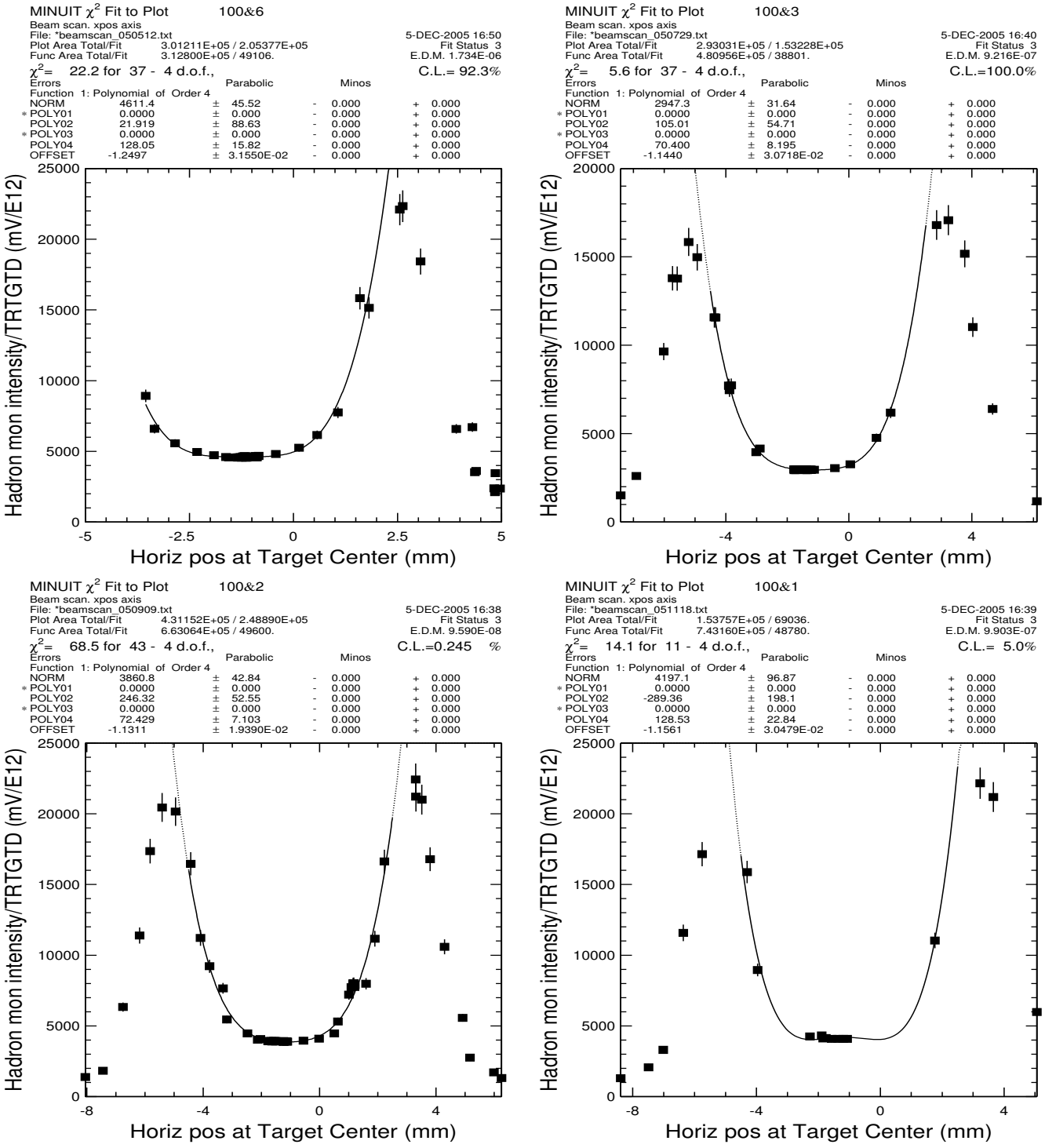

Figure 30: Examples of horizontal target scans using BPMs taken during 2005. The fit to the central "trough" region is to a 4th order polynomial of the form $Y = NORM + POLY01 * (x - OFFSET) + POLY02 * (x - OFFSET)^2 + ...$ The OFFSET is what determines the misalignment of the target in the BPM co-ordinate system. The vertical axis is the normalized hadron monitor intensity with a 5% uncertainty added to account for beam width variations and hadron monitor stability.

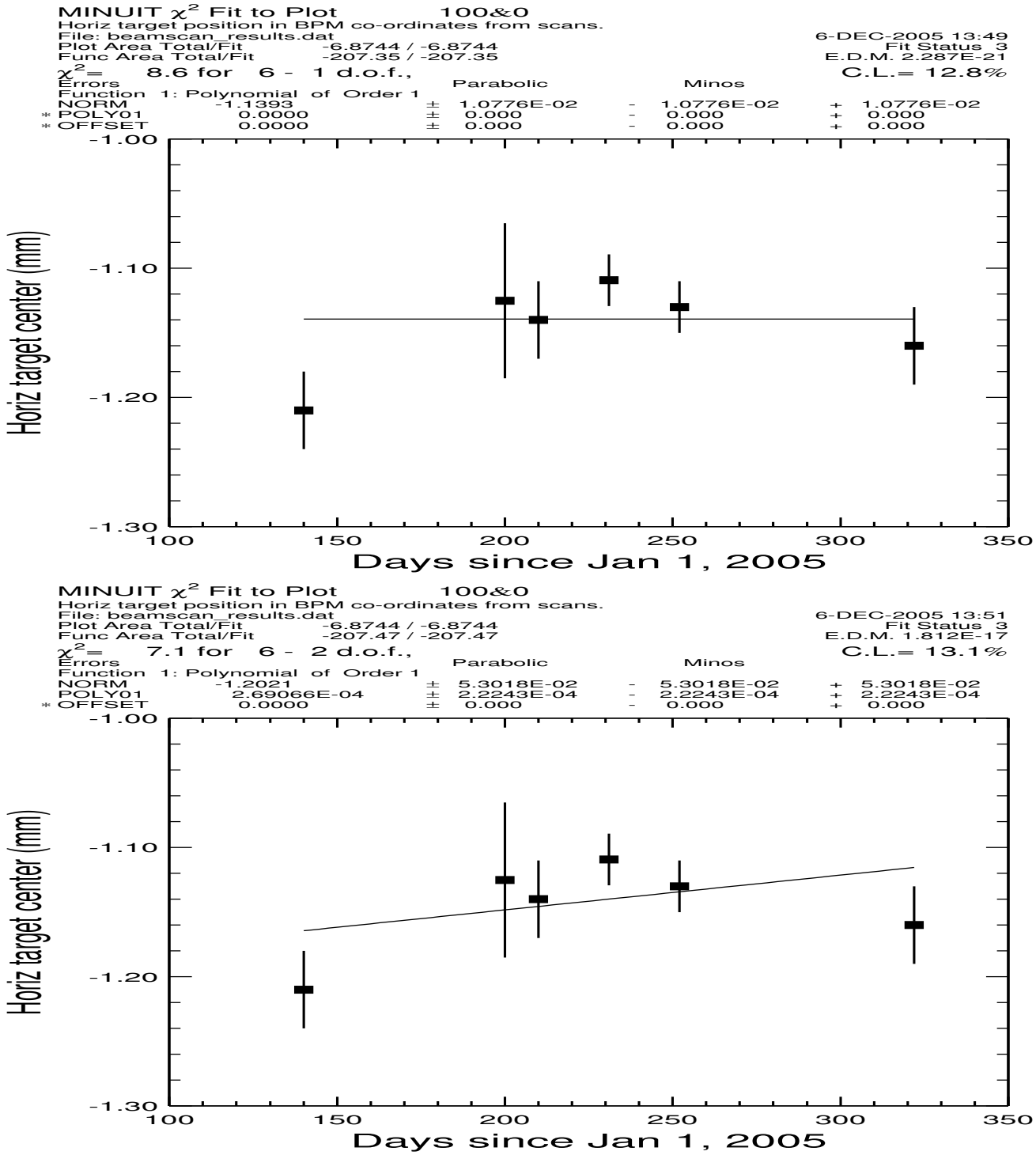

Figure 31: Stability of the fits to the target offset in BPM co-ordinates vs time.

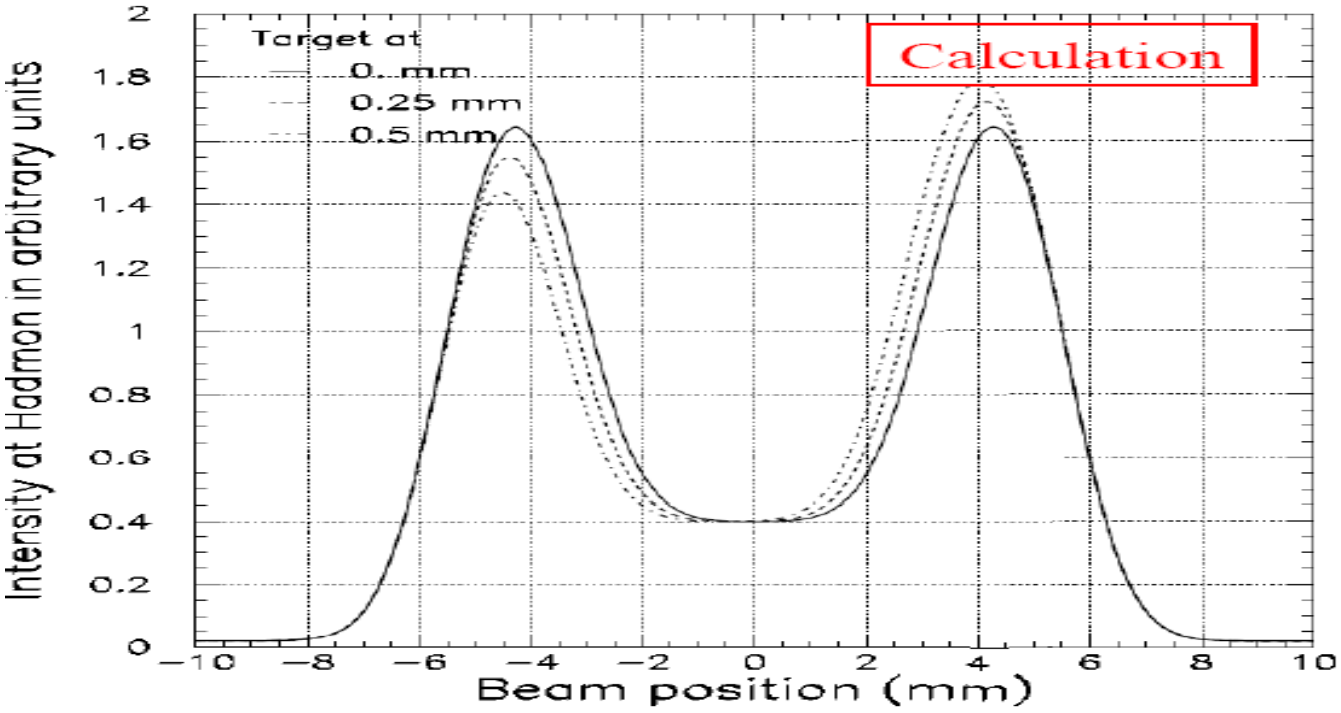

Figure 32: Calculation of the distribution of the hadron monitor charge as a function of beam position on target in the horizontal using different target-baffle misalignments.

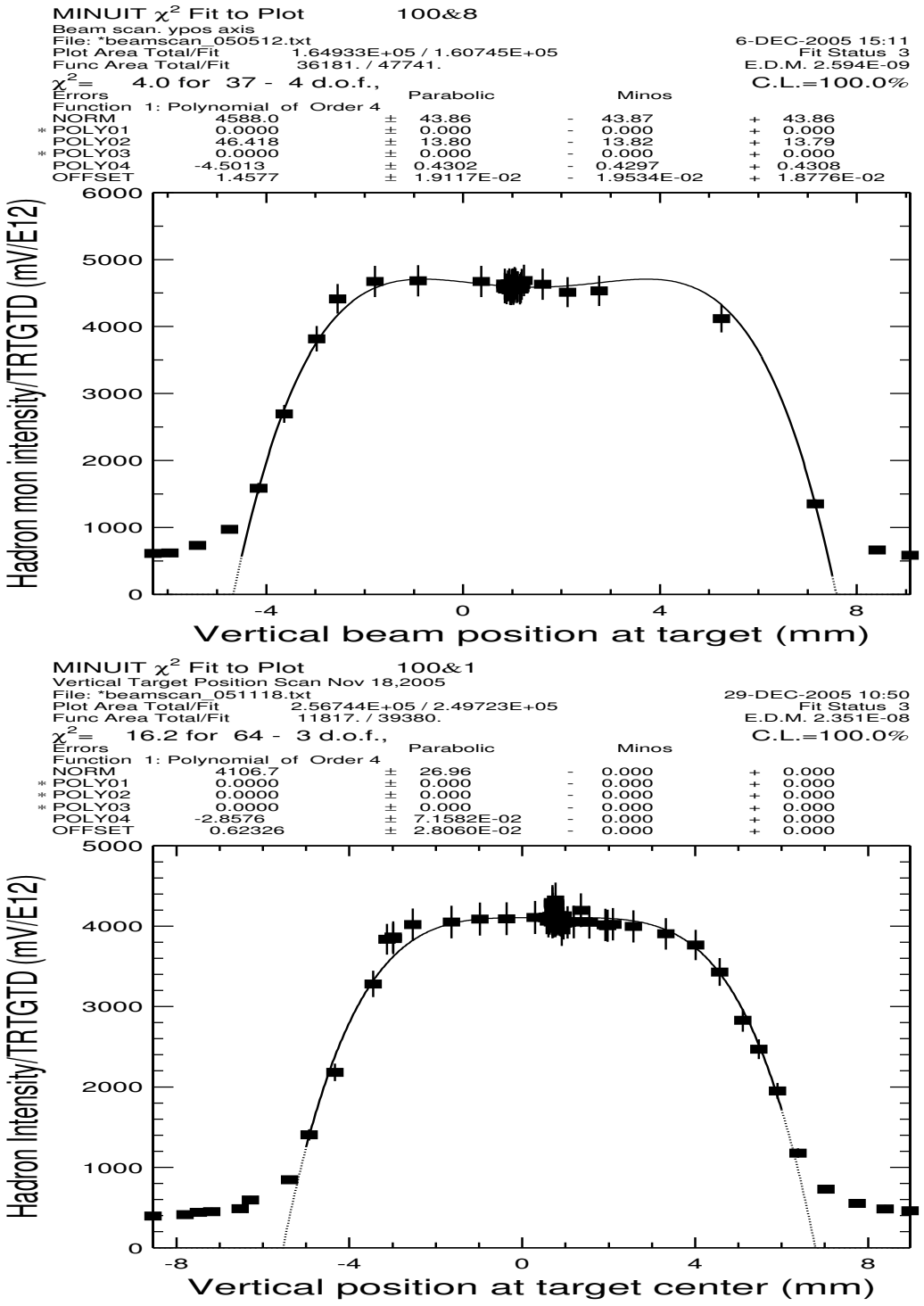

Figure 33: Data from a vertical target position scans using BPMs taken on May 12th (top), Nov 18 (bottom) 2005. The fit to the central region is to a 4th order polynomial of the form $Y = NORM + POLY01 * (x - OFFSET) + POLY02 * (x - OFFSET)^2 + ...$ The OFFSET is what determines the misalignment of the target in the BPM co-ordinate system. The vertical axis is the normalized hadron monitor intensity with a 5% uncertainty added to account for beam width variations and hadron monitor stability.

5.2 Beam profile and stability

In the discussions in Section 5.6, we will illustrate the effect of varying beam profiles on the neutrino flux in the near and far detectors. The NuMI design specifications call for a Gaussian beam with a width of 1mm in the horizontal and vertical at the target. Segmented electron multipliers (SEM) [1] are used to measure the beam profile along the beamline. PMTGT is the SEM closest to the target region and is located 9 meters from the target face when the target is in the LE position. It has a segmentation of 0.5mm. The beam profile measured by PMTGT on May 18th, 2005 and September 16th, 2005 is shown in Figure 34. On July XX, 2005 the SEM bias voltages were lowered and the measured beam profile after that date is consistent with a Gaussian shape as shown in Figure 34.

The vertical and horizontal width of the beam are strongly correlated. In Figure 35, the width of the beam from a single Gaussian fit as measured at PMTGT in the horizontal and vertical is plotted. We require the beam to be within 1mm of target center. The data is taken from the period Aug-Nov,2005 after the SEM voltages had been adjusted. Two seperate linear fits to the profile histogram of vertical vs horizontal beam width are performed in the region $0 < \sigma_x < 1.5$ mm and $\sigma_x > 1.5mm$ where σ is the fit value using a single Gaussian for the beam profile. We find $\sigma_y = 0.14 + 0.96\sigma_x,\ \sigma_x < 1.5$ mm and $\sigma_y = 0.26 + 0.82\sigma_x,\ \sigma_x > 1.5$ mm.

The width of the beam varies with the batch intensity. In Figure 36, the variation of the beam area, defined as $(\pi\sigma_x\sigma_y)$, is plotted as a function of main injector state. We chose data from only a few days in October, 2005 for this study to limit the dependance on changing accelerator conditions. The proton batch positions at the target vary depending on whether the main injector cycle includes an extraction to pbar source or whether all 6 batches are sent to NuMI. Since the SEM measures the width integrated over all 5-6 batches, there may be some differences in the observed beam width when running in the two different modes. We see no significant differences in the distribution of beam widths from the main injector in the two modes of running as shown in Figure 36. We observe large variations in beam area ($> 50\%$) occuring at fixed batch intensity as well as a general trend of increasing beam width with batch intensity. Currently, the instability in the beam widths at fixed beam intensities has been attributed to instabilities in the Booster beam. To model the overall dependence of beam width on batch intensity we studied the profile histograms of beam width versus average batch intensity in the period Aug-Nov, 2005. We find that the average beam widths increase until around 4.5 E12 protons/batch and then plateau (see Figure 37). We conclude that $\bar{\sigma_x} \sim 1.15$ mm and $\bar{\sigma_y} \sim 1.25$ mm for batch intensities > 4.5 E12 protons/batch.

We studied the stability of the beam widths as a function of time from May - Dec, 2005. The distribution of the beam profiles for each spill verses time is shown in Figures 38 to 41. We note that the largest instabilities in beam width occured at the end of May,2005, the beginning of June, 2005 and during December, 2005. The cause of these instabilties has been attributed to Booster RF problems.

So far we have only discussed the measurement of the beam width as measured by the SEM 9 meters away from the NuMI target face. To relate the measurement at PMTGT to the actual beam profile at the target, we need to use the beam optics to transport to the target location. The calculations predict the beam profile at the target location will be 3.3% wider than at PMTGT. On March 14, 2005 a study using several profile monitors along the beamline was conducted to verify the beam optics used to extrapolate to the target. The results of that study are discussed in [8]. The study concludes that the profile σ is matched well by calculation except at PM101 (the first profile monitor in the beamline) due to the current at quad 101 being at 60% of design strength. The current setting was corrected in mid-June,2005.

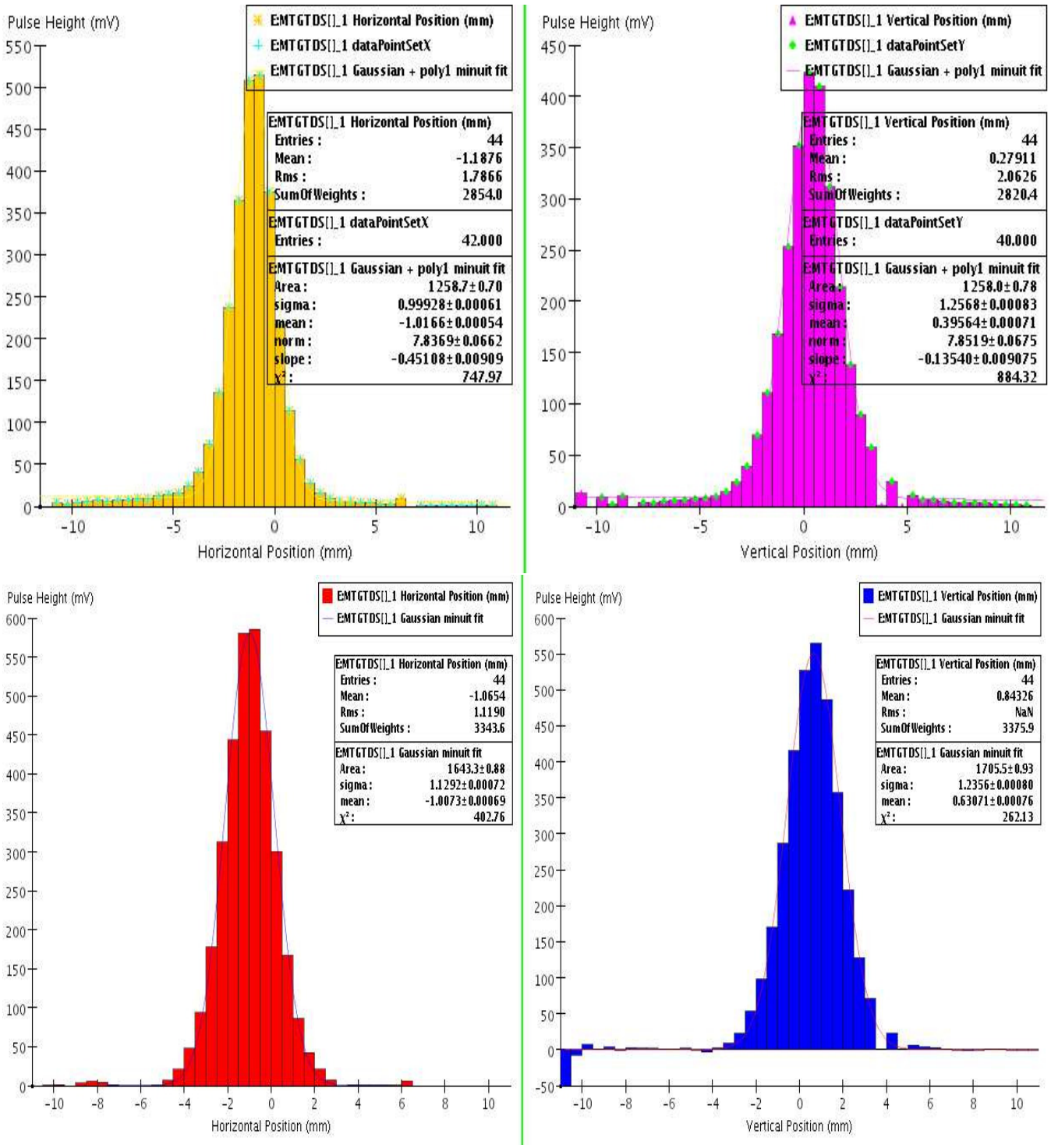

Figure 34: Beam profile as measured by PMTGT on 5/18/2005 (top) and 9/16/2005 (bottom). The SEM bias voltages were changed on July XX, 2005. After the voltage change the beam profile is found to be consistent with a Gaussian hypothesis.

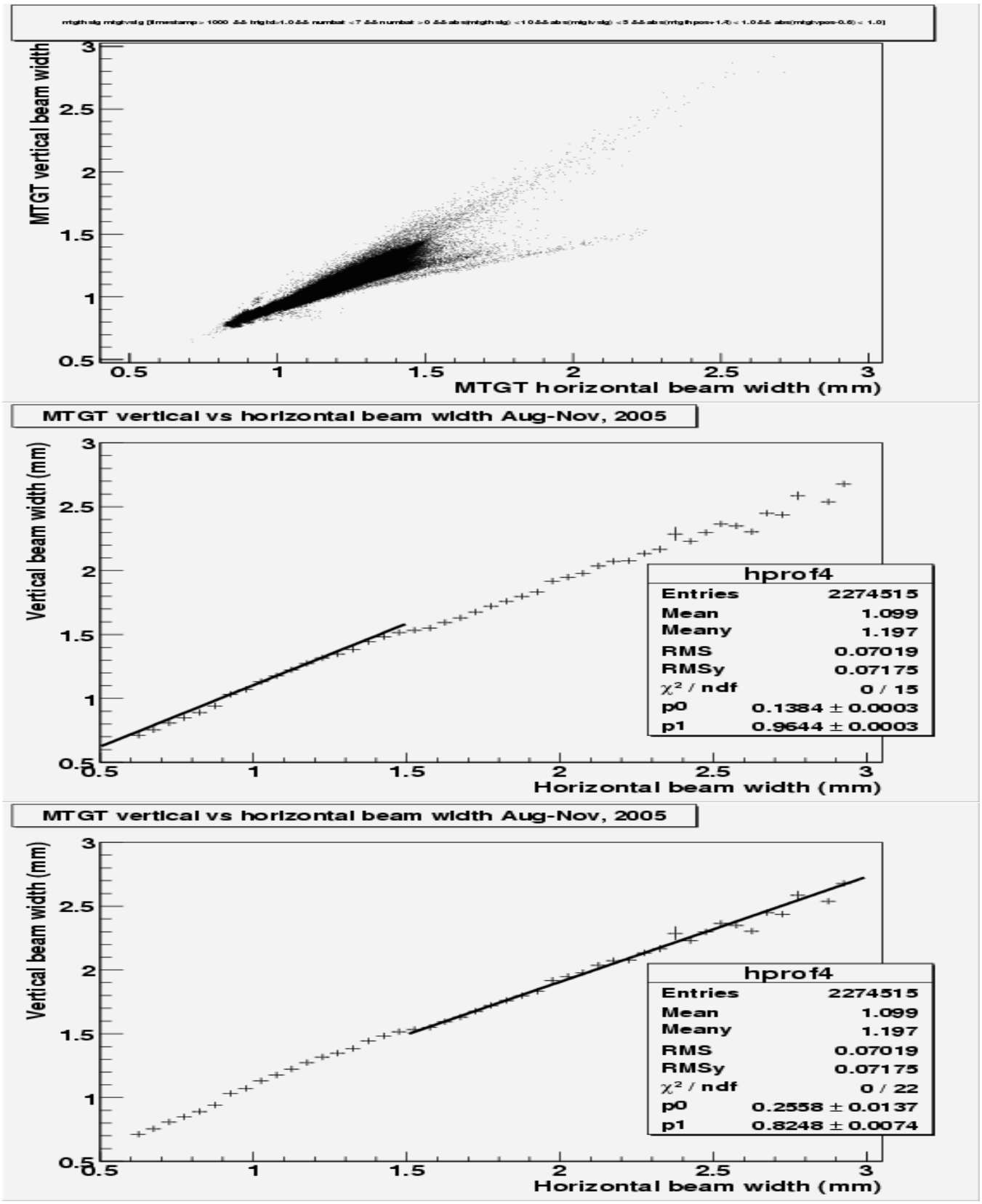

Figure 35: Vertical vs horizontal beam width correlations

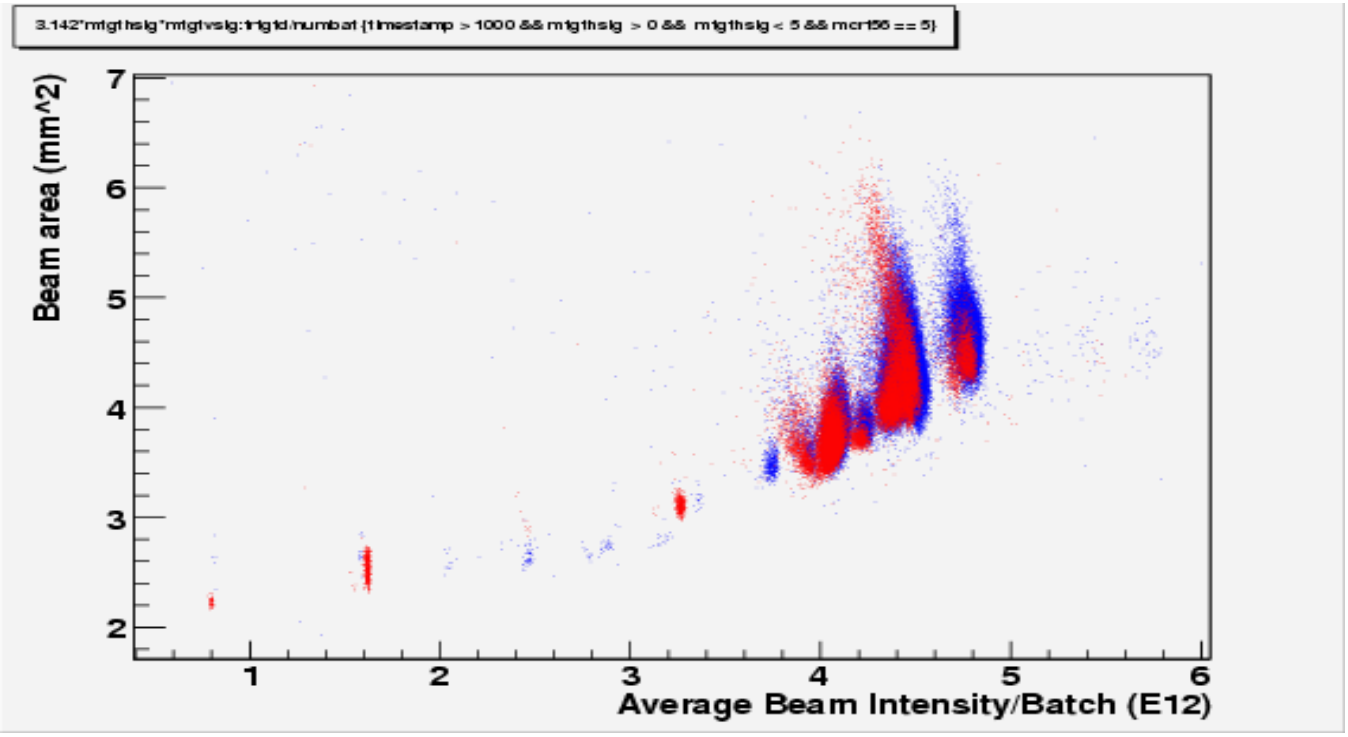

Figure 36: The variation of beam area ($\pi\sigma_x\sigma_y$) with MI state. Blue points are for NuMI only and red points are for NuMI mixed mode, Oct 14-18, 2005

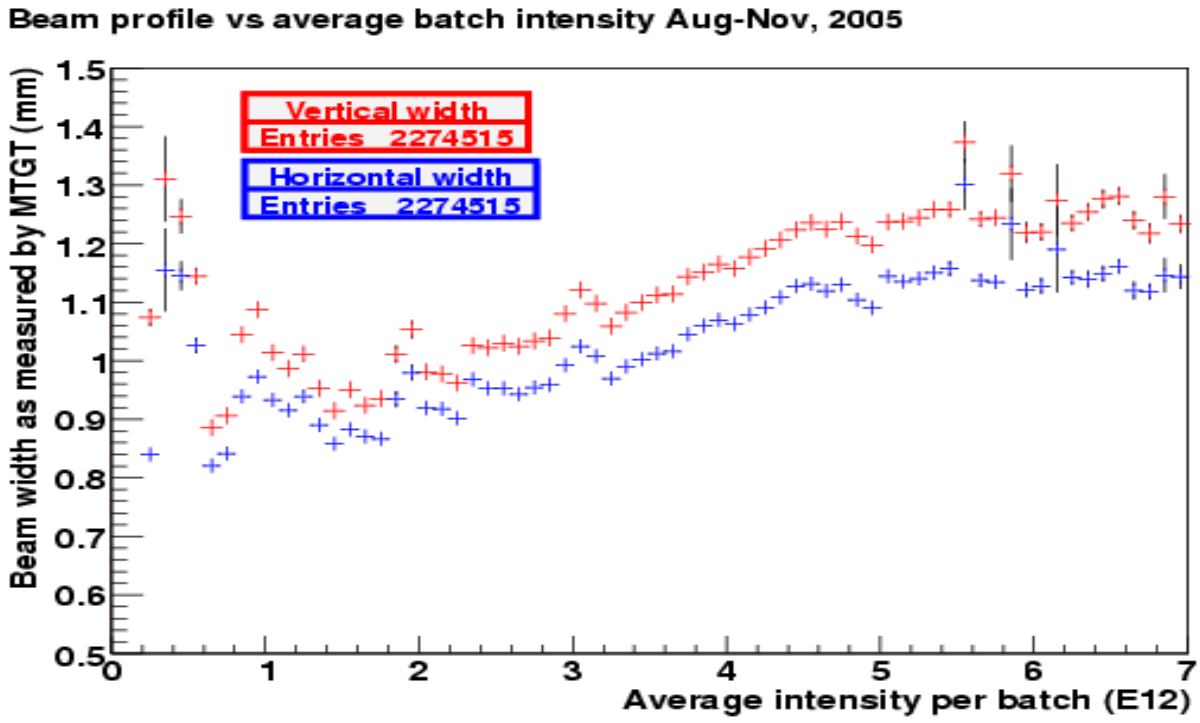

Figure 37: The variation of beam width with average batch intensity.

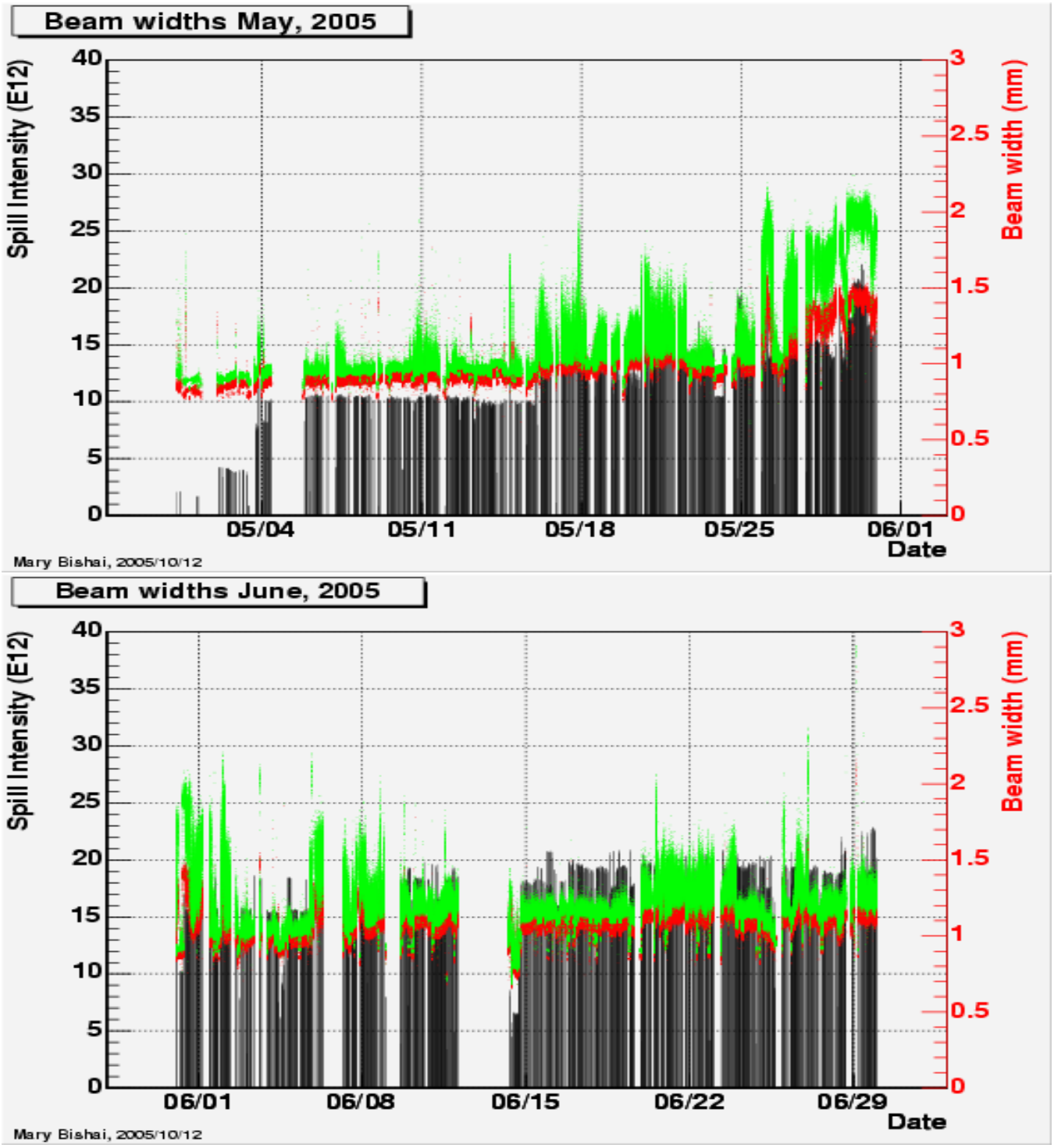

Figure 38: Beam width variation as measured by MTGT function of time, total intensity. The green points are for the vertical beam widths and the red points are horizontal beam widths.

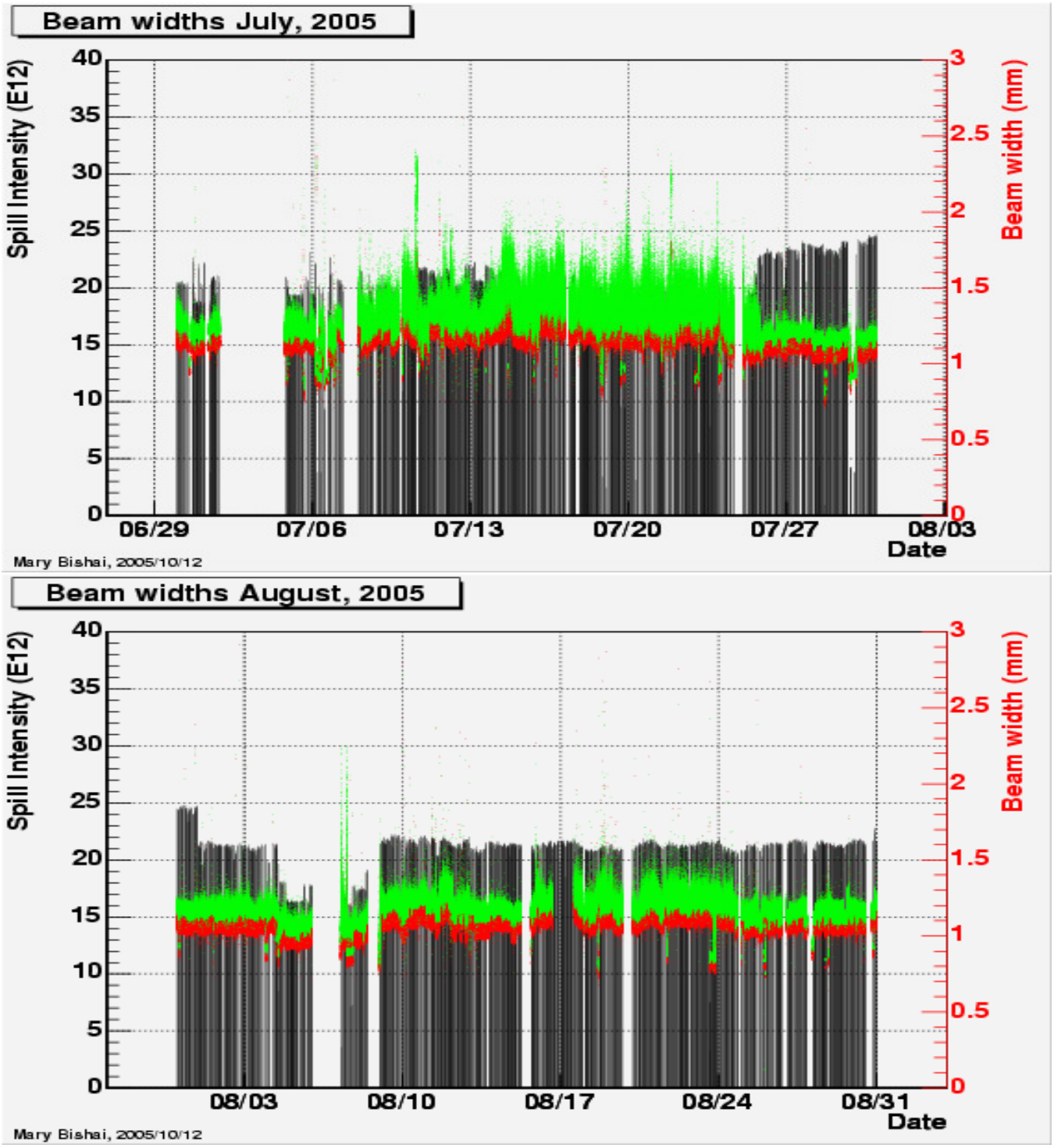

Figure 39: Beam width variation as measured by MTGT function of time, total intensity. The green points are for the vertical beam widths and the red points are horizontal beam widths.

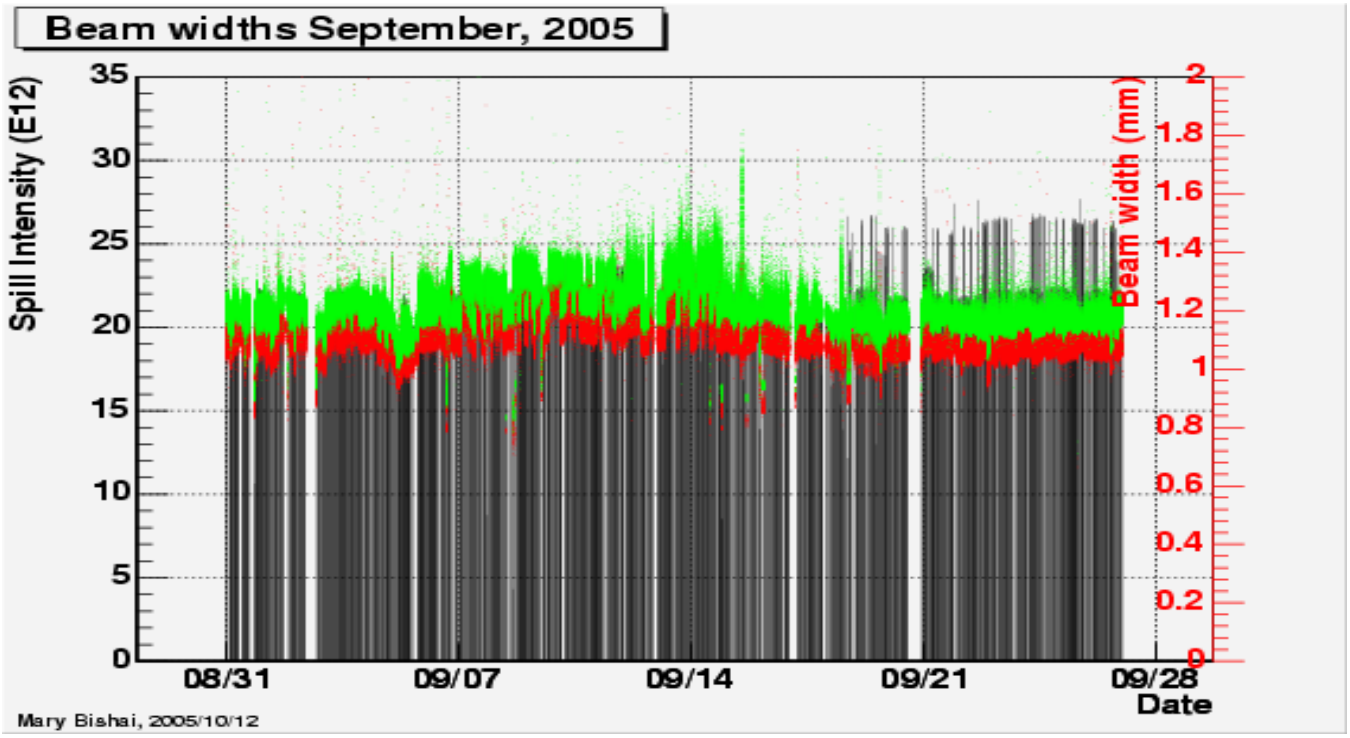

Figure 40: Beam width variation as measured by MTGT function of time, total intensity. The green points are for the vertical beam widths and the red points are horizontal beam widths.

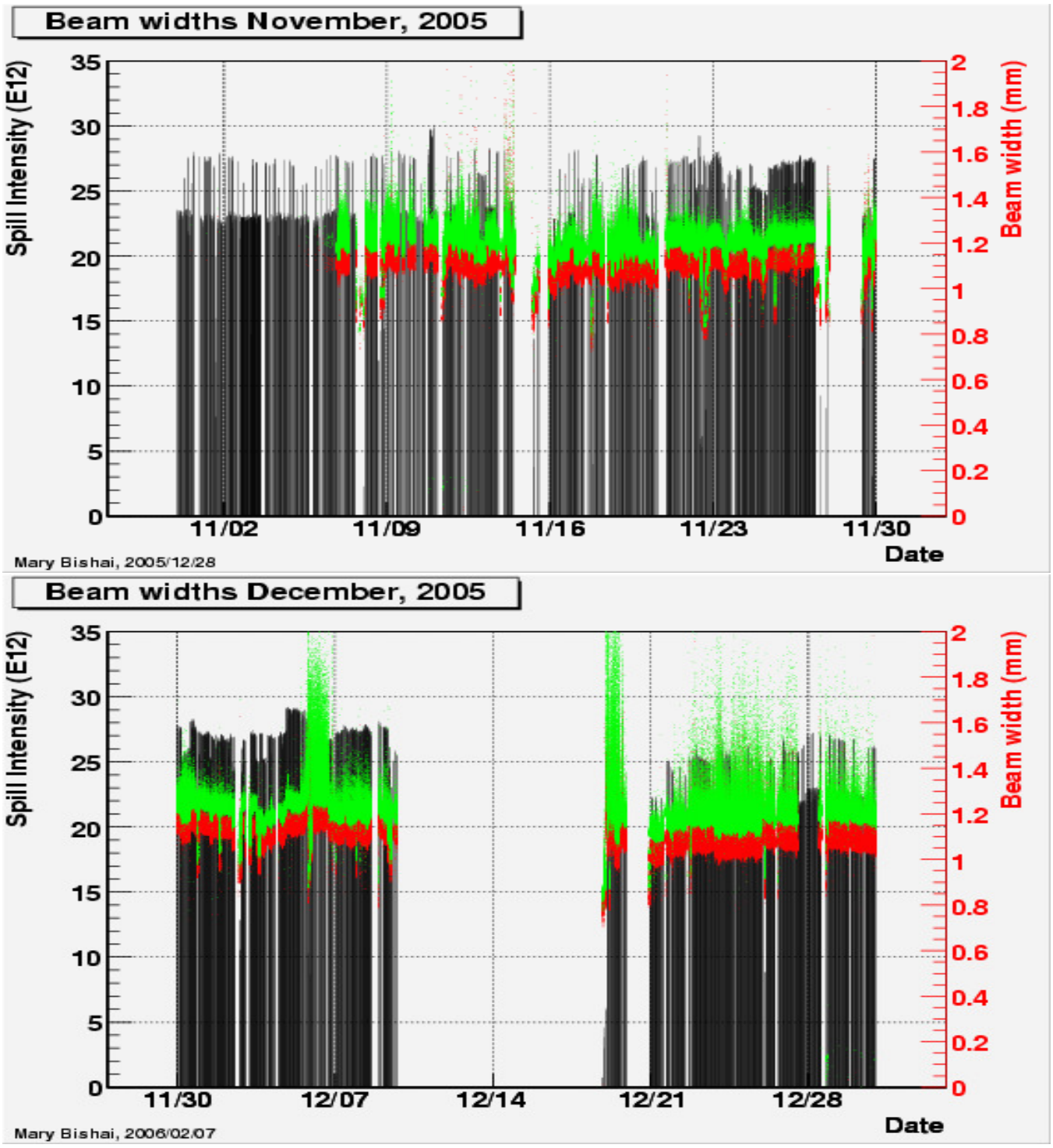

Figure 41: Beam width variation as measured by MTGT function of time, total intensity. The green points are for the vertical beam widths and the red points are horizontal beam widths.

5.3 Beam position stability on the target

The Main Injector stores up to 6 proton batches from the Booster. Two booster batches can be "slip-stacked" into 1 Main Injector batch. The first batch in the Main Injector is typically extracted to the pbar source for anti proton production. There currently 3 modes of Main Injector operation relevant to NuMI:

NuMI only cycle: All 6 MI batches are sent to the NuMI beamline in one MI cycle.

NuMI mixed-mode cycle.: The first batch in the MI which is usually two slip stacked booster batches is first extracted to the pbar source. The remaining 5 batches are sent to NuMI. In this cycle, the MI52 kicker magnet which extracts beam to the pbar source fires first, followed by the NuMI kicker.

Interleaved mode: As the anti-proton stack in the pbar accumulator increases, the stochastic cooling process takes longer to cool the pbar beam and the rate at which antiprotons can be added to the accumulator decreases. In this mode it is possible to run the Main Injector in an interleaved mode with 1 NuMI only cycle followed by a NuMI mixed-mode cycle and so on. Interleaving MI cycles began in July, 2005.

The beam position monitors measure the position and intensity of each batch in the MI and NuMI beamline. In Figure 42 the horizontal position of each batch projected to the target center for NuMI only and NuMI mixed-mode cycles as measured on May 24th and 31st is plotted. Since the NuMI target is much larger in the vertical than the horizontal we will concentrate in these studies on the stability of the batch positions in the horizontal. We find that the distribution of batch 1 horizontal position at the target during NuMI mixed-mode has a bimodal structure and the mean batch position at each node is the furthest removed from the target center ($target^{x}_{center} = -1.20 \pm 0.01$ mm) [9]. In NuMI mixed-mode, noise from the MI52 kicker perturbs the first 20-30 bunches of first batch sent to NuMI causing them to deviate from the desired positions along the beamline. The time between MI52 firing and the first NuMI bucket varies every other turn, hence the bimodal distributions of batch 1 positions. The values of the mean and standard deviation of the the batch position at the target for different MI cycles measured during May, 2005 is summarized in Table 11. We find that the largest deviation of the mean batch position from the target center is -0.5mm in the horizontal for batch 1 in NuMI mixed mode. The standard deviation of the batch positions at the target can be used to estimate the beam stability during normal running. We find the largest standard deviation to be 100 μm. This includes the BPM resolution which is xxx μm.

The Autotune program uses a feedback mechanism to adjust the trim magnet currents and steer the beam towards target center. Autotune has been used since January, 2005. The program typically uses the batch position average of a subset of NuMI batches 2,3,4 to set the trim currents for the next spill. A more sophisticated version of the program called Vernier Autotune was launched on August 31st, 2005. This significantly improved the batch stability at the target. This latter version of Autotune also averages the batch positions measured over six spills before adjusting the trim magnets. The horizontal batch positions at the target center measured during the period Oct 14-18, 2005 are shown in Figure 43. The mean and standard deviations are summarized in Table 12. For the data period after Sept 30th, 2005, We find that the largest deviation of the mean batch position from the target center is -0.2mm in the horizontal for batch 1 in NuMI mixed

[9] For this study, the BPM scale factors were not used - hence the target center location should be -1.21 not -1.14 mm

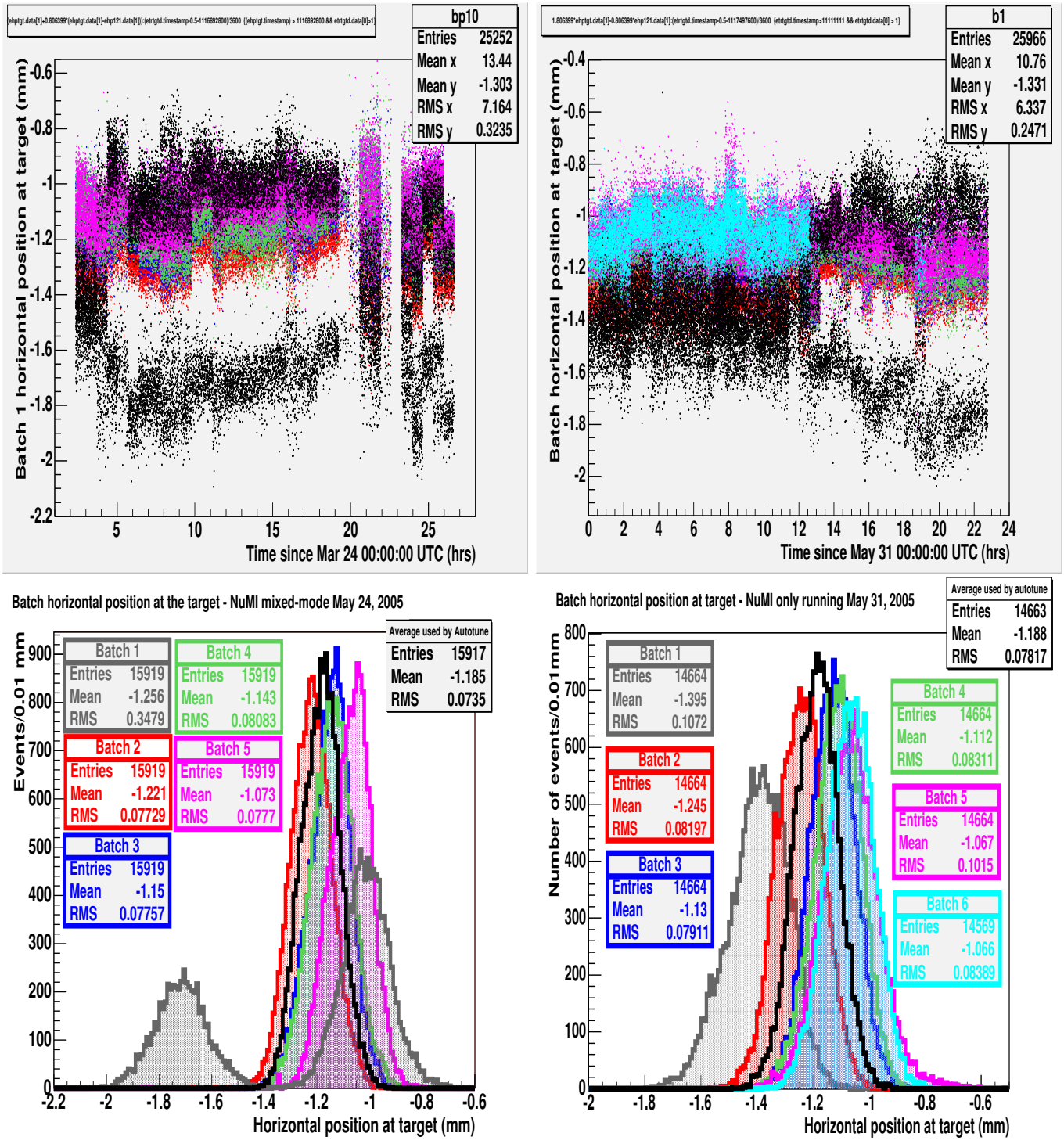

Figure 42: Horizontal batch positions projected to target center in NuMI only and NuMI mixed mode measured on May 24th and May 31st, 2005. The batch numbers are the NuMI batch number conventions.

mode. The standard deviation of the batch positions at the target can be used to estimate the beam stability during normal running conditions. We find the largest standard deviation to be 80 μm. This includes the BPM resolution which is xxx μm. Our previous studies have indicated that the deviation between the average batch positions at the target during May-Dec, 2005 is on the order

Table 11: Means and standard deviations of the 6 batch positions at the NuMI target for different MI cycles. The data from May, 2005. The batch numbers here are for MI batches. NuMI batch 1 is MI batch 1 in NuMI only mode and MI batch 2 in NuMI mixed-mode. The value to use for the target center is -1.21 ± 0.01 mm.

MI Batch	NuMI only cycle	NuMI mixed-mode
1	-1.40 ± 0.11 mm	pbar batch
2	-1.25 ± 0.08	-1.26 ± 0.35
3	-1.13 ± 0.08	-1.22 ± 0.08
4	-1.11 ± 0.08	-1.15 ± 0.08
5	-1.07 ± 0.10	-1.14 ± 0.06
6	-1.07 ± 0.08	-1.07 ± 0.08

Table 12: Means and standard deviations of the 6 batch positions at the NuMI target for different MI cycles. The data is from Oct, 2005. The batch numbers here are for MI batches. NuMI batch 1 is MI batch 1 in NuMI only mode and MI batch 2 in NuMI mixed-mode. The value to use for the target center is -1.14 ± 0.01 mm.

MI Batch	NuMI only cycle	NuMI mixed-mode
1	-1.32 ± 0.08 mm	pbar batch
2	-1.19 ± 0.05	-1.13 ± 0.17
3	-1.10 ± 0.05	-1.12 ± 0.06
4	-1.04 ± 0.05	-1.09 ± 0.05
5	-1.04 ± 0.05	-1.11 ± 0.05
6		-1.07 ± 0.05

of 0.5mm. The studies also indicate the batch position stability at the target is of the order 100 μm during normal running. The studies sampled only a small snapshot in time of beam performance. To better understand the relative batch position stability over the whole period from May to Dec, 2005, we studied the spill-by-spill differences in batch position at the target as a funciton of time. The maximum difference between batch positions in the horizontal and vertical for each spill is plotted in Figures 44 to 48. We note large instabilities were observed in June and the end of November, 2005. The November, 2005 instabilities are suspected to have been caused by mode 1 longitudinal instabilities in the Main Injector.

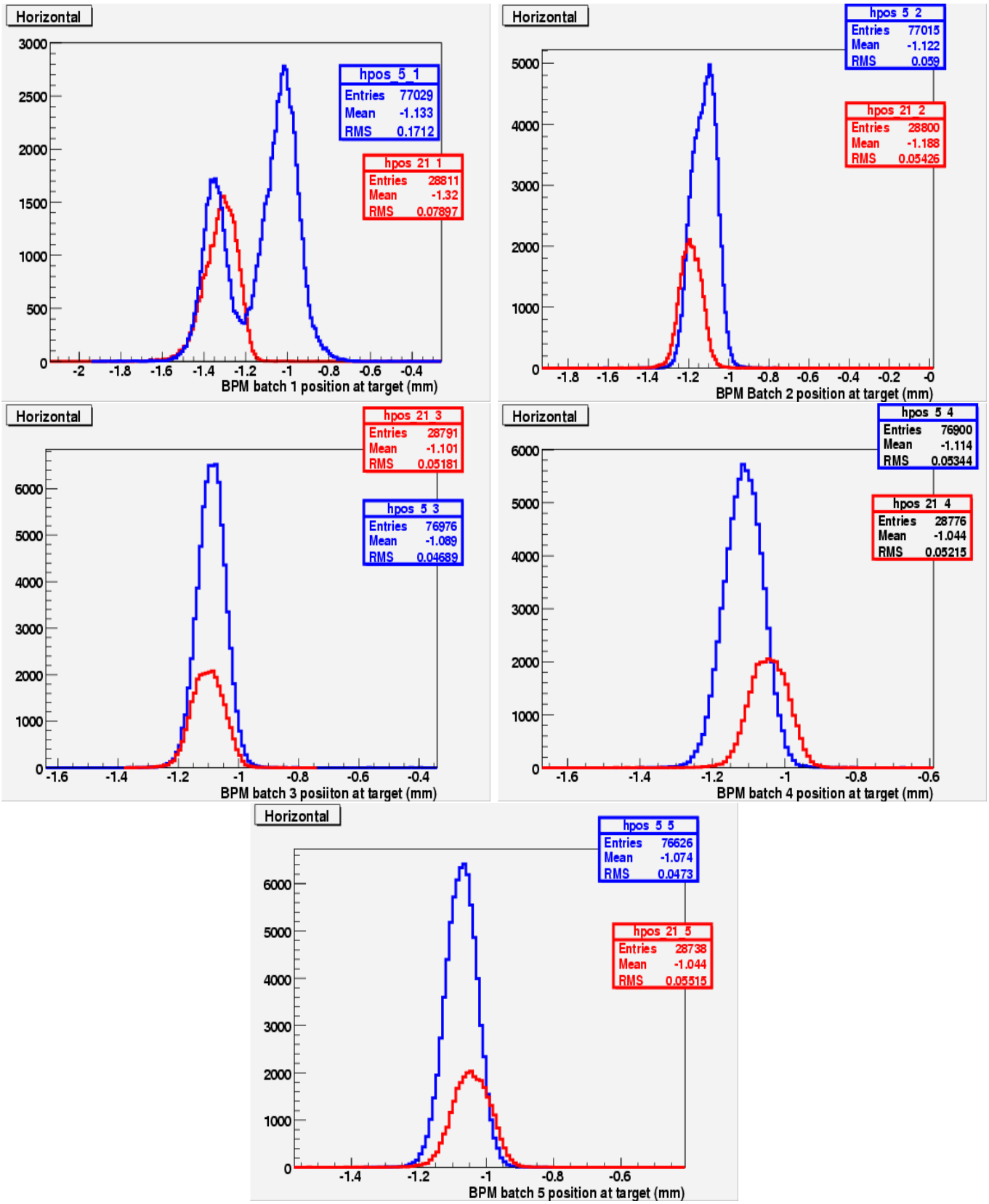

Figure 43: Batch positions projected to target center in NuMI only (red) and NuMI mixed mode (blue) measured Oct 14-18, 2005. Note that batch 1 position in the Main Injector in NuMI mixed mode actually corresponds to batch 2 in NuMI only mode.

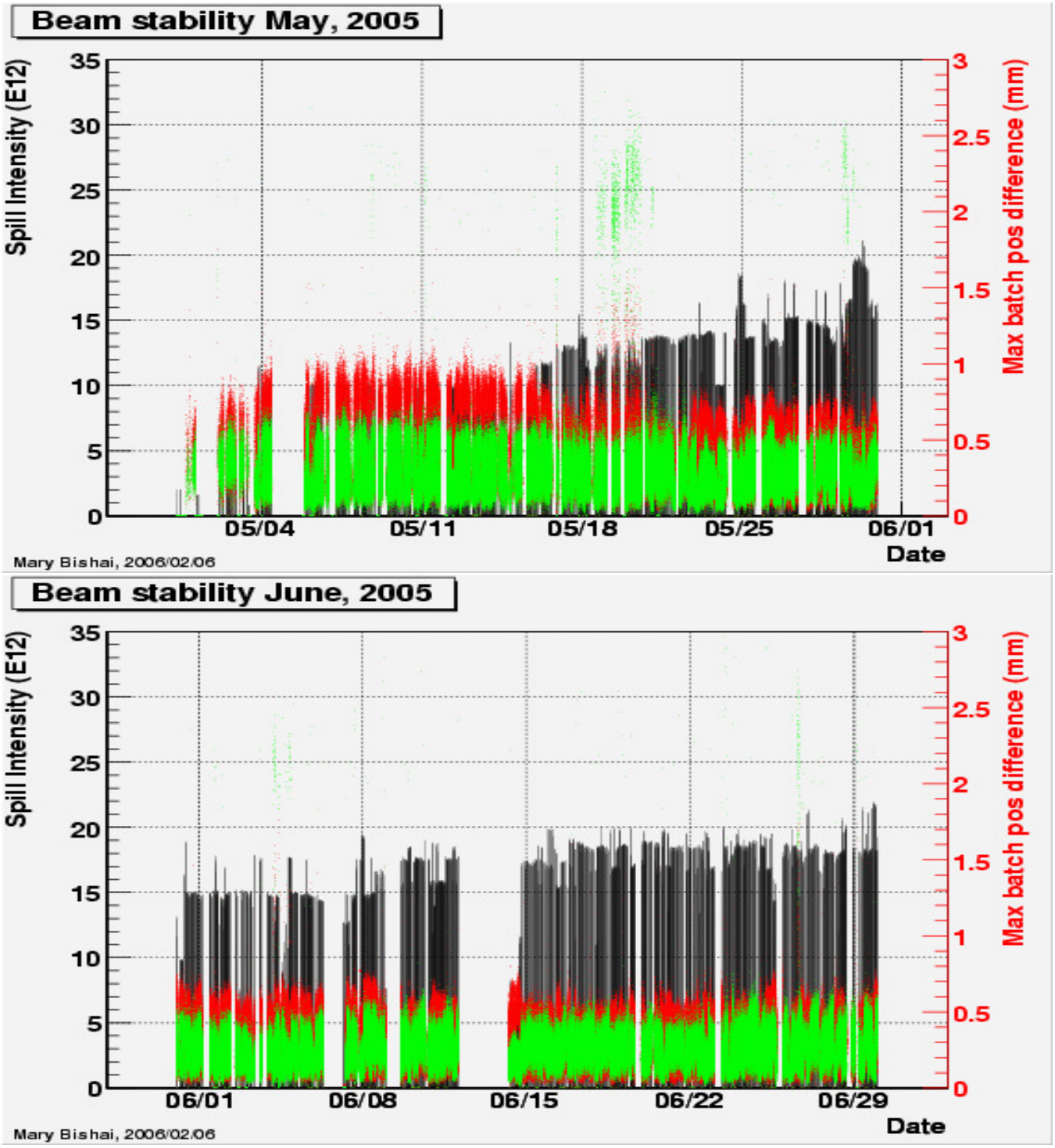

Figure 44: Maxmimum batch position variation as projected on the target as a function of time, total intensity. The green points are for the vertical batch positons and the red points are horizontal batch positions.

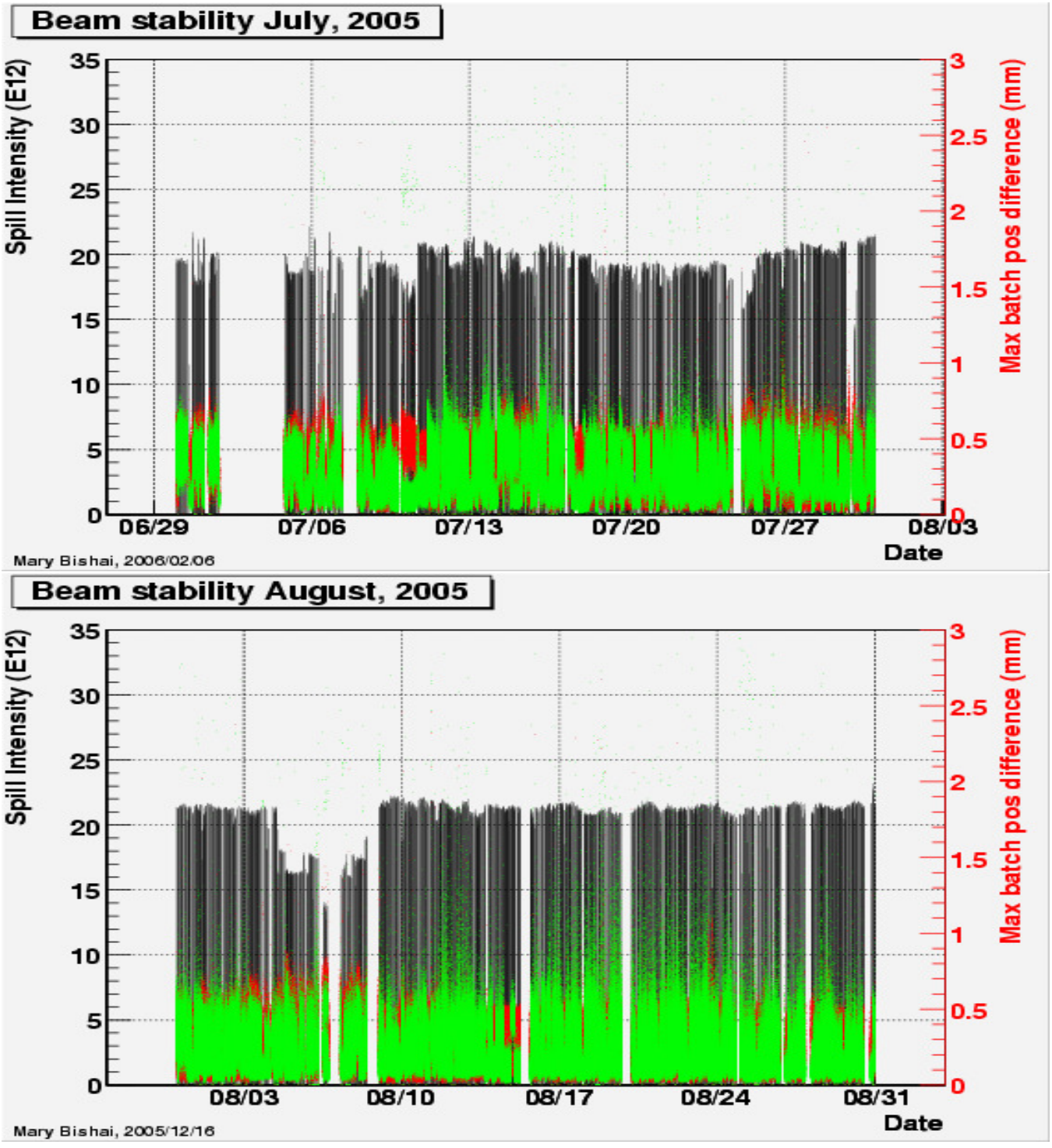

Figure 45: Maxmimum batch position variation as projected on the target as a function of time, total intensity. The green points are for the vertical batch positons and the red points are horizontal batch positions.

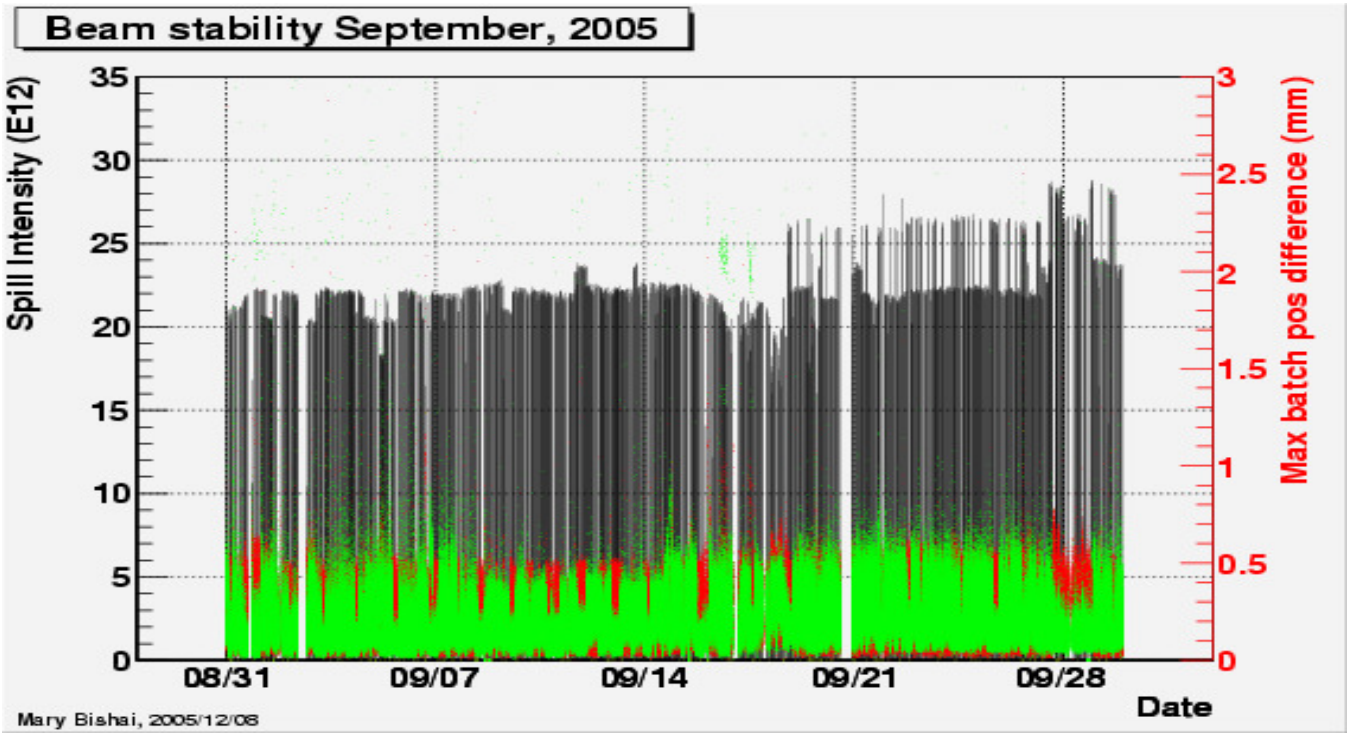

Figure 46: Maxmimum batch position variation as projected on the target as a function of time, total intensity. The green points are for the vertical batch positons and the red points are horizontal batch positions.

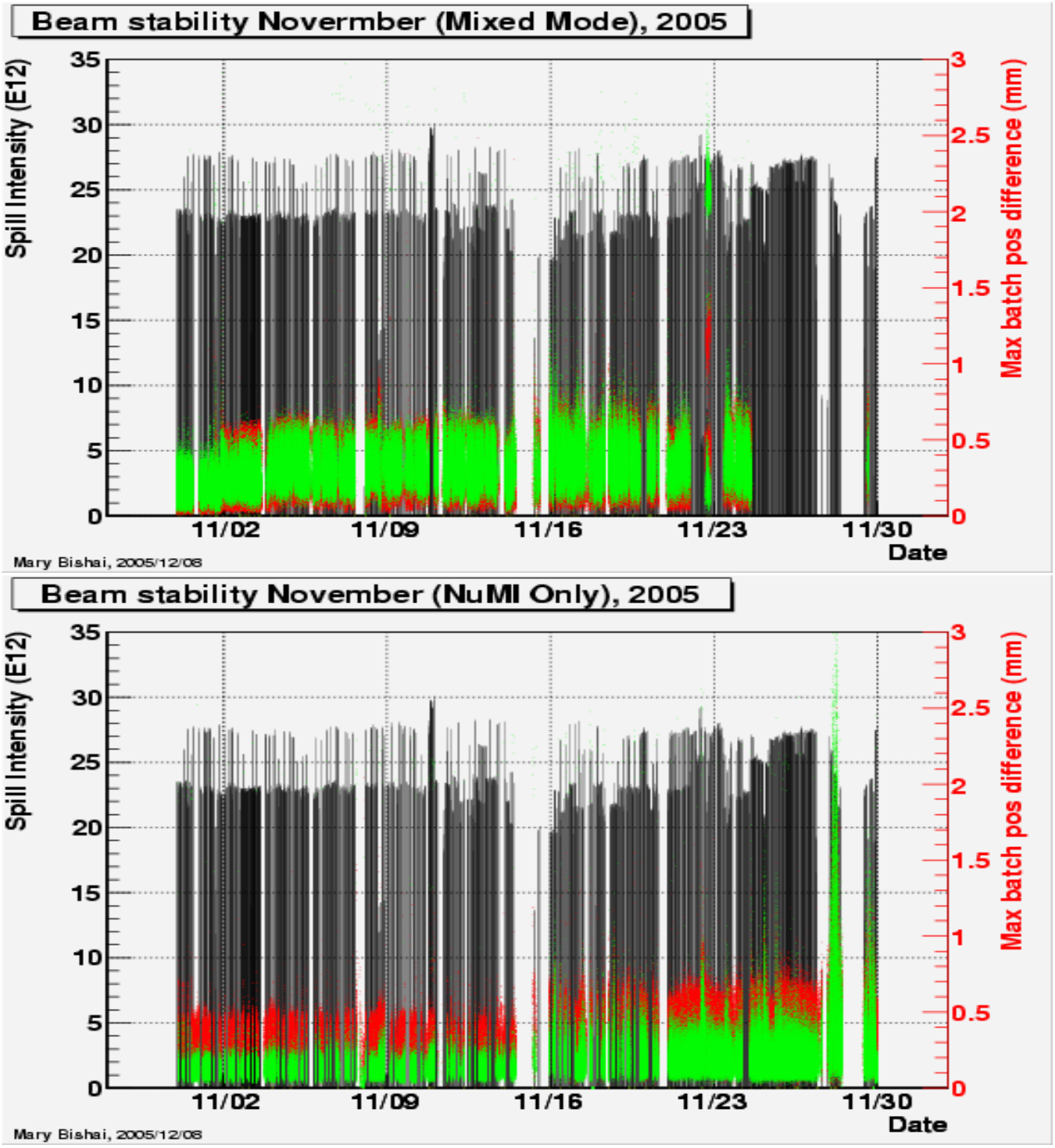

Figure 47: Maxmimum batch position variation as projected on the target as a function of time, total intensity and MI state. The green points are for the vertical batch positons and the red points are horizontal batch positions.

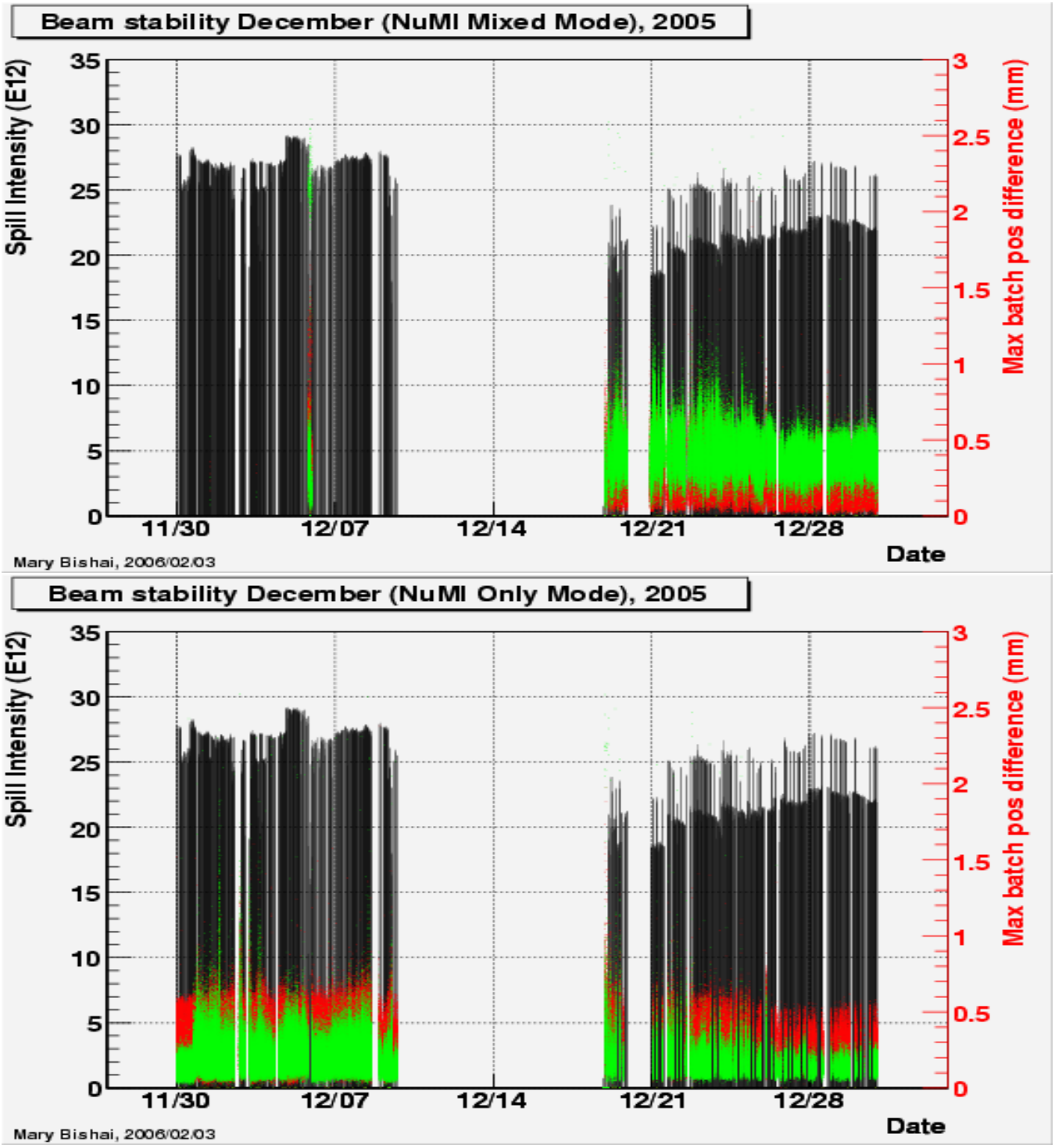

Figure 48: Maxmimum batch position variation as projected on the target as a function of time, total intensity and MI state. The green points are for the vertical batch positons and the red points are horizontal batch positions.

5.4 Beam incident angle on the target

5.5 Beam losses

We consider the case where losses in the NuMI beamline could change the actual beam intensity at the target location as compared the measurement at TORTGT. In general, we find that beam losses along the beamline are negligible. A typical pulse and the loss monitor readout from several locations along the beamline is shown in Figure 49. The readout from the loss monitors is consistent with pedestals. There have been only 4 instances of significant losses down the NuMI beamline during

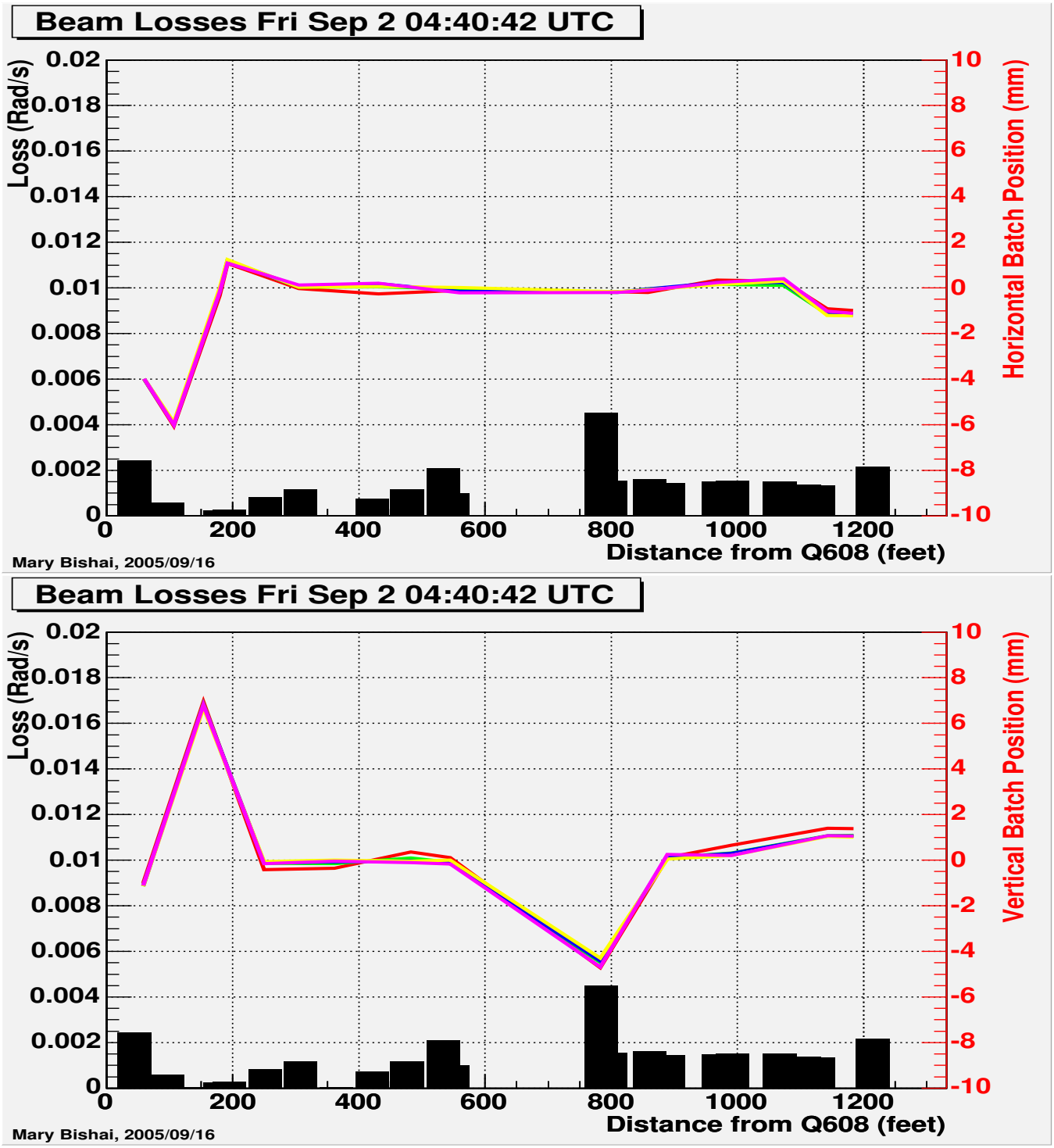

Figure 49: Typical losses - Sept, 2005.

2005 where the loss was large enough to be recorded as a significant difference between the intensity reading at TOR101 and TORTGT (> 0.5 E12). For future reference, we present a snapshot of the beam trajectory and the loss monitor readout from one of these pulses recorded on Sep 2nd, 2005 in Figure 50. We conclude that there are no significant losses in the NuMI beamline that could

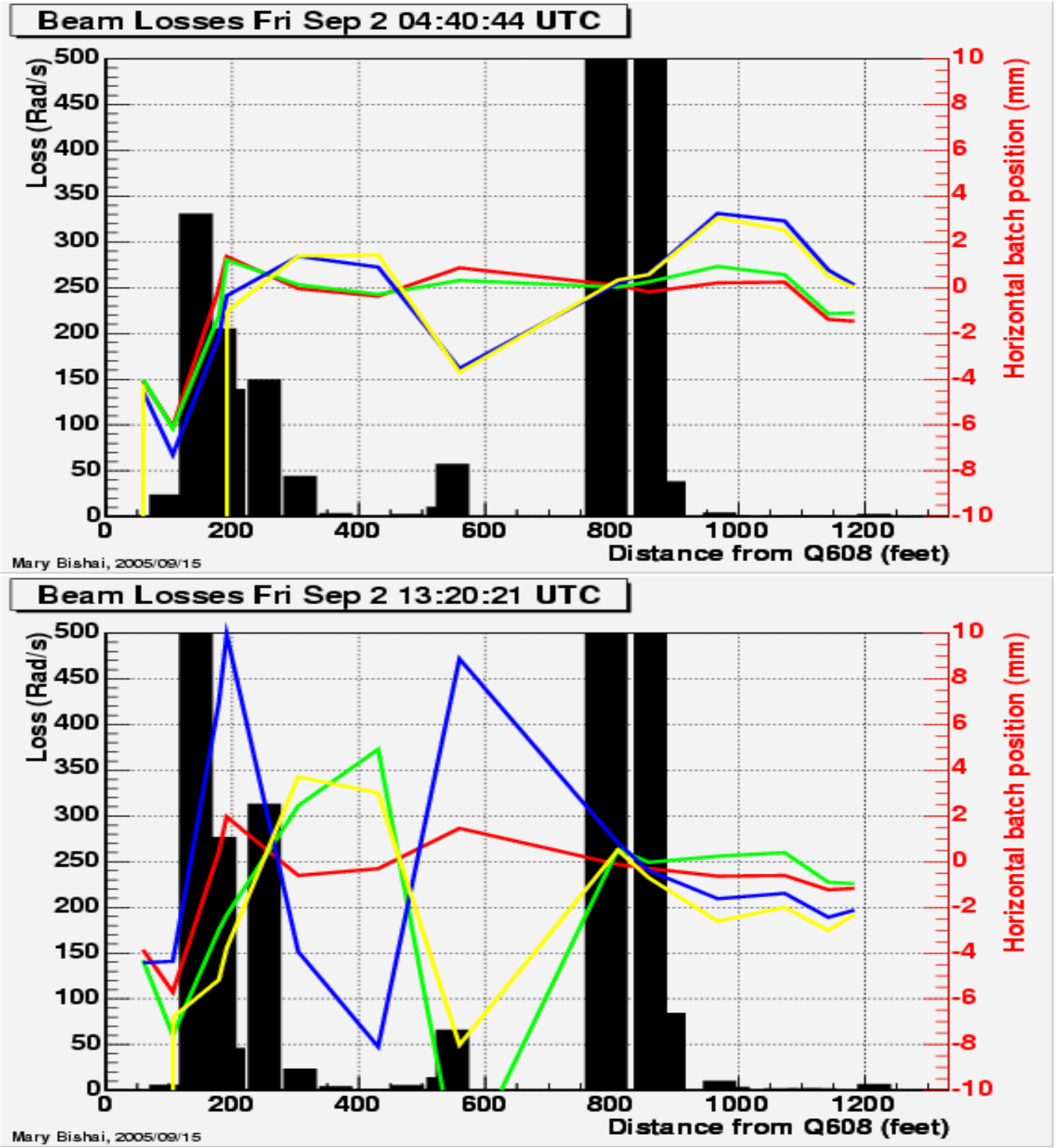

Figure 50: Bad loss pulses - only 4 recorded May-Nov, 2005

change the actual beam intensity at the target as compared to the measurement of intensity at TORTGT.

5.6 Beam quality selection critiria and efficiency

In this section we consider the fraction of POT that are useful to the physics goals of MINOS. Although in principal every POT should count, variations in beam conditions will affect the neutrino flux at the near and far detectors. For physics analysis that depend on the absolute normalization of the POT using the beam data, it is desirible to select spills where the beam quality is within acceptable limits. The choice of beam quality selection critiria is driven by limiting the systematic uncertainties on the neutrino flux at the near and far detectors due to protons lost per spill and to bad beam conditions. Firstly, we consider the effect of protons delivered that do not actually hit the target. We can estimate the fraction of protons lost per spill using a Gaussian assumption for the beam shape and the projected position at the target. By requiring the fraction of protons on target to be $> 95\%$, we can limit the uncertainty on the POT normalization due to our incomplete knowledge of the beam shape to a negligible level. In Figure 51 the fraction of the beam on the target as a function of horizontal and vertical beam widths for all spills collected between May and Sep, 2005 is shown. We see that for horizontal beam widths of < 1.5mm when the beam is centered on the target the fraction of beam on the target is $>$ Secondly, the hadron flux from the target will depend on where the protons hit the target. This depends on the shape of the beam and the position at which the beam maximum hits the target. Using GNUMI V1.17 we studied the overall change in the neutrino flux at the near and far detectors for the following beam conditions:

1. The beam is centered on the target but is 1.5 mm wide in the vertical and horizontal. This is consistent with what we observe in the data (see Figure 35) where we find that in data a 1.5 mm wide beam in the horizontal is approximately 1.5 mm wide in the vertical as well.

2. The beam is the nominal width of 1mm but is off target center by 1.5mm.

3. The beam is 1.5 mm wide in the vertical and horizontal and off the target center by 1.5 mm in the horizontal.

The ratio of the neutrino flux obtained using non-standard beam conditions to that of the flux using the nominal beam shape which is a circle with a Gaussian width of 1mm centered at the target is shown in Figure 52. We find that a beam which is 1.5 mm wide or 1.5 mm off target center produces a change in the flux at the near detector of 5% in the 0-5 GeV region. When taking the ratio between far detector and near detector the deviation from the nominal flux is much smaller. Based on this study we choose the beam data quality cuts to maximise efficiency for accepting spills. The default beam data quality cuts we have selected are

1. Horn intensity: $-200 <$ horn$_\mathrm{i}$ < 163 kA. This cut will exclude the special horn current scan runs taken in August.

2. Beam intensity: $0.5 <$ beam$_\mathrm{i}$ < 50 E12. This cut excludes spills with very low intensity where the uncertainty on the toroid readout is large.

3. Beam on target: a) The target is in the beamline + b) the horizontal average batch position is ± 1 mm from target center c) the vertical average batch position is ± 1 mm from target center d)$0.1 <$ horizontal beam width < 1.5 mm e))$0.1 <$ vertical beam width < 2.2mm

The fraction of POTs that survive loose beam data quality cuts for each month from May to Dec 2005 are listed in Table 13. We find that the fraction of total POT excluded is $< 0.5\%$. The largest fraction of POT rejected is due to the horn current selection which excludes the special horn

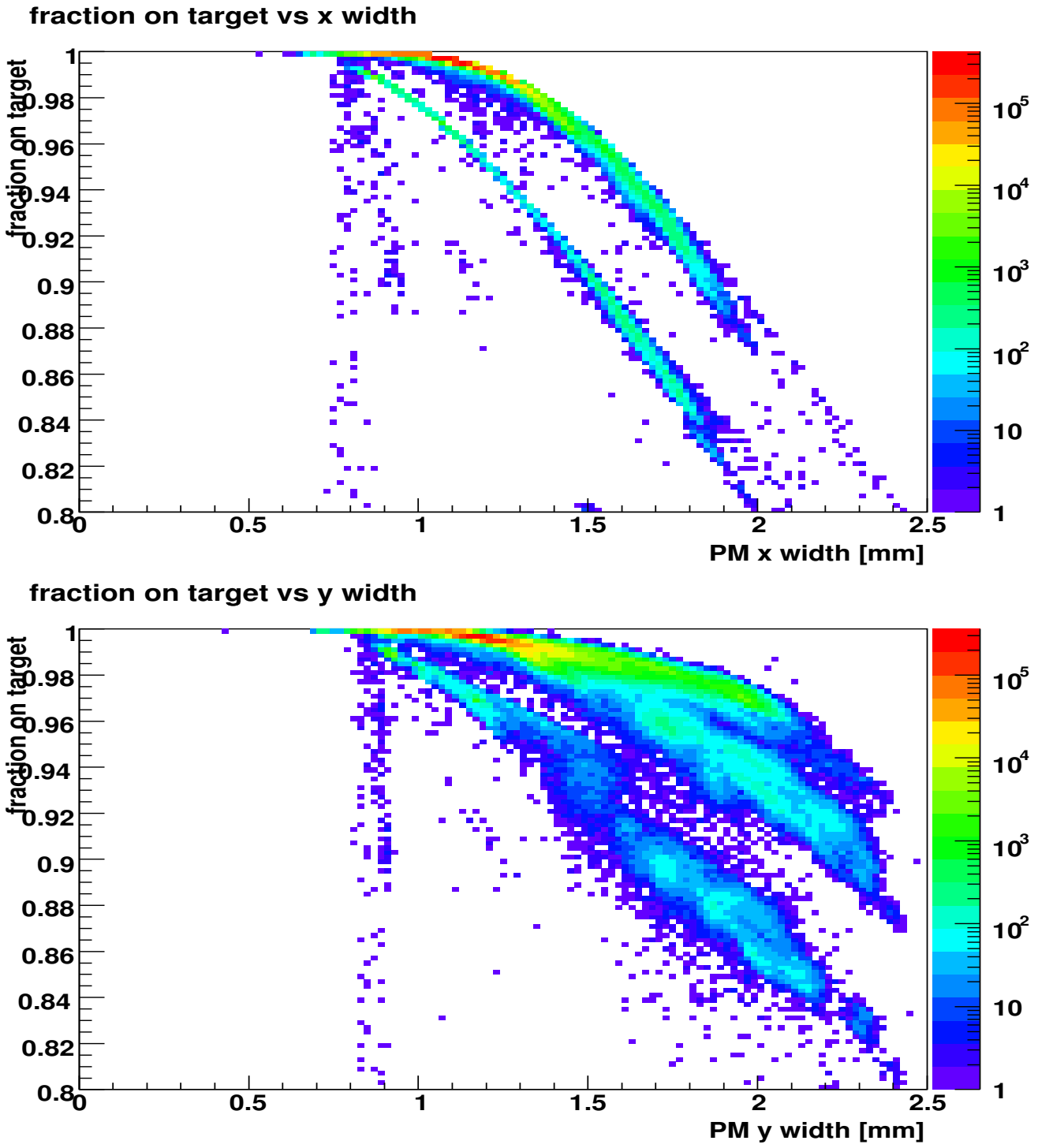

Figure 51: Fraction of the beam on the target horizontally and vertically using beam width and deviation from target center for all data May-Sep, 2005. There are 3 bands in the horizontal distribution and corresponding bands in the vertical distribution. Target position scans show up as the vertical bands to the left of the distributions. The central band corresponds to readout failures of the beam position monitors used to project to the target center.

current study runs taken in August, 2005. Prior to May 4th, 2005 the BPM read out in the MINOS datastream was unreliable. We recommend that the profile monitors be used to project the beam

position at the target for quality cuts for this earlier dataset.

Table 13: Summary of data selection efficiencies.

Month	BDP POT	Intensity > 0.5 E12	+Horn current	+Beam on target
March	7.04 E17	99.97	98.97%	72.98 %
May	67.4 E17	99.98 %	99.98 %	99.23 %
June	103.7 E17	99.98%	99.34%	99.27%
July	130.9 E17	99.98%	99.98%	99.69%
August	170.5 E17	99.998%	97.27%	97.25%
Sept	192.1 E17	99.998%	99.85%	99.81%
Oct	101.4 E17	100.00%	99.69%	99.57%
Nov	185.6 E17	100%	99.99%	99.81 %
Dec	147.3 E17	100%	99.64%	99.51 %
Total	1.111 E20			

Several classes exist in the MINOS offline framework which implement a loose set of default beam data quality cuts on a spill-by-spill basis. A detailed description of the default cuts applied in the MINOS offline analysis framework and instructions on how to use the spill quality selection classes is found in reference [10].

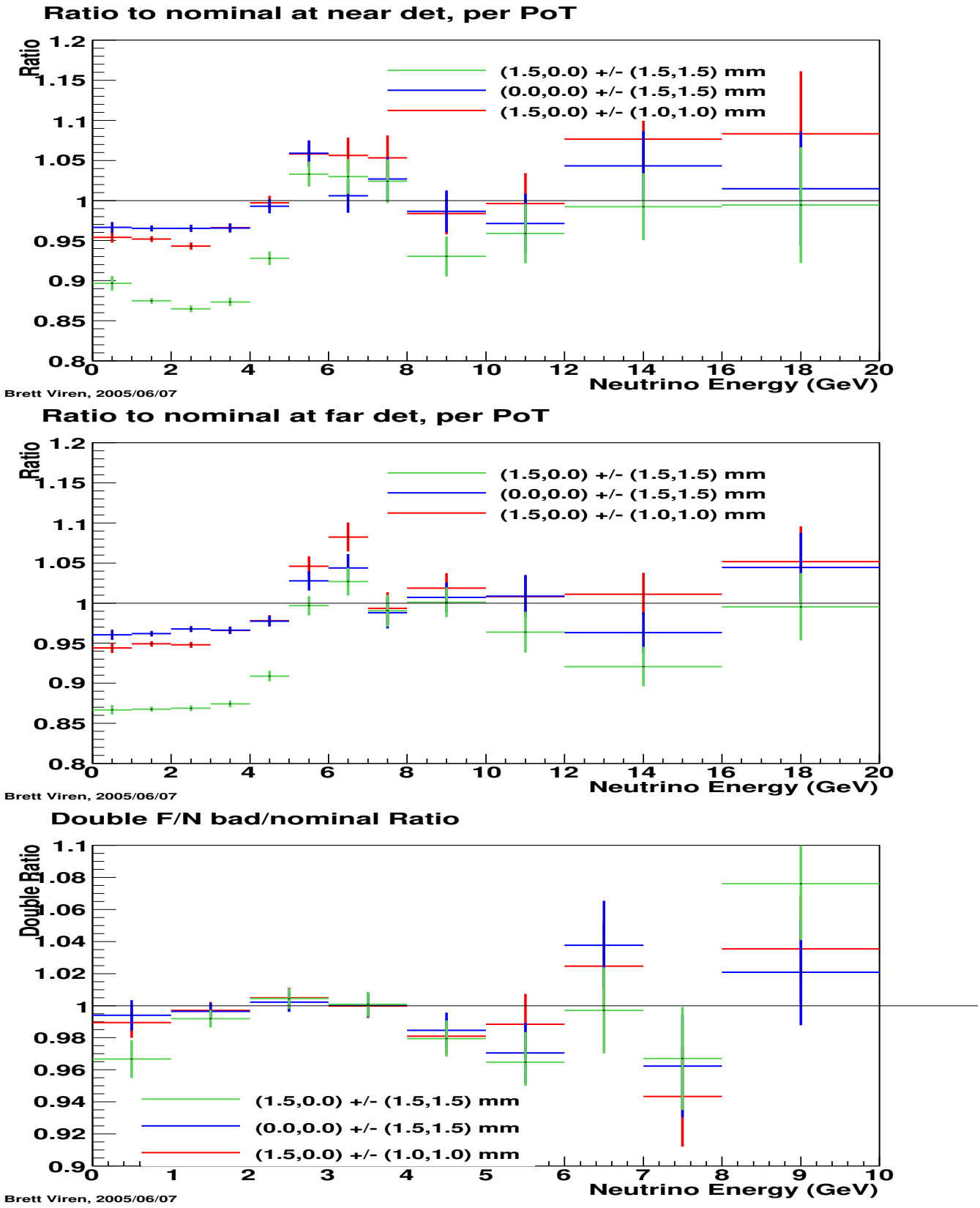

Figure 52: Effect of wide beams and beams hitting of target center on the neutrino flux at the near and far detectors and the ratio. The nominal flux is obtained using a circular beam with a Gaussian width of 1mm perfectly centered on the target.

5.7 SUMMARY

We have examined the sources of further corrections to the POT delivered to MINOS from beam spilling off the target and good beam selection critiria. We have shown previously that a Gaussian approximation for the beam shape is an adequate description. We recommend that the POT normalization per spill include a correction for the fraction of beam spilling off the target using the Gaussian widths measured at the PMTGT SEM and corrected for the expected 3.3% increase in width at the actual target location. The fraction of the beam contained on the target assuming a Gaussian beam is estimated using the error function:

$$\begin{aligned} f_{\text{on target}} = 0.25 \quad \times \quad & \left[erf\left(\frac{-(x_1-\bar{x})}{\sqrt{2}\sigma_x}\right) + erf\left(\frac{(x_2-\bar{x})}{\sqrt{2}\sigma_x}\right)\right] \\ \times \quad & \left[erf\left(\frac{-(y_1-\bar{y})}{\sqrt{2}\sigma_y}\right) + erf\left(\frac{(y_2-\bar{y})}{\sqrt{2}\sigma_y}\right)\right] \end{aligned} \tag{1}$$

where the error function, $erf(x)$ is defined as

$$erf(x) = \frac{2}{\sqrt{\pi}} \int_0^X e^{-u^2} du \tag{2}$$

a$x_{1,2}$ and $y_{1,2}$ are the four corners of the target in BPM co-ordinate system, $\sigma_{x,y}$ are the horizontal and vertical profiles of the beam as measured by PMTGT $\times 1.033$ and $\bar{x}$ and $\bar{y}$ are the average batch positions at the target. We find that the average value of σ_x and σ_y for beam intensities > 4.5E12 protons/batch to be ≈ 1.15 and 1.25 mm respectively. From the studies in Section 5.1 we find the location of the target center horizontaly in BPM co-ordinates to be $target^x_{center} = -1.14 \pm 0.011$mm and the target center vertically in BPM co-oridinates is $target^y_{center} = 1.0 \pm 0.4$ mm. We assume the target to be 6.4mm wide in the horizontal and 22mm wide in the vertical. The sources of uncertainty on the fraction of beam on target calculated for each spill are thus

1. Non-Gaussian tails, which we assume to be negligible for now.

2. The uncertainty on σ_x and σ_y is determined by the SEM resolution of the beam width which we take to be 150 micron (0.5mm pitch/$\sqrt{(12)}$).

3. The uncertainty on the target location obtained from the target scan measurements of the BPMs and the stability of BPM measurements of the target location. To accomodate the variation in the target horizontal center location observed during different target scans we recommend a conservative uncertainty of 100 microns on $target^x_{center}$ and 0.5mm in $target^y_{center}$.

4. The uncertainty on the spill-by-spill measurement of the average batch position at the target ($\bar{x}$ and $\bar{y}$ in Equation 1). The position at the target is calculable for each batch. The uncertainty in the location is determined by the BPM resolution which is nominally 50 microns for the pretarget and batch-batch variations. We find the location of batches 3,4,5 and 6 at the target are stable in both NuMI only and NuMI mixed mode to 50 microns after Vernier Autotune was introduced. Since batch 1 average position can be off by 200 microns from target center, we will therefore use 100 microns as the conservative uncertainty on $\bar{x}$ and $\bar{y}$ for each spill.

By combining the above uncertainties together we estimate that the the uncertainty on the POT per spill from the estimation of the fraction of the beam on target to be 1% (???).

We have identified a loose set of beam quality cuts to apply when selecting spills. Our primary motiviation was to maximize efficiency. For the given set of cuts described in Section 5.6 and [10] we find that for the data collected from May to December, 2005 with nominal horn currents, less than 1% of the POT delivered to NuMI are rejected due to bad beam conditions with the loose beam quality critiria currently recommended.

6 Near Detector POT studies

The primary purpose of the MINOS Near Detector is to provide an experimental measurement of the NuMI beam spectrum, components and absolute normalization. Therefore the Near Detector provides the final measurement of the NuMI beam quality and stability and vice-versa. The Near Detector event rate per spill vs the number of POT in a spill as measured in the pME beam configuration is shown in Figure 53. The average number of tracks vs POT from the pME data fit to a straight line is also shown in Figure 53. We find that the rate is linear with POT for intensities up to 2.5E13. The Near Detector event rates as a function of time normalized by POT should be constant if both the beam quality, toroid calibrations and the near detector are stable. The Near Detector event selection and daily event rates are discussed in reference [9]. A preliminary measurement of the average daily event rates, normalized by POT, as a function of time from May through December, 2005 for events with total energy $<$ and $>$ 10 GeV are shown in Figure 54 [9]. The rates are shown for the pLE data. We find that the POT normalized daily event rate is stable to within 3 % for pLE at nominal horn current. The notable outliers on the rate plot in August, 2005 correspond to dates when the horn current scans where carried out.

6.1 Beam Quality Effects in the Near Detector

In section 5.6 we discussed the results of MC studies when beam quality, specifically the width and location of beam centroid on the target, is severely degraded. We studied the effect of varying beam width on the Near detector neutrino spectrum in the data by selecting two ND data samples with different beam widths: Sample 1 is for spill with beam width $<$ 1.2 mm in the horizontal and Sample 2 which is all events for which the beam width is $>$ 1.3 mm in the horizontal. The data is taken from May 21st to the 31st. As noted earlier we had our worst beam width performance on May 28-31st. The ratio of the reconstructed neutrino spectrum as measured in the near detector of Sample 2/Sample 1 is shown in Figure 55. Although the data seems to show the same trends as the MC the statistics of Sample 2 (wide beam widths) is too small to provide a conclusive comparison. Note that Figure 52 shows the ratio in the generated neutrino flux at the near detector location for wide versus nominal beam width, whereas the plots in Figure 55 are for the ratio of the *reconstructed* neutrino event spectrum in the near detector.

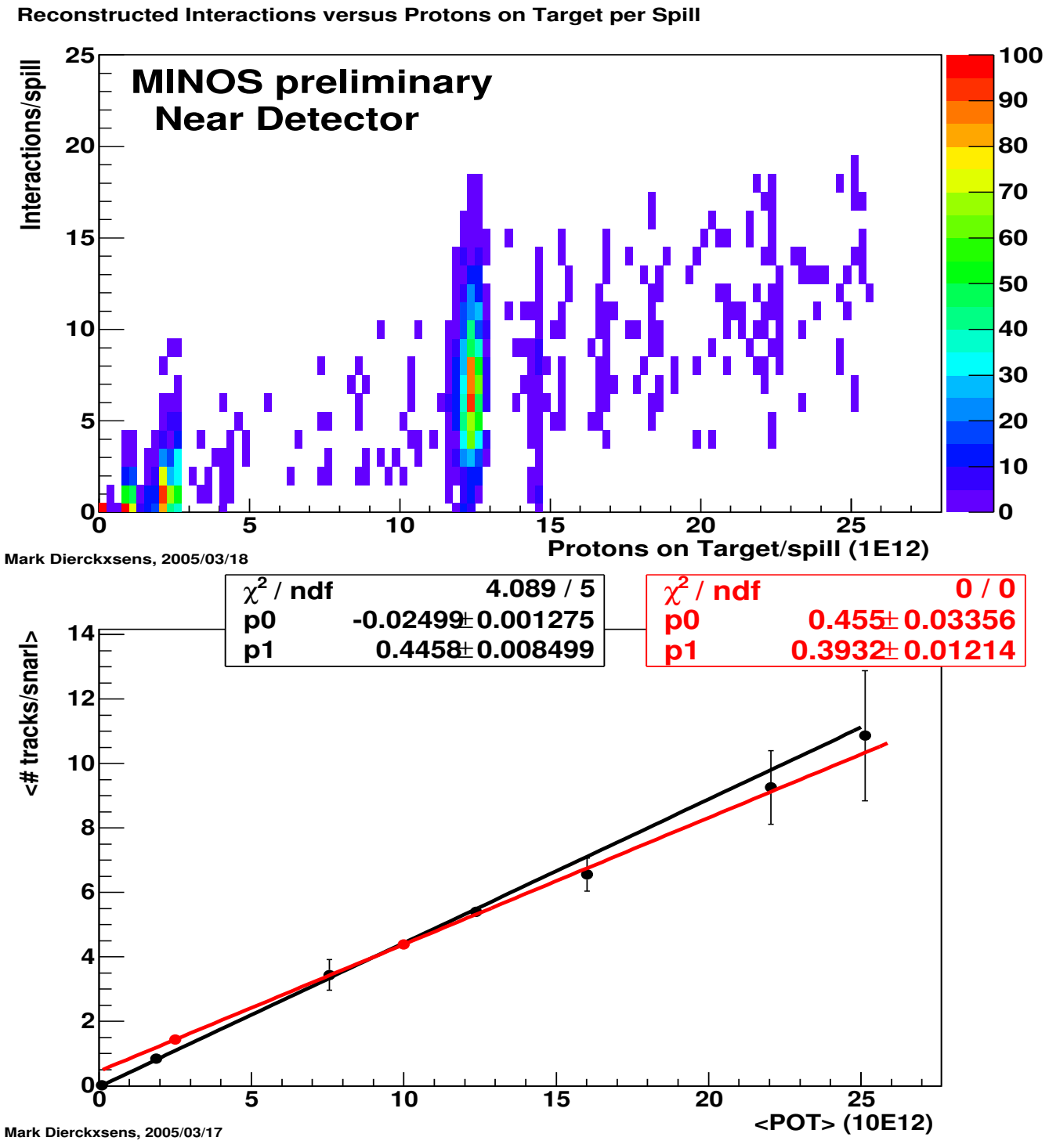

Figure 53: The Near Detector event rate per spill vs POT per spill as measured in the pME data taken in March 2005 (top). The average number of tracks per spill for pME data (black points) and the MC prediction (red points) is hown in the bottom plot. A straight line fit to data and MC average track rates is also shown.

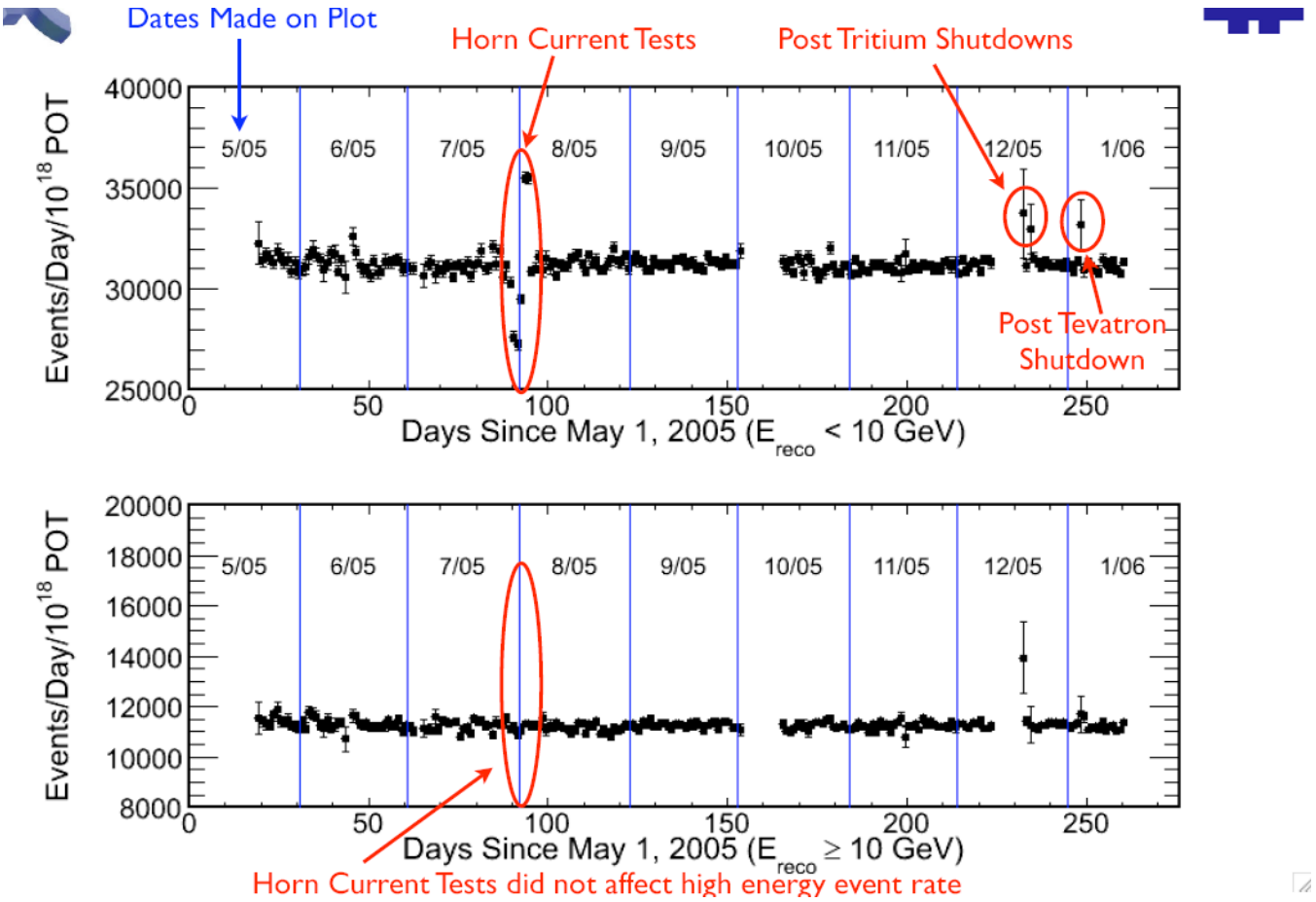

Figure 54: The near detector event rates as a function of POT since May 1, 2005 for the pLE data.

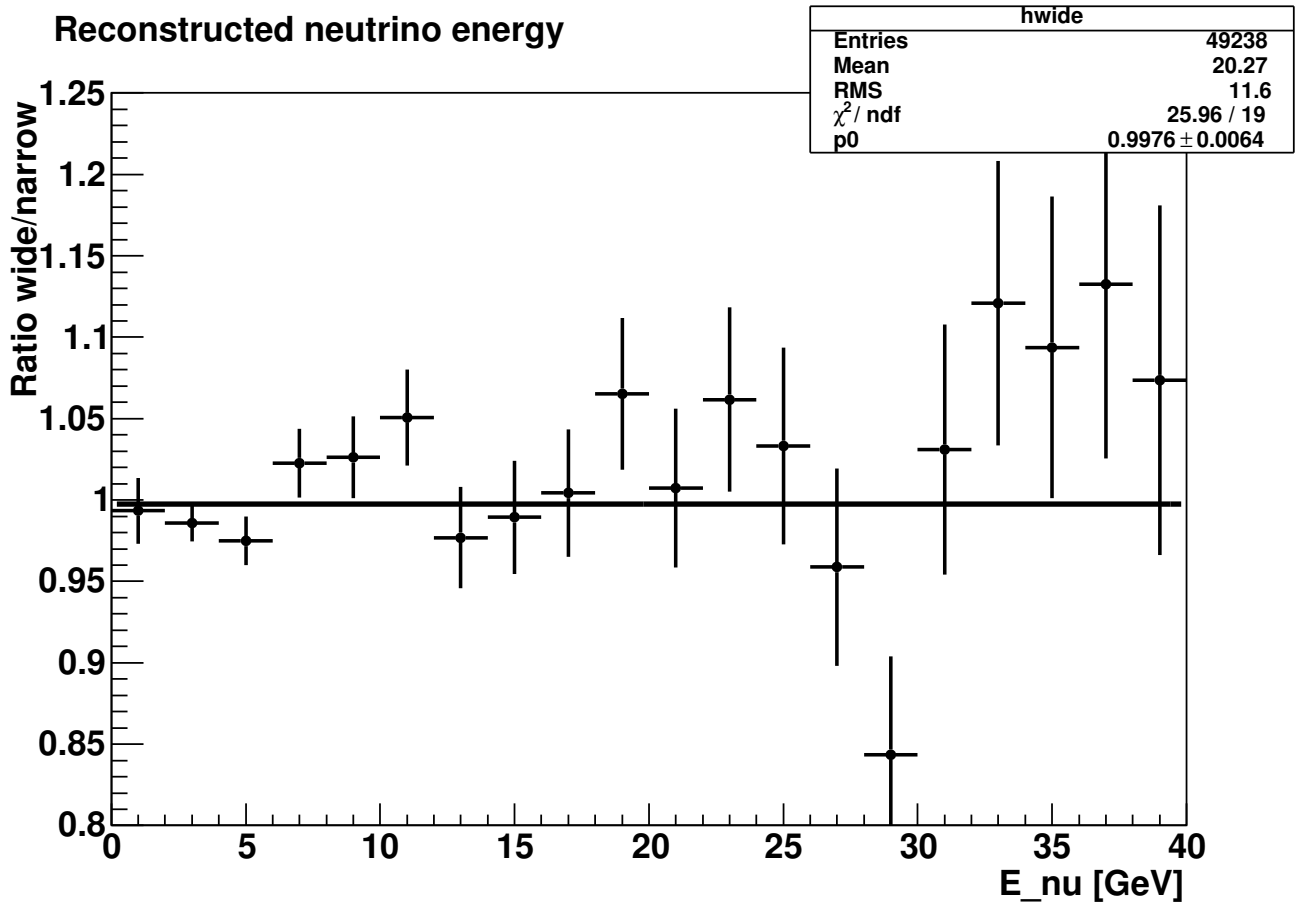

Figure 55: Ratio of the reconstructed neutrino event spectrum in the near detector with wide beam width versus narrow beam width. Wide beam width is defined as $\sigma_x > 1.3$ mm and narrow beam width is defined as events with $\sigma_x < 1.2$ mm.

7 Conclusions

In this report we have presented a detailed study of the estimation of the fraction of protons delivered to NuMI during 2005.

Firstly, we documented the calibrations of the NuMI toroids which measure the absolute proton intensity per spill. A very preliminary estimate of the uncertainty on the absolute toroid calibration and stability is listed in Table 14. We find that the absolute toroid calibration and stability for the period after July 26, 2005 to be better than 1%. This number is very preliminary.

Table 14: Uncertainties on the number of POT per spill

Absolute toroid calibration	$\approx 3\%$ prior to July 26,2005 $\approx 1\%$ after July 26,2005
Estimation of fraction of protons on the target using beam instrumentation	1% (???)
Logging uncertainties (sample time)	0.03%

Secondly, we presented a detailed study of the performance of the MINOS beam data stream logging. The MINOS beam data stream logs the readout from > 300 NuMI instrumentation devices every spill. We found that the logging efficiency varied throughout 2005 as the logging software was improved and commisioned. In Dec, 2005 we estimated that the beam data logging efficiency was 99.7%. The fraction of spills where the NuMI toroids readout successfully is $> 99.9\%$. The fraction of spills where all critical ACNET devices needed to determine the beam quality at the target read out properly is $> 99.0\%$.

Thirdly, we conducted a detailed study of the beam quality as determined by 1) the beam profile at the target 2) the position of the beam centroid at the target and its stability and 3) beam lost in the beamline. By using the NuMI beamline instrumentation in the beam target region, we can estimate the fraction of the beam spilling off the target and correct the measurement of the proton beam intensity measured by the toroids on a spill-by-spill basis. The resolution and stability of the NuMI instrumentation determines the uncertainty on the fraction of the beam on target estimated for each spill. We estimate that the accuracy of the NuMI instrumentation in the pretarget region will allow us to measure the fraction of the beam on the NuMI target with an accuracy of 1% (???).

Fourthly, we have studied the effect of beam quality on the Near Detector neutrino events. Based on MC studies of the effect of bad beam quality on the neutrino flux measured at the near detector and the ratio of near to far, we have selected a very loose set of beam quality critiria to maximize spill selection efficiency. We estimate that the integrated POT rejected from requiring loose beam quality cuts to be $< 1\%$. We have also studied the stability of the Near Detector reponse as a function of the POT. We find that the number of reconstructed neutrino events in the Near Detector when normalized by POT for the period May 20-Dec 31,2005 is stable to within 3%.

Overall, the performance of the NuMI beamline and its instrumentation in 2005 has exceeded expectation. The quality of the beam delivered has been tightly controlled which has resulted in the rejection of less than 1 % of the total POT due to bad beam conditions. The extensive beam instrumentation has allowed us to characterize the beam quality on a spill-by-spill basis to great accuracy as well as measure the absolute numbers of protons delivered each spill with an uncertainty of $\approx 1\%$ (after July 26, 2005).

A Fermilab accelerator complex timing signals

There are four special purpose communication links that broadcast time, beam synchronization, and machine data throughout the Fermilab Accelerator complex. The most sophisticated of these links is the Tevatron Clock (TCLK). Up to 256 unique events may be encoded onto TCLK with typical resolution of 100 nanoseconds. Beam Sync clocks have been implemented for both the Main Injector and Tevatron. The Main Injector Beam Sync Clock is refered to as MIBS. The beam sync clocks operate at approximately 7.5 MHz and are derived from the Main Injector and Tevatron RF systems. Beam diagnostics, beam transfers between machines, and placement of MI proton and p-bar bunches are coordinated by encoded events on these clocks. A custom integrated circuit was designed to accommodate detection of the serially encoded events present on both Tevatron and Beam Sync clocks with a minimum of circuit overhead. Each of these links is distributed throughout the accelerator complex and is integrated into a significant number of control system components. The NuMI production MI timeline showing the TCLK events used for NuMI timing is shown in Figure 56. The NuMI and Pbar mixed mode MI timeline is shown in Figure 57 Here are some of

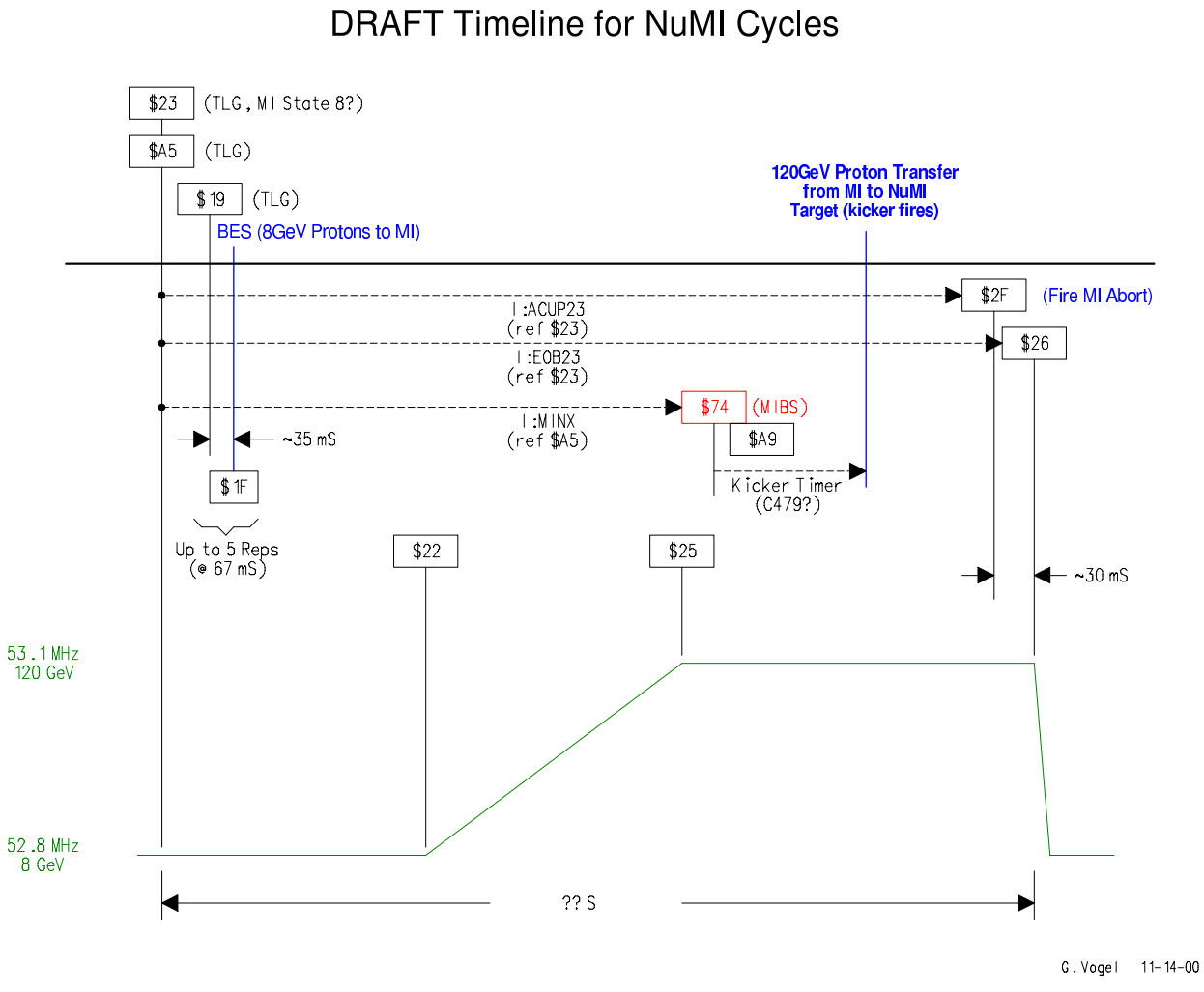

Figure 56: NuMI only MI timeline

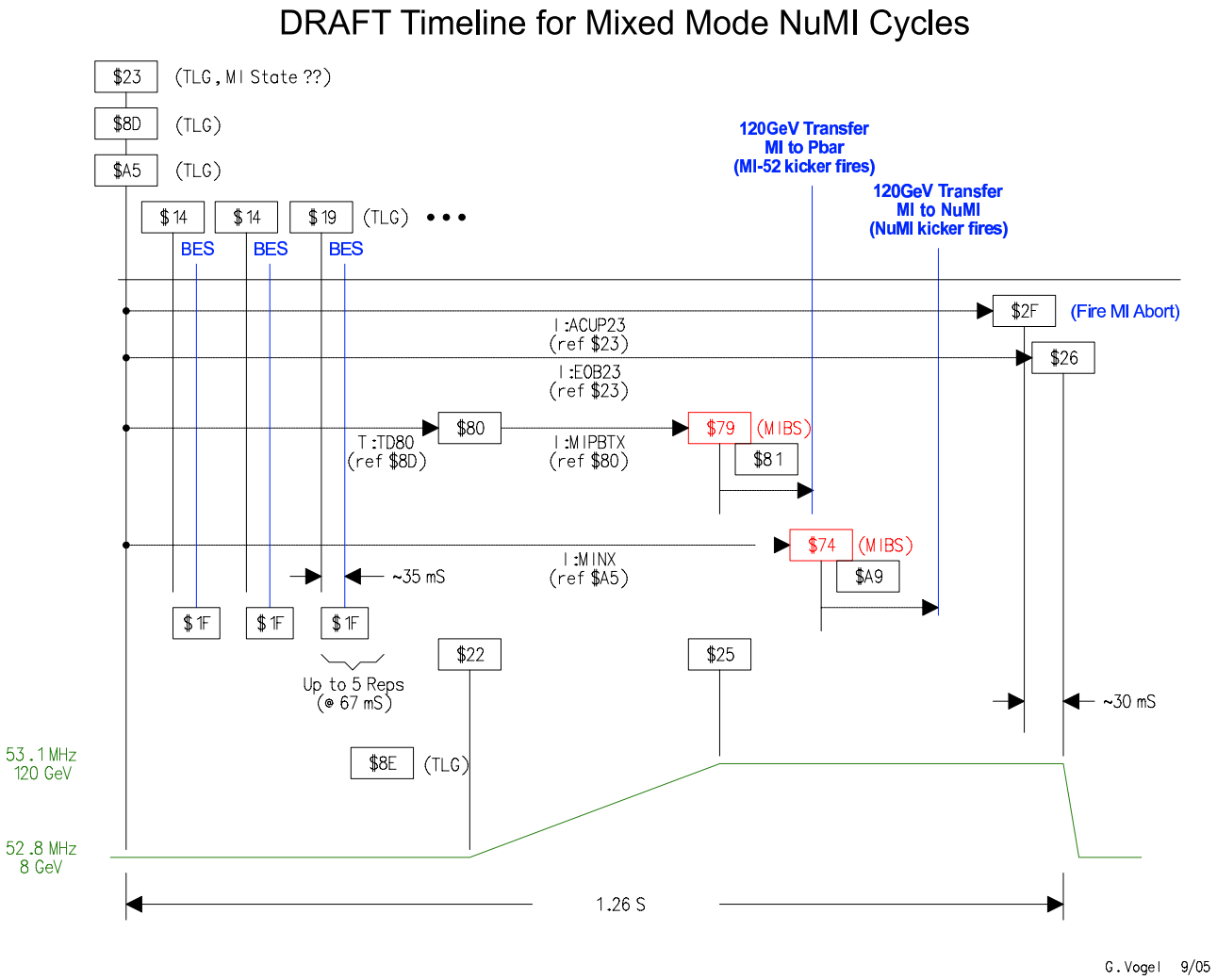

Figure 57: NuMI only MI timeline

the TCLK and MIBS timing events most relevant to readout of the NuMI beamline instrumentation including the toroids:

- TCLK $23=MI reset for NuMI Beam Cycle
- TCLK $25=Start of MI ramp Flattop
- TCLK $A4= NuMI Cycle sample
- TCLK $A5= NuMI extracted beam reset (Datalogged Event)
- TCLK $A6= NuMI permit has fallen
- TCLK $A9 is the reflected TCLK for MIBS $74 (P+ transfer from MI for NuMI)
- NuMI Kicker fires about 200usec after $74

B Horn Alignments

To measure the horn alignments, a proton beam scan across the horn cross-hairs was performed on March 3rd, 2005. The target was removed for this study. As the beam moves across the cross-hair, scattered radiation is recorded by the beam loss monitors (BLMs) mounted on the horns (see Figure 58). The more the beam is on the cross-hair, the larger the amount of ionization recorded by the

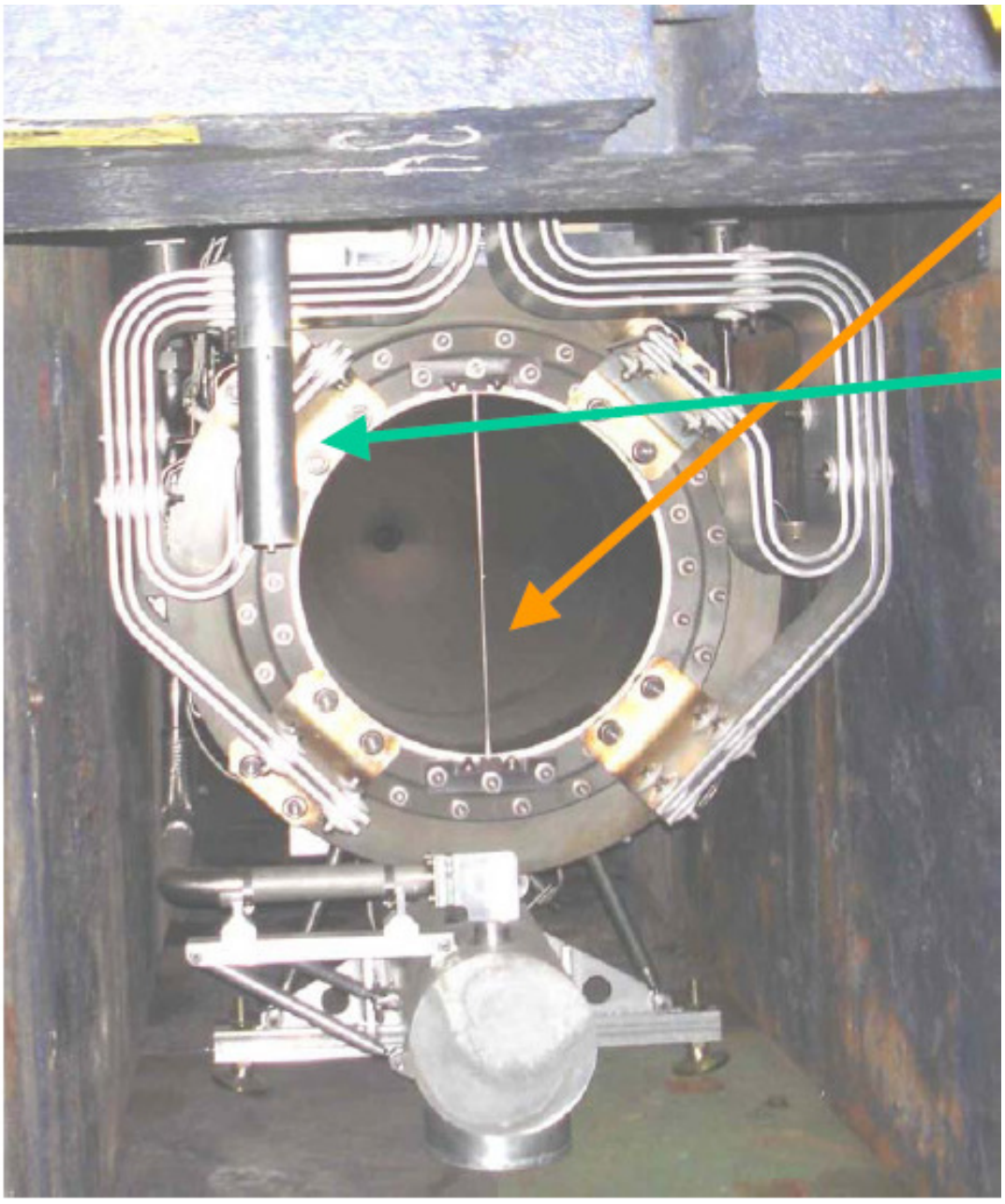

Figure 58: Photograph of horn 1 showing the location of the cross-hair (orange arrow) and the beam loss monitor (green arrow). The BLM is the cylinder on the top left.

BLMs. There are two loss monitors: H1ALM on horn 1 and H2ALM on horn 2. In Figure 59 the ionization signal from H1ALM and H2ALM is plotted versus location at the horn 1 cross hair location and the horn 2 location. The maximum ionization signal which corresponds to the beam hitting the cross hair at horn 1 is clearly visible in both loss monitors. A fit to a Gaussian and a

flat line indicates that the horn 1 cross-hair is at -4 ± 0.7 mm in the horizontal as measured by the BPMs. The horn 1 cross-hair should be at -2.5 mm if BPM $x = 0$ is the axis of the beamline. This indicates that with the current BPM readout horn 1 appears to be at $horn_x^1 = -1.5 \pm 0.7$ mm. A similar analysis of the much smaller bump in the loss monitor readout shown in Figure 59 at the horn 2 location indicates that in BPM readout the horn 2 cross-hair appears at $\approx x = 1$ mm. The signal amplitude is small and should be taken as a rough estimate as best. Horn 2 cross-hair should be at +2.5 mm if BPM $x = 0$ is the axis of the beamline. This indicates that $horn_x^2 \approx -1.5$ mm as measured by the current BPMs. Since the target center is estimated to be at $target_{center}^x = -1.14 \pm 0.011$ mm in the BPM co-ordinate system, we conclude that there is a target-horn misalignment in the range $target_x - horn_x^{1,2} = 0.4 \pm 0.7$ mm in the horizontal. Data from a vertical beam scan of the horns is also shown in Figure 59. The vertical scan seems to indicate that the horns are located at $horn_y = +1$ to 2 mm in the vertical in agreement with the target scans that also indicates the target is at $target_y = +1.5$ mm in the BPM co-ordinate system.

The effect of horn misalignments and horn currents on the neutrino flux is discussed in detail in [6].

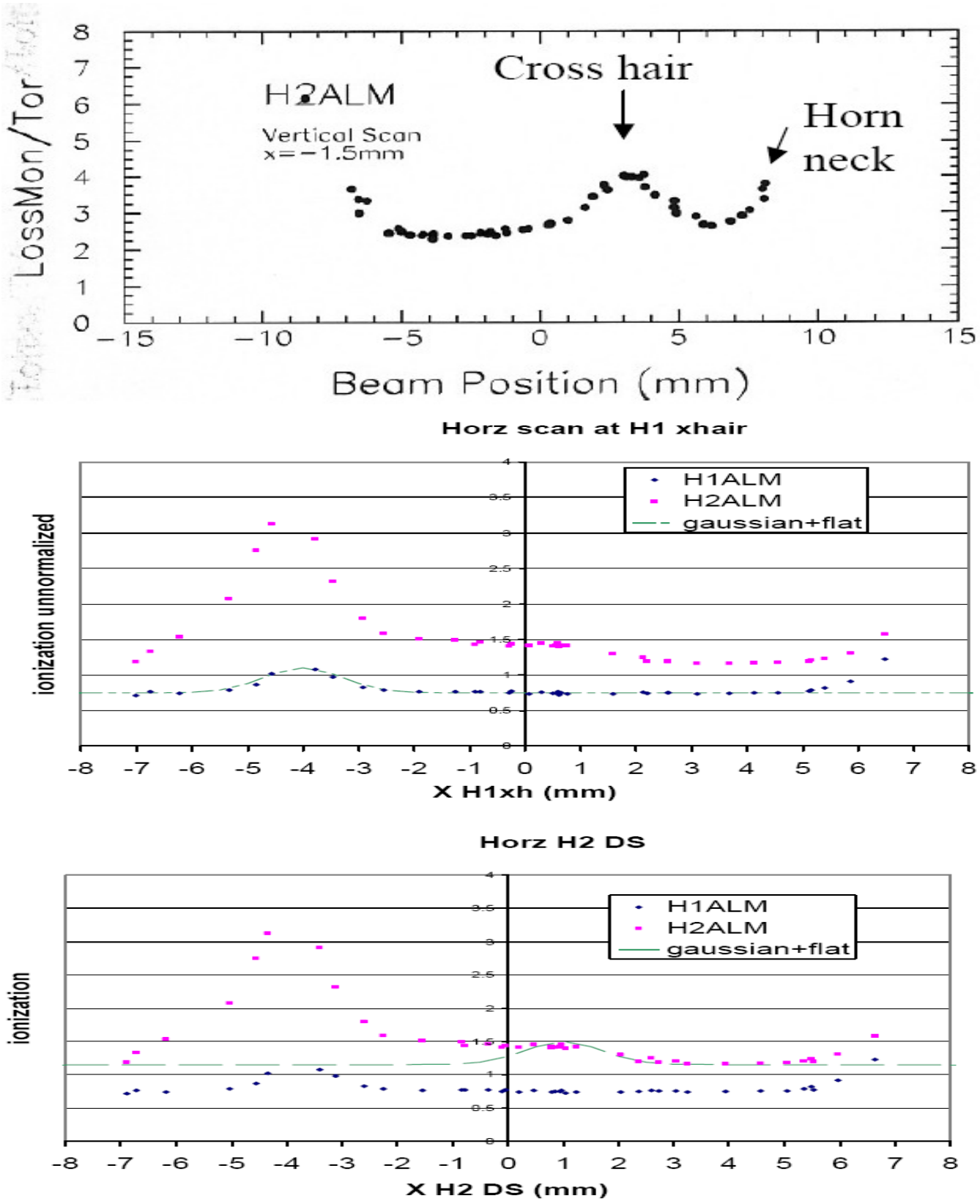

Figure 59: Beam scan of Horn 1 and Horn 2 cross hairs. A vertical horn scan is shown in the top figure. A fit to a Gaussian + straight line is used to measure the horizontal location of the cross hairs at the Horn 1 and Horn 2 position along the beamline (center and bottom plot).

C Summary of different NuMI running conditions

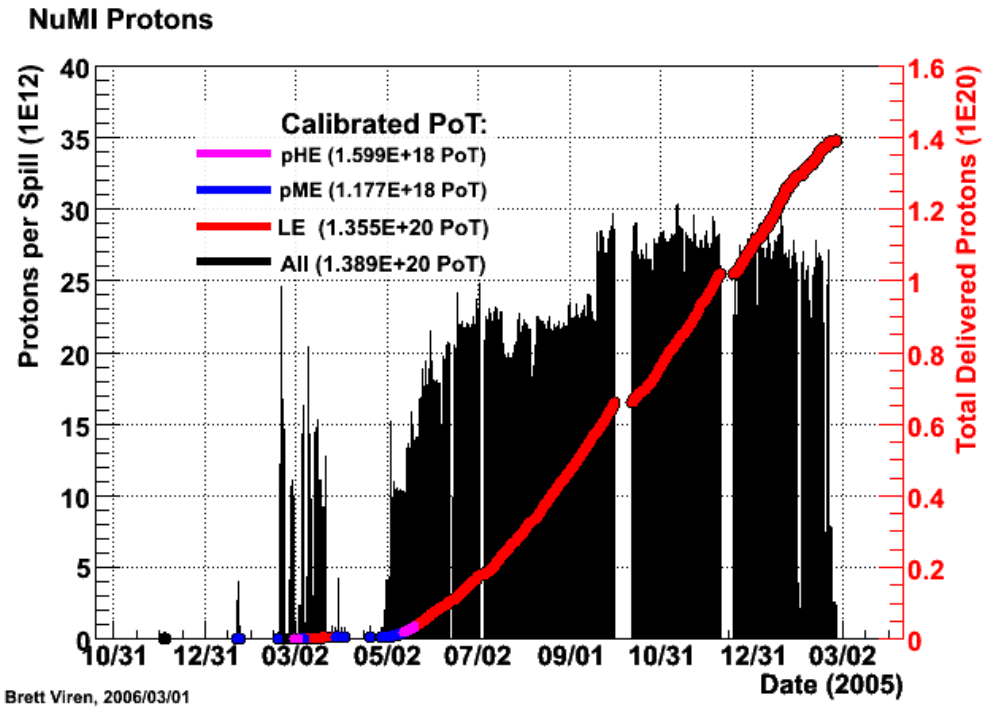

Figure 60: NuMI integrated and instantaneous POT as recorded by the BDP. POT calibration corrections are applied.

Table 15: Summary of different NuMI beam running conditions Feb, 2005 through Feb, 2006. These are for planned changes, unplanned changes in beam conditions such as horn current trips are not indicated in this list. Times are UTC. POT have calibrations applied. *Throw away spills with < 0.1E12 to exclude noise/pedestals. **Variation in toroid readouts.

Target location	Horn current	Start time	End time	POT*
-100 cm	-200 kA	2005-02-01	2005-02-27 21:30:50	2.39-3.10 E16 **
-250 cm	-200 kA	2005-02-27 21:43:35	2005-03-04 01:22:05	3.57-3.66 E15 **
-100 cm	-200 kA	2005-03-04 01:32:18	2005-03-07 23:52:44	5.73-5.84 E15 **
0 cm	-200 kA	2005-03-08 23:16:23	2005-03-23	6.68-6.83 E17 **
-100 cm	-200 kA	2005-04-30 20:19:37	2005-05-12 19:53:03	1.168 E18
-250 cm	-200 kA	2005-05-12 22:37:18	2005-05-20 16:00:21	1.596 E18
-10 cm	-185 kA	2005-05-20 19:44:16	2005-07-29 17:54:28	2.519 E19
-10 cm	-170 kA	2005-07-29 17:58:06	2005-08-01 18:58:08	1.466 E18
-10 cm	-200 kA	2005-08-01 19:01:30	2005-08-03 23:44:34	1.366 E18
-10 cm	-185 kA	2005-08-03 23:46:43	2006-02-10 21:03:43	1.016 E20
-10 cm	0 kA	2006-02-10 21:05:43	2006-02-15 13:37:04	2.915 E18
-10 cm	-185 kA	2006-02-15 18:05:02	2006-02-25 23:02:59	2.949 E18
Total		2005-02-01	2006-02-25 23:02:59	1.390 E20

References

[1] NuMI-B-933 NuMI-B-1068

[2] http://pearsonelectronics.com/current-monitor-products/calibration-and-test.htm

[3] Beams-doc-1813

[4] B. Viren. Description of the Beam Data Process and beam data logging for the MINOS experiment. Upcoming note.

[5] Kevin Cahill, Charlie King. http://www-bd.fnal.gov/controls/public/JavaControls.htm

[6] S. Kopp, Z. Pavlovic, D. Indurthy. MINOS-doc-1283-v1

[7] R. Zwaska. U. Texas thesis and upcoming note.

[8] Min-Jen Yang, "NuMI Beam Optics Study" http://www-numi.fnal.gov/internal/local_restricted_access/protonwg/MY_optics_study_3_14_05.pdf

[9] MINOS-doc-1484-v1

[10] MINOS-doc-1486